A Study of Beam Position Diagnostics with Beam-excited Dipole Higher Order Modes using a Downconverter Test Electronics in Third Harmonic 3.9 GHz Superconducting Accelerating Cavities at FLASH

P. Zhang[†‡*], N. Baboi[‡], N. Eddy[#], B. Fellenz[#], R.M. Jones[†*],
B. Lorbeer[‡], T. Wamsat[‡], M. Wendt[#]
[†]The University of Manchester, Manchester, U.K.
[‡]DESY, Hamburg, Germany
[*]The Cockcroft Institute, Daresbury, U.K.
[#]Fermilab, Batavia, Illinois 60510, U.S.A.

August 13, 2012

Abstract

Beam-excited higher order modes (HOM) in accelerating cavities contain transverse beam position information. Previous studies have narrowed down three modal options for beam position diagnostics in the third harmonic 3.9 GHz cavities at FLASH. Localized modes in the beam pipes at approximately 4.1 GHz and in the fifth cavity dipole band at approximately 9 GHz were found, that can provide a local measurement of the beam position. In contrast, propagating modes in the first and second dipole bands between 4.2 and 5.5 GHz can reach a better resolution. All the options were assessed with a specially designed test electronics built by Fermilab. The aim is to define a mode or spectral region suitable for the HOM electronics. Two data analysis techniques are used and compared in extracting beam position information from the dipole HOMs: direct linear regression and singular value decomposition. Current experiments suggest a resolution of 50 μm accuracy in predicting local beam position using modes in the fifth dipole band, and a global resolution of 20 μm over the complete module. Based on these results we decided to build a HOM electronics for the second dipole band and the fifth dipole band, so that we will have both high resolution measurements for the whole module, and localized measurements for individual cavity. The prototype electronics is being built by Fermilab and planned to be tested in FLASH by the end of 2012.

Contents

Chapter 1

Introduction

1.1 FLASH and the third harmonic cavities

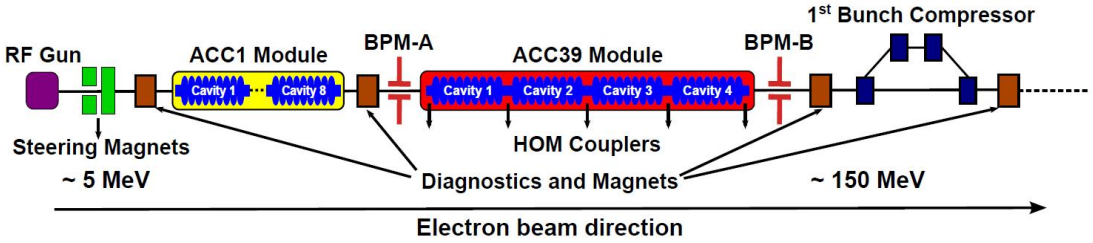

Figure 1.1: Schematic of injector section of the FLASH facility (not to scale, cavities in ACC1 are approximately three times larger than those in ACC39).

FLASH [1] is a free-electron laser (FEL) user facility at DESY in Hamburg providing ultrashort radiation pulses with an unprecedented brilliance. A schematic of the injector section of FLASH is shown in Fig. 1.1. A laser-driven RF gun generates a high quality electron beam. Seven superconducting 1.3 GHz TESLA type [2] modules accelerate the electron beam to a maximum energy of 1.2 GeV. Then the electron beam goes through an undulator section to produce laser like coherent FEL radiation.

(a) The ACC39 module

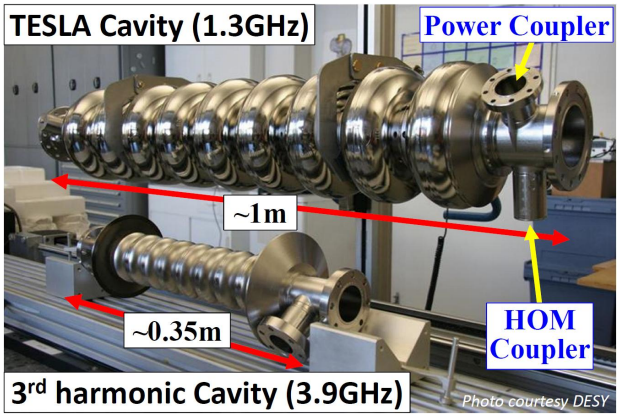

(b) Cavities

Figure 1.2: (a) The ACC39 module in FLASH beam line. The module in yellow, on the right, is ACC1. The direction of travel of the multi-bunch beam, is from right to left. (b) A TESLA style cavity operating at 1.3 GHz (top) and the corresponding third harmonic cavity (bottom).

A third harmonic module containing four 3.9 GHz superconducting cavities is installed in FLASH (Fig. 1.2(a)) in order to linearize the longitudinal phase space of the electron bunch [3]. Due to a special design [4], most higher order modes (HOMs) are above the cutoff frequency of the connecting beam

pipes, therefore are able to propagate among cavities. This leads to a significantly complex HOM spectrum of the 3.9 GHz cavity. Moreover, wakefields are much stronger in the 3.9 GHz cavities than those in the TESLA 1.3 GHz cavities. This is due to the smaller iris of the 3.9 GHz cavity which consequently scales up the wakefield with the second power for the longitudinal components and the third power for the transverse components [5]. Fig. 1.2(b) shows a comparison of the 1.3 GHz TESLA cavity and the 3.9 GHz cavity. If left unchecked, these HOMs will add adverse effects on the beam resulting a dilution of the beam quality. On the other hand, dipole higher order modes have linear dependence on the transverse beam position [5], and this enables the beam position to be determined remotely by monitoring these modes [6, 7, 8].

Higher order mode beam position monitors (HOMBPM) have the capability of measuring the beam position inside the accelerating cavity without additional vacuum components, while the traditional beam position monitors (BPMs) fall short of providing this information directly. However, a careful study on the cavity spectrum is required in order to secure an appropriate dipole mode. Since the cavity is not designed to be used as a diagnostics tool, the position resolution might be limited by the characterizations of the cavities.

Prior to designing any electronics for HOM-based beam diagnostics, extensive studies on the third harmonic cavities have been conducted. Concerning simulations, at first, eigenmode simulations have been performed on an ideal third harmonic cavity without couplers using three different simulation codes: MAFIA®[9, 10], HFSS®[11, 12] and CST Microwave Studio®[13, 14]. Then the entire third harmonic module consisting of four 3.9 GHz cavities have been simulated with three different schemes: Generalized Scattering Matrix (GSM) [15, 16], Coupled S-Parameter Calculation (CSC) [15, 17] and direct calculation using the ACE3P code suite [18, 19]. Regarding the measurement, a series of transmission measurements without beam excitations were conducted [15, 20], then beam-excited HOM spectra were measured [21, 20] and the dipole dependence on the beam offset were studied [20, 22, 23, 24]. Three modal options are therefore narrowed down [25] and the test electronics are subsequently designed and built by FNAL in order to study these modal options using both amplitude and phase of each mode for beam position diagnostics. Then a dedicated study has been conducted with the test electronics and the results are presented in this report.

In this report, the principle of the test electronics is introduced in Chapter 2 along with example output signals and various modal options tested in this study. In Chapter 3, two analysis methods used to extract beam position information from the HOM signals are explained and compared: direct linear regression (DLR) and singular value decomposition (SVD). Then the position resolution using one 20 MHz band of signals from each modal option is described in Chapter 4. Both time-domain and frequency-domain signals are studied and compared. Extensive tables of position resolutions for all modal options studied are listed in Appendix C, while the number of SVD modes used to achieve these resolutions is listed in Appendix D.

Chapter 2

HOM Measurements with the Test Electronics

Previous studies suggest three promising modal options for beam position diagnostics [25]. These are dipole beam-pipe modes at approximately 4 GHz, the first two dipole cavity bands at 4–5.5 GHz and the fifth dipole cavity band at approximately 9 GHz. A test electronics has been built to study these options in FLASH as explained in this chapter.

2.1 The Principle of the Test Electronics

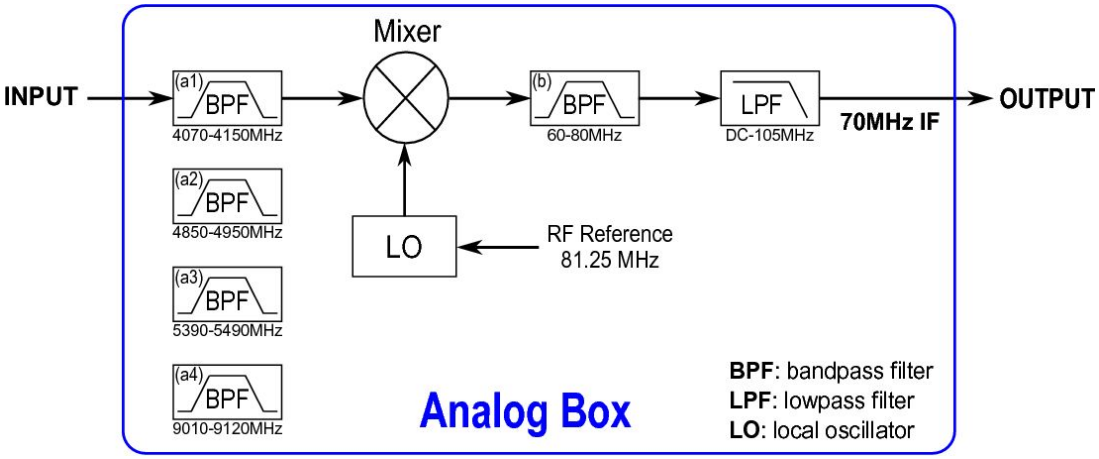

Figure 2.1: Schematics of the analog box. Only one of the four BPFs (a1-a4) is connected in the chain during each measurement.

The analog electronics was designed to have the flexibility to study various modal options of interest as well as accommodate the large mode bandwidths (BW) of these options. Its simplified block diagram is shown in Fig. 2.1. One of four different analog bandpass filters (BPF) can be connected into the chain to study the localized dipole beam-pipe modes at ∼4.1 GHz, strong multi-cavity modes in the first dipole band at ∼4.9 GHz and in the second dipole band at ∼5.4 GHz, and the trapped cavity modes in the fifth dipole band at ∼9 GHz. After filtering, the signal is mixed with a selectable local oscillator (LO) to an intermediate frequency (IF) of approximately 70 MHz. Then the 70 MHz IF signal is further filtered with a 20 MHz analog BPF to select the specific band of modes. In order to ensure that the possible remaining high frequency components of the IF signal generated during the mixing step are well suppressed, a lowpass filter (LPF) is applied to preserve only the frequency below 105 MHz with a dominant component from 60 MHz to 80 MHz. In Fig. 2.1, the "INPUT" is connected to a RF multiplexer to allow for a fast switching among HOM couplers as shown in Fig. 2.2. The 70 MHz IF out of the analog box is further split into two signals. One is digitized by a VME digitizer operating at 216 MS/s with 14 bit resolution[1] and 2 Volt peak to peak

[1]The output value from the VME digitizer has 16 bit with the last two digits both set to 0. It was for easy data processing

signal range along with a programmable FPGA for signal processing. The digitizer is triggered by a 10 Hz beam trigger, which is the RF-pulse repetition rate of FLASH. Both the selectable LO and the digitizer clock of 216 MHz are locked to the FLASH accelerator by using RF signals delivered from the FLASH master oscillator as a reference. This locking allows correct phase information of the digitized signal. The other IF signal is processed by a μTCA [26] digitizer with 16 bit resolution and 2 Volt peak to peak signal range operating at 108 MS/s. Since the IF is approximately 70 MHz, the μTCA ADC is undersampled. Both the trigger and the clock of the μTCA digitizer are directly delivered from the FLASH master oscillator, which is automatically locked to the FLASH accelerator. All the devices are set up in the FLASH injector barrack outside the accelerator tunnel. The detailed circuit drawing of the analog electronics is shown in Appendix A along with photos of the device setup, the analog box and the digitizers. Digitized data is collected from the VME digitizer with an EPICS [27] software tool, while FLASH control system DOOCS [28] takes care of the data collection for the μTCA digitizer. The beam charge, steerer current and BPM readouts are recorded synchronously from DOOCS. The data processing for position diagnostics is conducted offline using MATLAB [29].

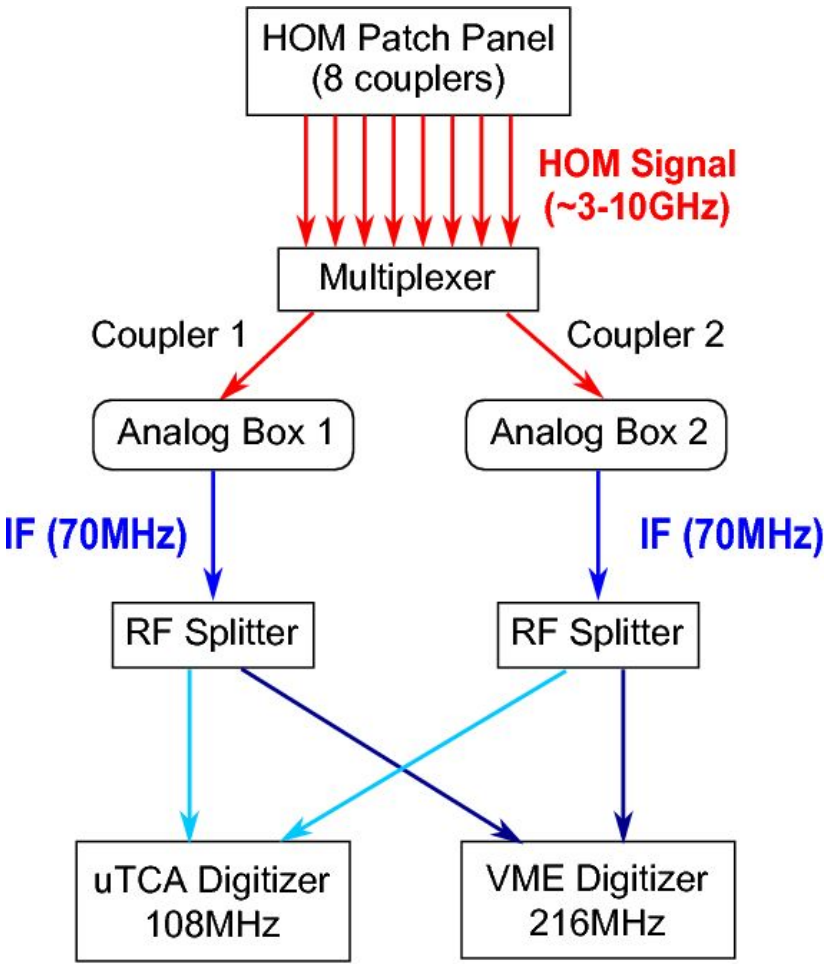

Figure 2.2: Schematic device setup in the injector barrack outside the FLASH tunnel.

Inside the analog box, individual attenuation and amplification was used for different frequency band. This is for the optimization of the signal level while accommodating the variation of HOM power amongst couplers. These are shown in Appendix B.

2.2 Downconverted HOM Signals

The downconverted HOM signals after splitting are processed by both the VME and μTCA digitizer. Fig. 2.3 shows the raw waveform of each HOM coupler for the 9066 MHz (BW: 20 MHz) digitized by VME. This

with the FPGA. The real resolution is still 14 bit.

frequency range is within the fifth dipole band. The strength of the signal varies dramatically among couplers. This might be due to the different coupling of the HOM couplers, which can also be contributed by the fact that modes within the 20 MHz band are trapped inside each cavity. Therefore dissimilar cavities attributed to fabrication tolerances give rise to the differences presented in the waveforms. Applying a fast Fourier transform (fft) on the waveforms in Fig. 2.3, the amplitude of each fft output is shown in Fig. 2.4. The spectra differ among cavities and HOM couplers.

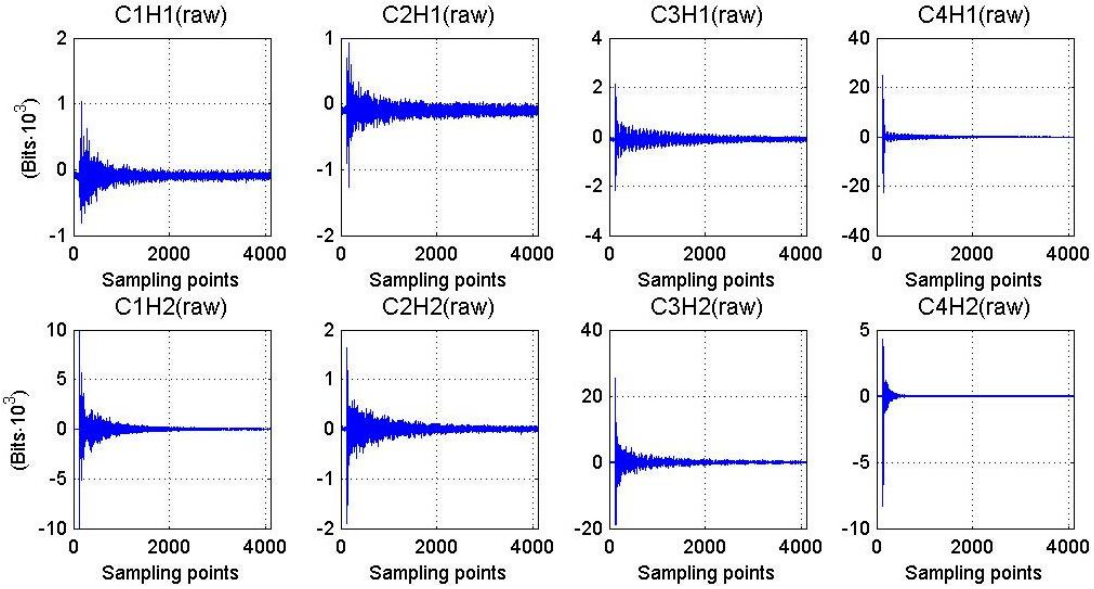

Figure 2.3: Raw waveforms measured by the VME digitizer for each HOM coupler. The center frequency is 9066 MHz with a 20 MHz BPF. Different vertical scale is used for each waveform.

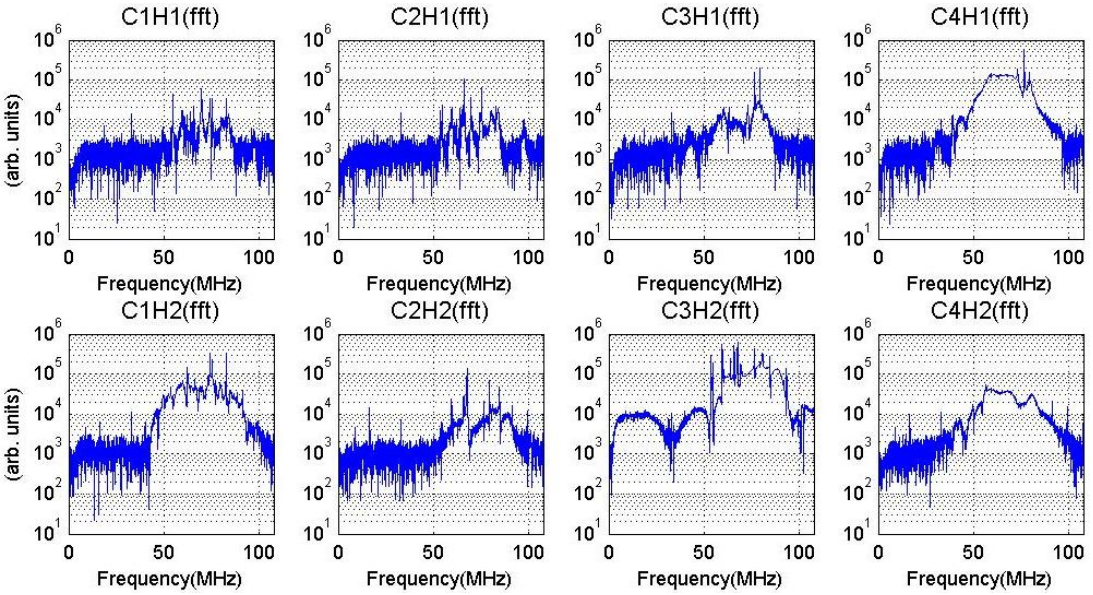

Figure 2.4: FFT amplitude of the raw waveform measured by the VME digitizer for each HOM coupler. The center frequency is 9066 MHz with a 20 MHz BPF.

Fig. 2.5 shows the waveforms for the 5437 MHz (BW: 20 MHz) digitized by VME. This frequency range is within the second dipole band. The signal strength is similar for each coupler. Since modes in this band propagate through the module, couplers pick up similar signals. The differences come from the couplers' dissimilar coupling and their locations. Fig. 2.6 shows the fft amplitudes of the waveforms.

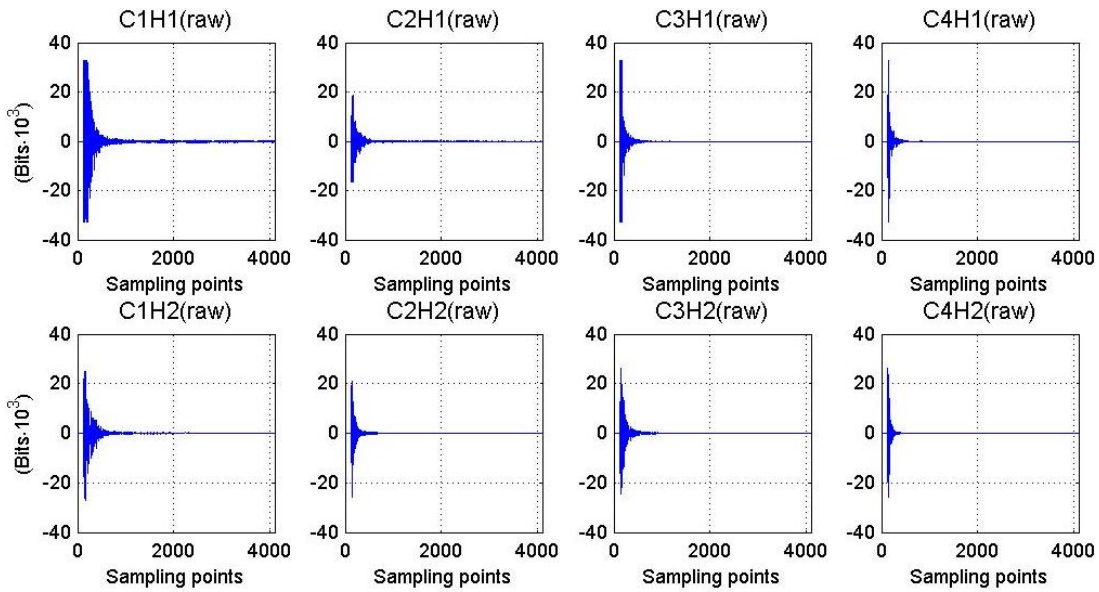

Figure 2.5: Raw waveforms measured by the VME digitizer for each HOM coupler. The center frequency is 5437 MHz with a 20 MHz BPF.

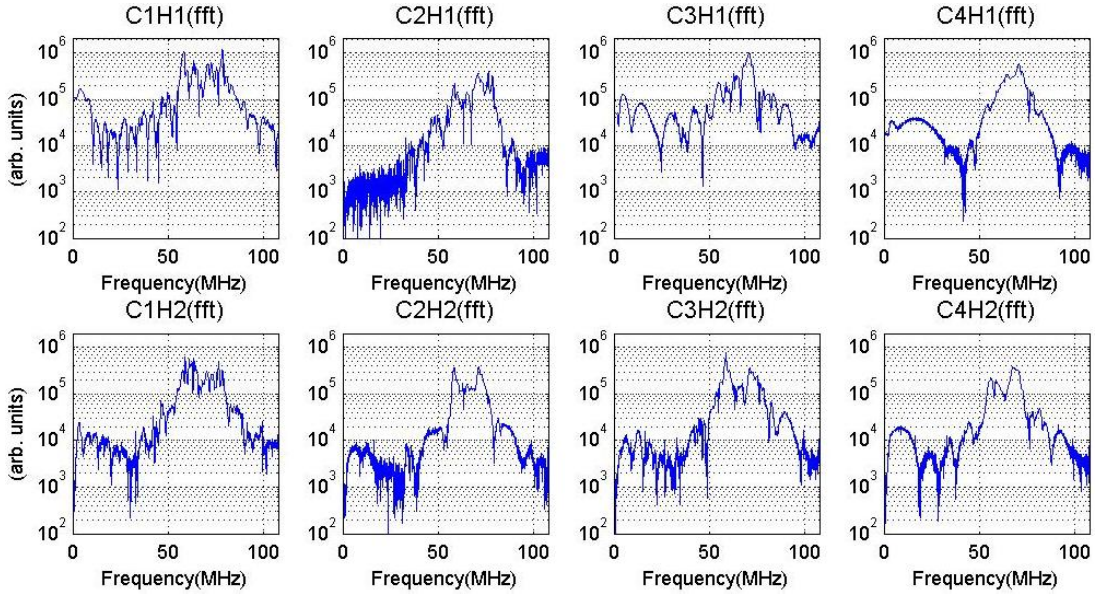

Figure 2.6: FFT amplitude of the raw waveform measured by the VME digitizer for each HOM coupler. The center frequency is 5437 MHz with a 20 MHz BPF.

2.3 Measurement Scheme

The schematics of the measurement setup is shown in Fig. 2.7. An electron bunch of approximately 0.5 nC is accelerated on-crest through ACC1 before entering the ACC39 module. Two steering magnets located upstream of ACC1 are used to produce horizontal and vertical offsets of the electron bunch in ACC39. Two beam position monitors (BPM-A and BPM-B) are used to record transverse beam positions before and after ACC39. Switching off the accelerating field in ACC39 and all quadrupoles close to ACC39, a straight line trajectory of the electron bunch is produced between those two BPMs. Therefore, the transverse offset of the electron bunch in the module can be determined by interpolating the readouts of the two BPMs.

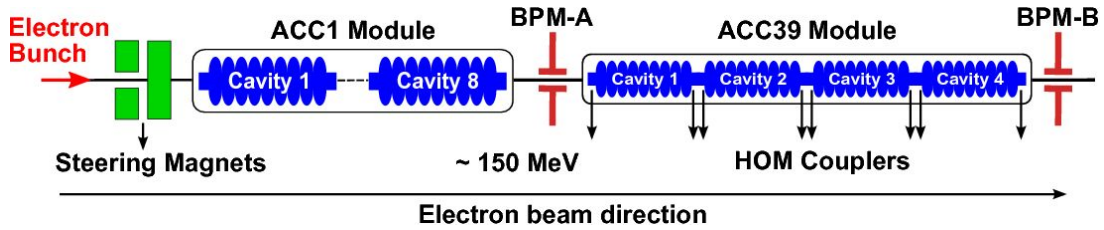

Figure 2.7: Schematic of measurement setup for HOM study (not to scale, cavities in ACC1 are approximately three times larger than those in ACC39).

To study the position dependencies of HOMs, we moved the beam in a 2D grid manner. Fig. 2.8(a) shows the steerer current during the movement. The samples in blue are used for calibration, and then validation[2] samples were taken as shown in red. The usage of the samples are explained in Chapter 3. Fig. 2.8(b) and Fig. 2.8(c) show the relations of the steerer current to the readings of BPM-A (dots) and BPM-B (asterisks). Fig. 2.8(d) and Fig. 2.8(g) show the readings of BPM-A and BPM-B during the beam movement. The angle of the beam trajectory is represented by x' and y', and its relations to the bpm readings are shown in Fig. 2.8(e)(f)(h)(i). When the readings of BPM-A were close to zero for both x and y plane, the readouts jumped between positive and negative unpredictably. In order to cure this, we use the currents of steering magnets to correct the problematic BPM readings. From the measurement results, the jumping in x plane is not severe, therefore only the readings of y have been corrected for all measurements shown in this report.

[2] A set of coefficients is first generated during calibration. Then the newly measured HOM signals are applied with these coefficients to make predictions of beam positions. This is called validation.

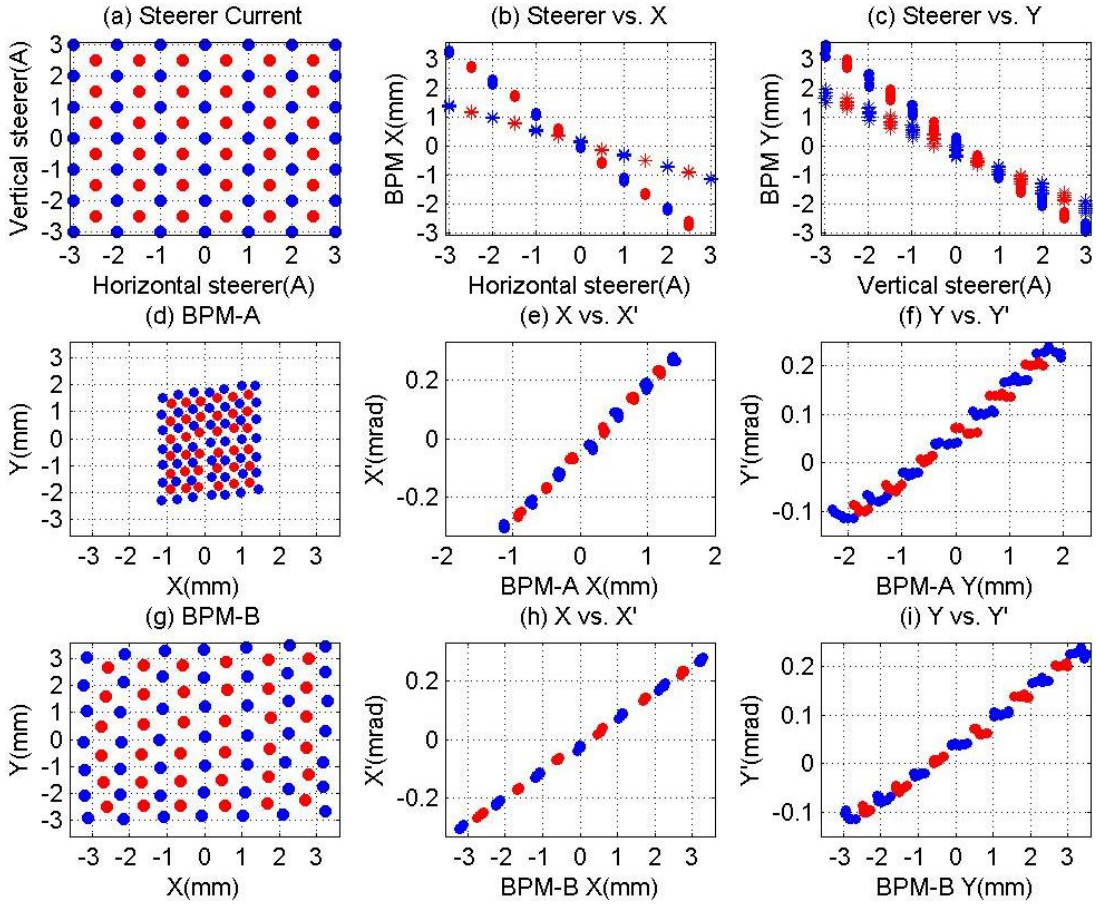

Figure 2.8: 2D grid-like beam movement. The calibration samples are in blue while the validation samples are in red. In (b) and (c), dots represent the readings from BPM-A while asterisks for BPM-B.

As we are dealing with trapped and coupled modes, two schemes of position interpolations are used. The transverse beam position is interpolated into each cavity center for trapped modes as shown in Fig. 2.9. Fig. 2.10(a) shows the interpolated position of each cavity center. This enables the local positions in each cavity to be determined by the non-propagating modes extracted from each cavity. Since the coupled modes are propagating through the four-cavity module, we decide to interpolate the beam position into the center of the whole module considering the four cavities in its entirety. The interpolation is shown in Fig. 2.11 and the interpolated position of the module center is shown in Fig. 2.10(b). One notices some non-straight lines in Fig. 2.10(a) on the bottom right, and it might be due to the beam jitter as only one cavity was measured at each time.

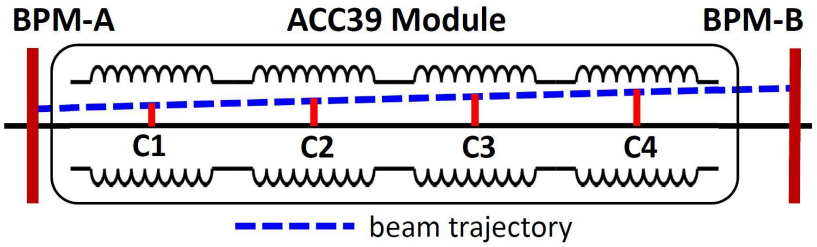

Figure 2.9: Position interpolation into the center of each cavity for localized modes.

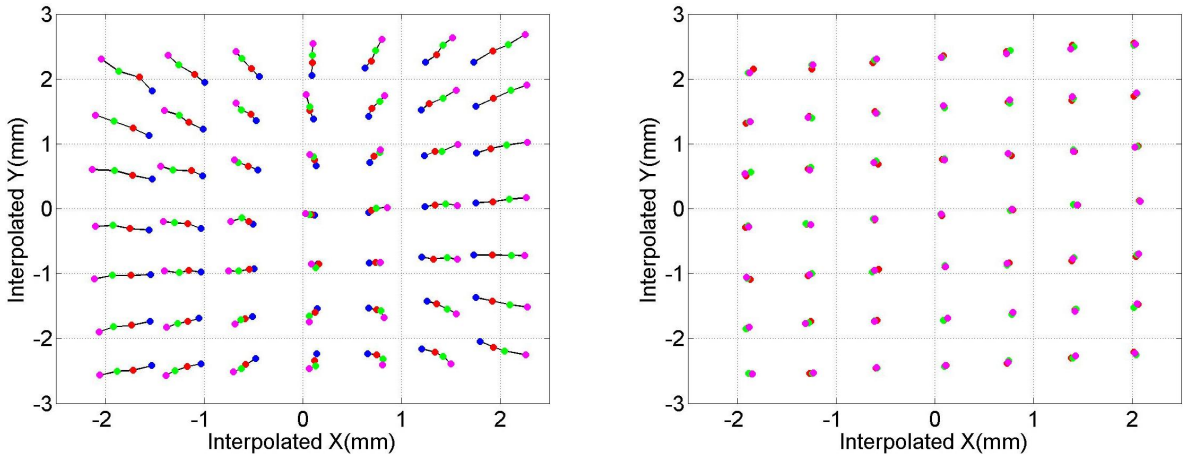

(a) Interpolation into each cavity

(b) Interpolation into module center

Figure 2.10: (a) Interpolated position at each cavity center colored as C1 (blue), C2 (red), C3 (green) and C4 (magenta). Points connected with black lines belong to the same beam position. (b) Interpolated position at the module center when measuring C1 (blue), C2 (red), C3 (green) and C4 (magenta). Only the calibration samples are shown.

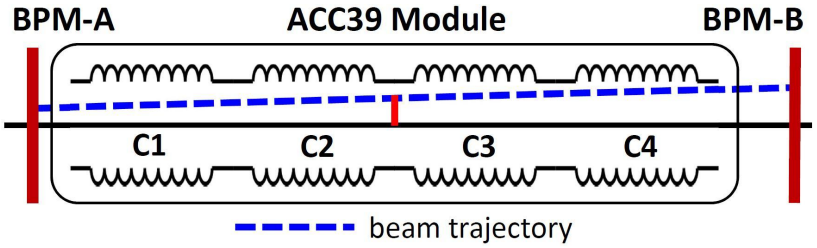

Figure 2.11: Position interpolation into the center of the whole module for coupled modes.

In this report, three modal options have been studied. The center frequencies and the BWs for these options that we have set on the test electronics during the measurement are listed in Table 2.1. For the first and second dipole band, we also studied the diagnostics with a broadband signal by removing the 20 MHz BPF after the mixer. In this case, the BW of the IF signal was 100 MHz determined by the BPF in front of the mixer and the LPF.

Table 2.1: Modal options studied with the test electronics.

Beam-pipe modes		1^{st} dipole band		2^{nd} dipole band		5^{th} dipole band	
Center	BW	Center	BW	Center	BW	Center	BW
4082 MHz	20 MHz	4859 MHz	20 MHz	5437 MHz	20 MHz	9048 MHz	20 MHz
4118 MHz	20 MHz	4904 MHz	20 MHz	5464 MHz	20 MHz	9066 MHz	20 MHz
		4940 MHz	20 MHz	5482 MHz	20 MHz		
		4900 MHz	100 MHz	5450 MHz	100 MHz		

Chapter 3

Analysis Methods for Beam Position Diagnostics

Two different analysis methods are used to extract beam position information from the HOM signals: direct linear regression and singular value decomposition. These are explained and compared in this chapter.

3.1 Data Samples

In this chapter, waveforms measured from HOM coupler C3H2 with the VME digitizer are used to describe two data analysis techniques. The center frequency has been set to 9066 MHz with a 20 MHz BW. One example of the downconverted waveforms is shown in Fig. 3.1(a). The downconverted waveforms are applied with a mathematical ideal filter to keep the range from 56 MHz to 101 MHz in order to cut away the coupling modes at approximately 55 MHz. Fig. 3.1(b) shows one example of the spectrum after a fft was applied on the waveform shown in Fig. 3.1(a). The filtered waveform is shown in Fig. 3.1(c) in blue as one example. Since the signal decays fast, a time window is further applied on the filtered signal which is shown as the red waveform in Fig. 3.1(c). All waveforms have been normalized to 1 nC bunch charge, and one of the them is shown in Fig. 3.2(a). The beam has been moved in a grid manner. As shown in Fig. 3.2(b), a 7×7 grid is used for calibration (49 samples, blue dots) and a 6×6 grid is used as validation samples (36 samples, red dots) in order to obtain full coverage in 2D space for both samples within the linear range of BPM-B (-3 mm to +3 mm).

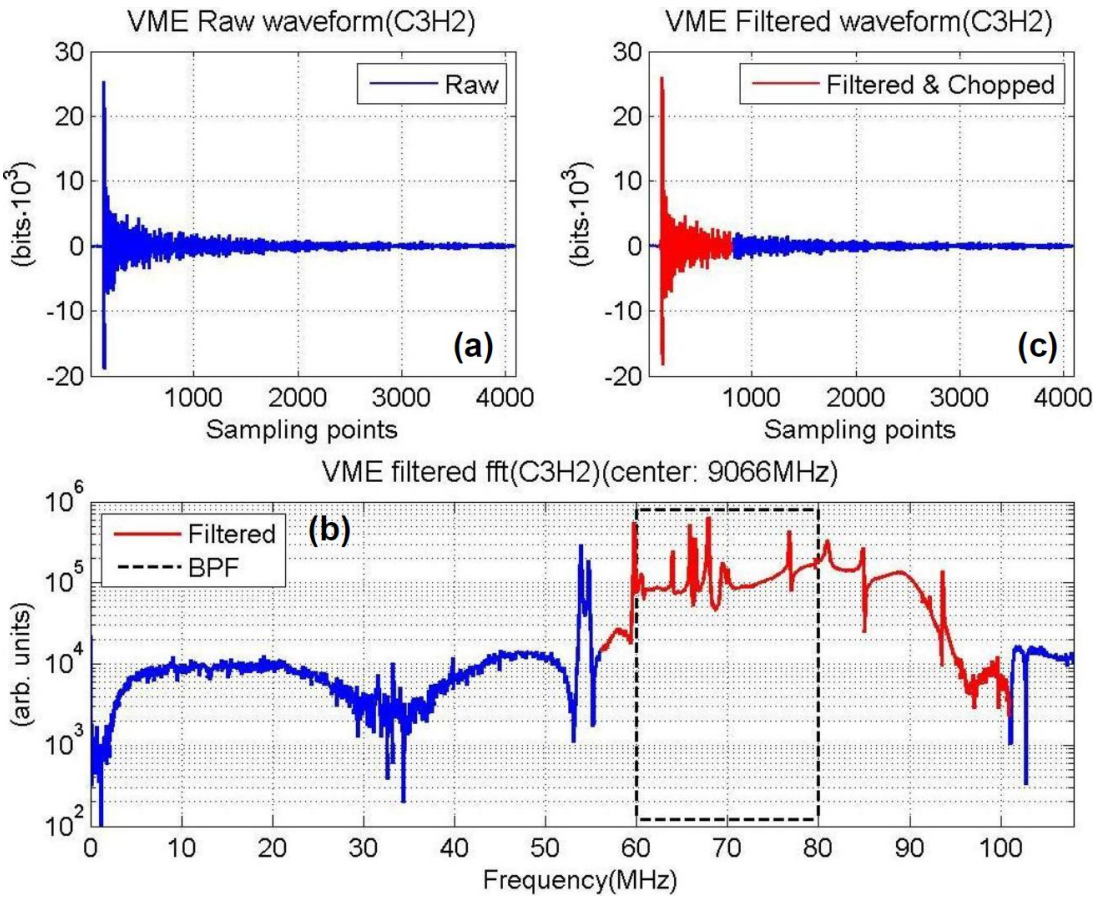

Figure 3.1: Waveform measured with VME-based digitizer (center frequency: 9066 MHz, BW: 20 MHz).

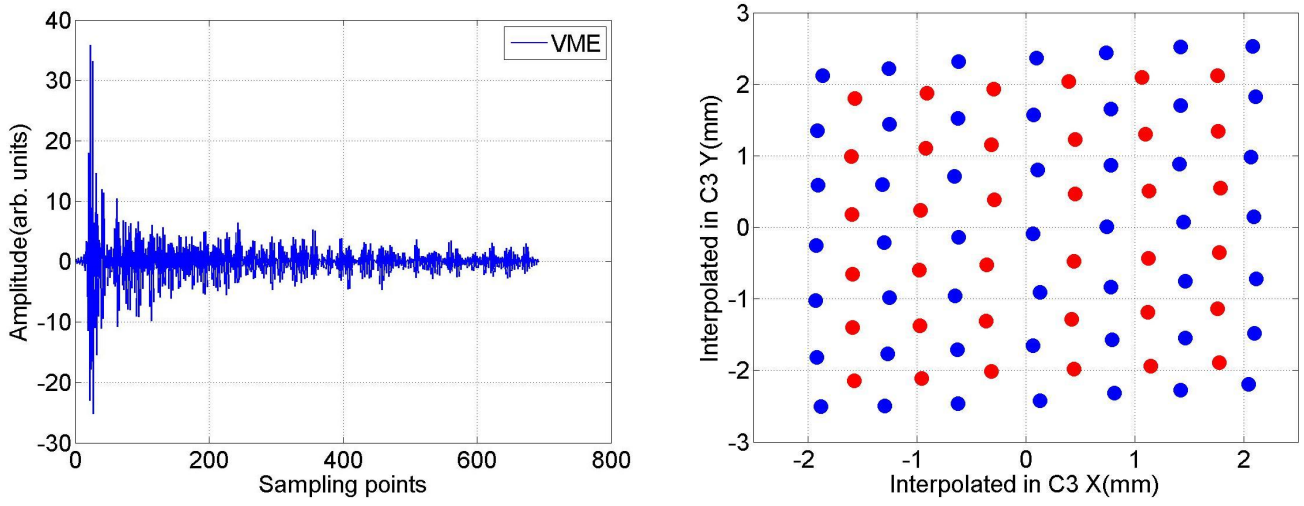

(a) One waveform

(b) Beam positions

Figure 3.2: (a) One waveform measured from C3H2. (b) Grid-like beam movement (calibration samples are in blue and validation samples are in red). The positions are interpolated in C3.

3.2 Direct Linear Regression

To extract beam position information from the dipole modes, a straightforward method is direct linear regression (DLR),

$$A \cdot M = B. \tag{3.1}$$

In this equation, matrix A contains the waveforms, B is the matrix of transverse beam position x and y interpolated from the two BPM readouts. The angle of the beam trajectory x' and y' is not the subject of this study. M is the matrix of regression coefficients. The arrangement of matrix A and B are

$$A = \begin{pmatrix} waveform_1 \\ waveform_2 \\ \vdots \\ waveform_m \end{pmatrix} = \begin{pmatrix} a_{11} & a_{12} & \dots & a_{1n} \\ a_{21} & a_{22} & \dots & a_{2n} \\ \vdots & \vdots & \ddots & \vdots \\ a_{m1} & a_{m2} & \dots & a_{mn} \end{pmatrix} = \begin{pmatrix} r_1^T \\ r_2^T \\ \vdots \\ r_m^T \end{pmatrix} = \begin{pmatrix} c_1^T \\ c_2^T \\ \vdots \\ c_n^T \end{pmatrix}^T \in \mathbb{R}^{m \times n}, \tag{3.2}$$

$$B = \begin{pmatrix} B_1 \\ B_2 \\ \vdots \\ B_m \end{pmatrix} = \begin{pmatrix} x_1 & y_1 \\ x_2 & y_2 \\ \vdots & \vdots \\ x_m & y_m \end{pmatrix} \in \mathbb{R}^{m \times 2}. \tag{3.3}$$

A is a $m \times n$ matrix. a_{ij} represents the value of j^{th} sampling point in $waveform_i$. The superscript T denotes the vector or matrix transpose. $r_i^T \in \mathbb{R}^n$ is the i^{th} row of A, which is the $waveform_i$ for a particular beam position. $c_i \in \mathbb{R}^m$ is the i^{th} column of A, representing the i^{th} regressor or variable. $B_i \in \mathbb{R}^2$ is the i^{th} row of matrix $B \in \mathbb{R}^{m \times 2}$. It represents the interpolated horizontal coordinate x_i and vertical coordinate y_i of the i^{th} beam position corresponding to the measurement of $waveform_i$. In order to characterizes the DC components in the waveforms, a intercept term is added into A and M by adding one column of 1 in A and one row of coefficients in M as

$$A^* = (I, A) \in \mathbb{R}^{m \times (n+1)}, \tag{3.4}$$

$$M^* = \begin{pmatrix} M_0 \\ M \end{pmatrix} \in \mathbb{R}^{(n+1) \times 2}, \tag{3.5}$$

where $I \in \mathbb{R}^{m \times 1}$ and $M_0 \in \mathbb{R}^{1 \times 2}$. Matrix M is obtained by solving linear system composed by A^* and B for calibration samples.

The predictions of B can be obtained by

$$B_{pre} = A^* \cdot M^* \tag{3.6}$$

for both calibration and validation samples. Applying DLR on the waveforms measured from HOM coupler C3H2 split as Fig. 3.2(b), we obtain the results for both samples. In Fig. 3.3(a), the prediction and the measurement almost overlap, which proves the linear dependence of the waveform on the transverse beam offset. Fig. 3.3(b) shows that the M obtained from calibration has good prediction power. To measure the consistency, the coefficient of determination r^2 is calculated ($r^2 = 1$, perfect fit; $r^2 = 0$, poor fit) [30]. The difference between the predicted position B_{pre} and the measured position B is defined as the *prediction error*,

$$prediction\ error = |B_{pre} - B|. \tag{3.7}$$

Fig. 3.4 shows the prediction error for calibration and validation samples by using DLR, together with the rms value of the prediction error, E_{RMS}. Then the position resolution is given by E_{RMS} of the validation samples. Therefore, the resolution achieved by DLR is 47 μm for x and 56 μm for y.

The algorithm used in solving the linear system (in the form of Eq. 3.1) is least squares, which is a standard method to solve linear regression problems. The method relies on minimizing the difference of prediction (B_{pre}) and measurement (B) whilst modifying the elements of the matrix M^*. In our case, the size of matrix M^* is related to the number of sampling points, therefore a considerable number of unknown variables (in this particular case, 701) needs to be determined. This is computationally expensive. As

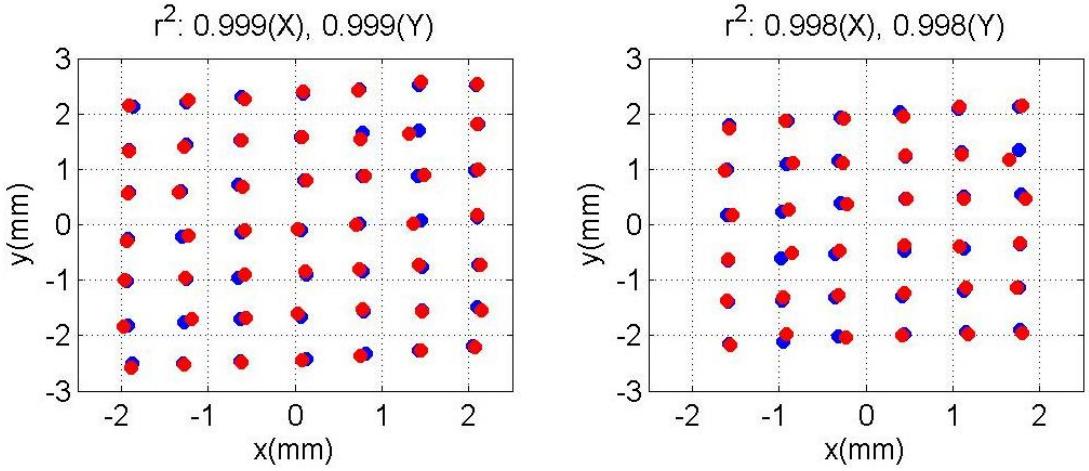

Figure 3.3: Measurement (blue) and prediction (red) of the transverse beam position from calibration (left) and validation (right) samples. The applied method is DLR.

all sampling points are used in the regression, each column of matrix A is a regressor. The correlation coefficients $R \in \mathbb{R}^{n \times n}$ of these regressors are calculated as

$$R(i,j) = \frac{\mathrm{Cov}(c_i, c_j)}{\sqrt{\mathrm{Cov}(c_i, c_i) \cdot \mathrm{Cov}(c_j, c_j)}}, \tag{3.8}$$

where c_i and c_j are i^{th} and j^{th} column of matrix A respectively defined in Eq. 3.2, $\mathrm{Cov}(c_i, c_j)$ is the covariance between two regressors c_i and c_j. In this definition, $R = \pm 1$ means strong correlation while R=0 means no correlation. Fig. 3.5 shows the correlation coefficients of the calibration samples. Most regressors are strongly correlated and this makes the linear system sensitive to the fluctuations of the calibration samples. In our case, the system is vulnerable to noise. Moreover, even though it is not the case here, overfitting is always a potential problem unless the calibration samples are fairly large. To avoid these risks, it is better to reduce the system size from multi-hundred to several tens, and then apply linear regression on the reduced system. The method we used for this purpose is described in the following section.

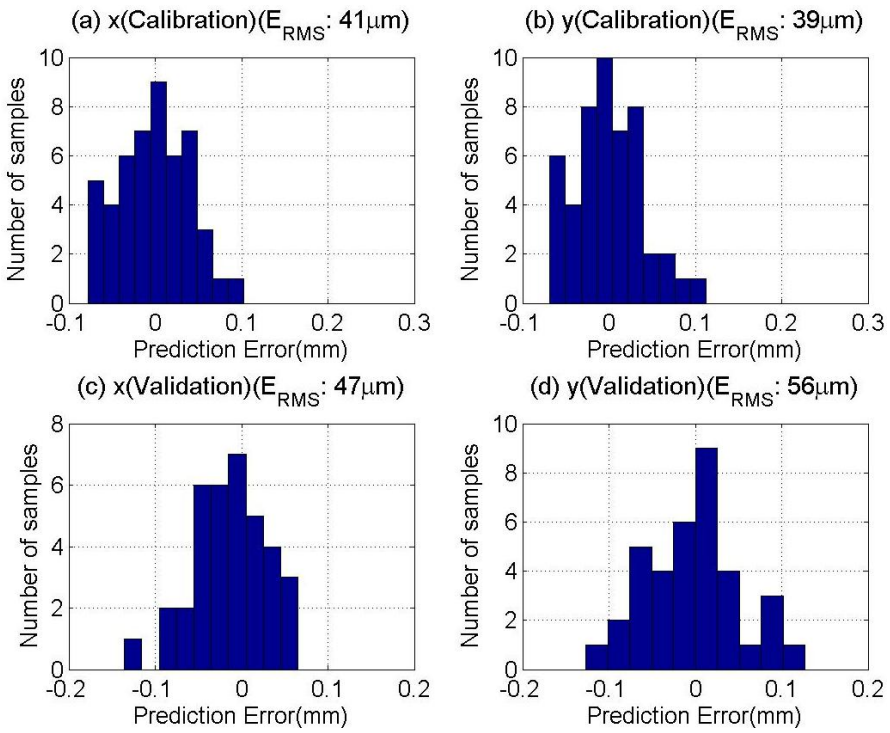

Figure 3.4: Difference of measured and predicted transverse beam position from calibration and validation samples. The applied method is DLR.

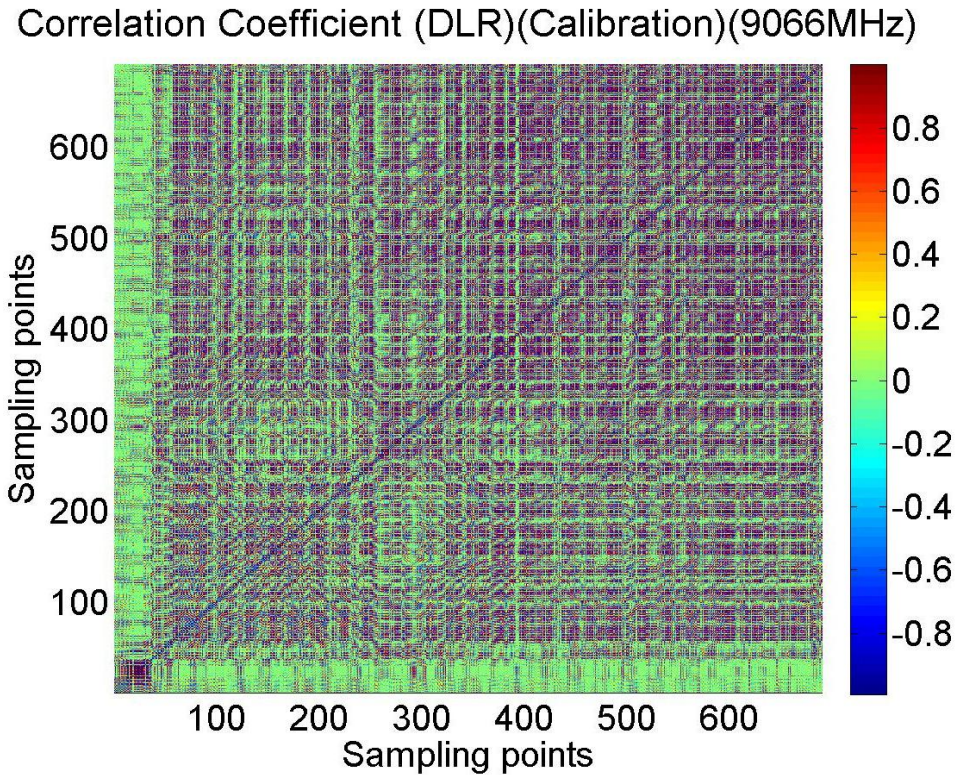

Figure 3.5: Correlation coefficients of the calibration samples.

3.3 Singular Value Decomposition

In order to find a small number of prominent components from the signal matrix A, a method known as *Singular Value Decomposition* (SVD) is used [31]. In general, SVD looks for patterns of a matrix in terms of SVD modes without relating them to any physical parameters (like dipole mode frequency, quality factor, beam position, etc.). Those SVD modes are natural groupings of the signal matrix, which are not clearly visible or explicitly defined in the matrix itself.

Applying SVD, the matrix A is decomposed into the product of three matrices,

$$A = U \cdot S \cdot V^T, \tag{3.9}$$

where $U \in \mathbb{R}^{m \times m}$ and $V \in \mathbb{R}^{n \times m}$. The columns of U and V^T are singular vectors of A, which form the bases of the decomposition[1]. S is a diagonal matrix whose non-zero elements are singular values. Applying SVD on the calibration samples (blue dots in Fig. 3.2(b)), the singular value of each SVD mode is obtained and shown in Fig. 3.6(a). It can be seen that the first few SVD modes have relatively large singular values, in other words, they are the dominant patterns of matrix A. The correlation coefficients of all SVD modes decomposed from the calibration samples are calculated as shown in Fig. 3.6(b). The first SVD mode has relatively strong correlations with the third and the fourth SVD mode. This is because the mean of the 49 calibration waveforms is not zero as shown in Fig. 3.7(a).

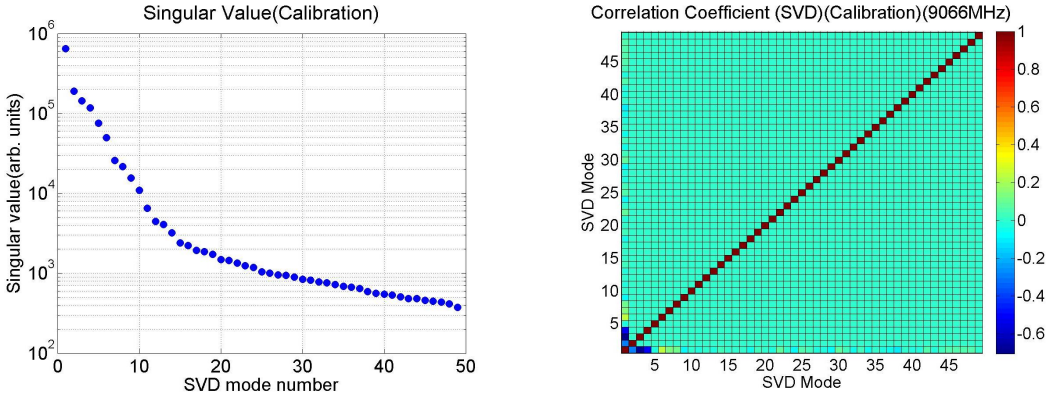

(a) (b)

Figure 3.6: (a) Singular values of SVD modes; (b) Correlation coefficients of SVD modes decomposed from the calibration samples.

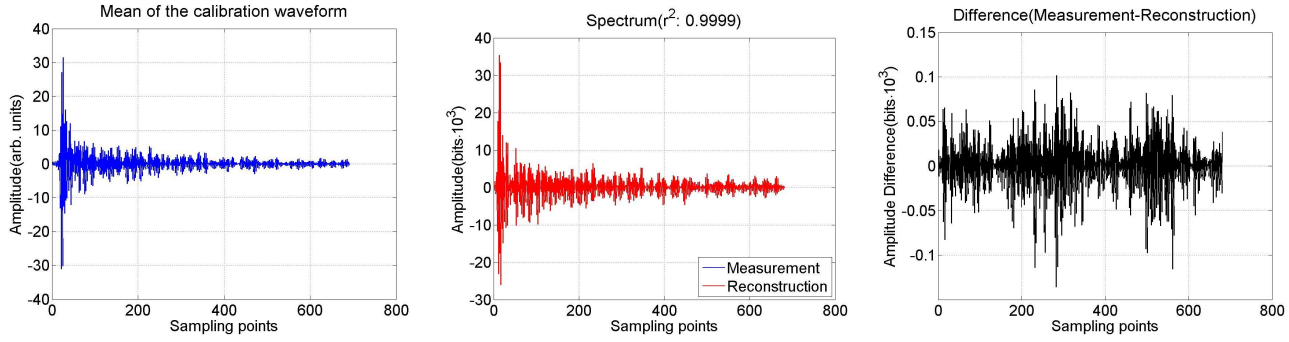

(a) (b) (c)

Figure 3.7: (a) Mean of the calibration waveforms; (b) Reconstructed waveform (red) from the first twelve SVD modes compared with original waveform (blue). (c) Difference of the original and reconstructed waveform.

[1] In general case, $U \in \mathbb{R}^{m \times m}$, $S \in \mathbb{R}^{m \times n}$ and $V \in \mathbb{R}^{n \times n}$. However, in the case of $m < n$, only the first m SVD modes have non-zero singular values.

Each of the SVD modes can be used to produce a spectra matrix by

$$A_i = U_i \cdot S_{ii} \cdot V_i^T, \tag{3.10}$$

where U_i is the i^{th} column of U, and V_i^T is the i^{th} row of V^T. S_{ii} denotes the i^{th} diagonal element of S. A_i has the same size as the original spectra matrix A. Fig. 3.8 shows one spectrum for each of the first twelve A_i's. The approximation A_{reco} can be calculate by simply summing over the related A_i by

$$A_{reco} = \sum_{i=1}^{p} A_i. \tag{3.11}$$

By combining the first twelve SVD modes ($p = 12$), A_{reco} is plotted together with the original spectra matrix A in Fig. 3.7(b) and the difference of A and A_{reco} is shown in Fig. 3.7(c). The spectrum can be well represented by using only the first twelve SVD modes.

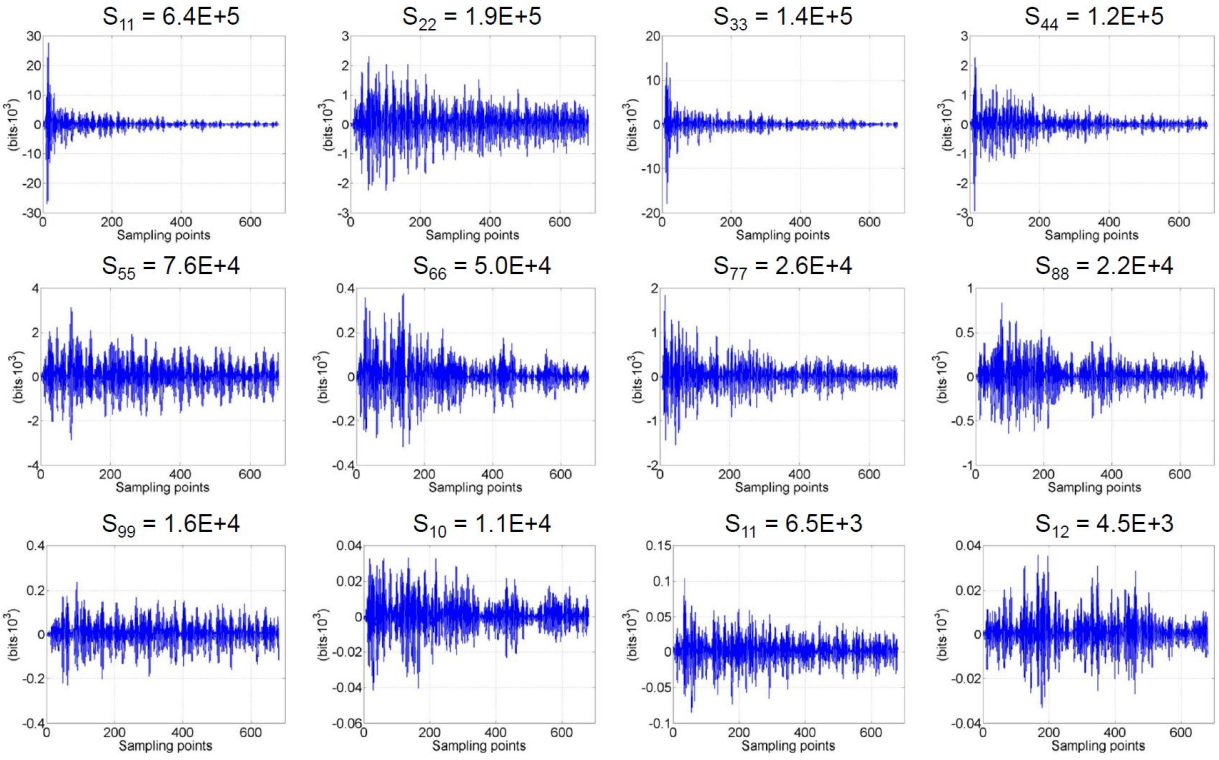

Figure 3.8: Spectra reconstructed from each of the first twelve SVD modes.

Having the SVD base vectors from the decompositions of spectra matrix A, the amplitude of all SVD modes, $A_{svd,full}$, can be obtained for each beam movement by

$$A_{svd,full} = A \cdot V \tag{3.12}$$

The first twelve columns of the matrix $A_{svd,full}$ constitute the matrix A_{svd} along with one column of 1 representing the intercept term. The size of the matrix A_{svd} is significantly smaller (13 columns, representing 12 SVD modes and one intercept term) compared to the original matrix A (701 columns, representing 700 sampling points and one intercept term). Replacing A by A_{svd} in the regression (Eq. 3.1), the linear system composed by A_{svd} and B is now over-determined, which has a well-known best solution in least-square sense. The position prediction B_{pre} can then be obtained using Eq. 3.6 by replacing A with A_{svd} for calibration samples. The prediction for the validation samples has two steps: first, project A onto the base vectors obtained from calibration samples to get the amplitude of the first twelve SVD modes using Eq. 3.12; second, substitute the SVD amplitude matrix in Eq. 3.6 to get the position prediction.

The contribution of combining the first p SVD modes to determine the transverse beam position x and y is measured by rms prediction error as shown in Fig. 3.9. Using the first twelve SVD modes is seen to

give an optimal performance for the x plane. It is also a reasonable choice for the y plane (Fig. 3.9(b)) even though less SVD modes would be sufficient. This confirms, with Fig. 3.6(a) and Fig. 3.7(b), that the first few modes contain most of the information. By combining the first twelve SVD modes, one can get the majority of beam position information.

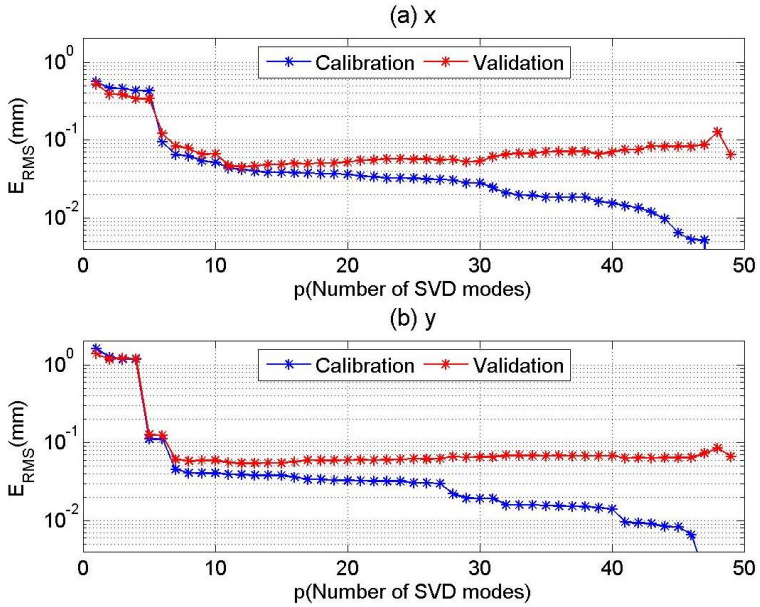

Figure 3.9: Contribution of the first p SVD modes to determine the transverse beam position x and y measured by the E_{RMS}.

Fig. 3.10 shows the HOM response from calibration and validation samples by using the first twelve SVD modes to determine the transverse beam position x and y. The prediction errors remain small and comparable for calibration and validation samples as shown in Fig. 3.11. The position resolution is 45 μm for x and 55 μm for y.

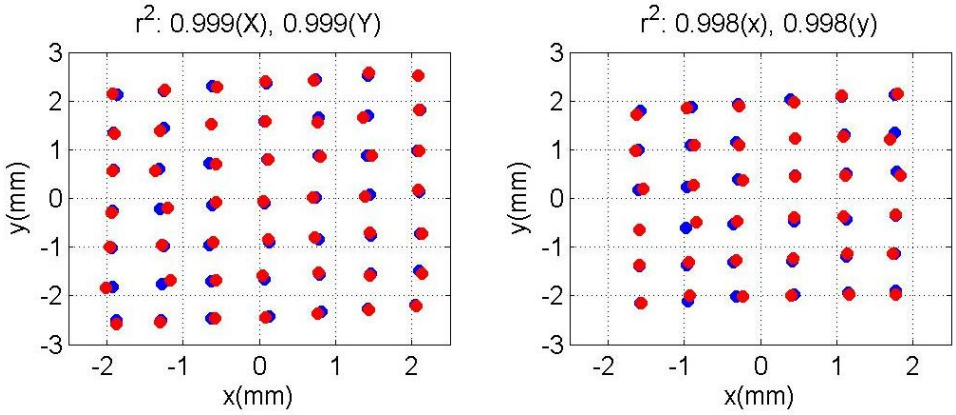

Figure 3.10: Measurement (blue) and prediction (red) of the transverse beam position from calibration (left) and validation (right) samples. The applied method is SVD with the first twelve SVD modes.

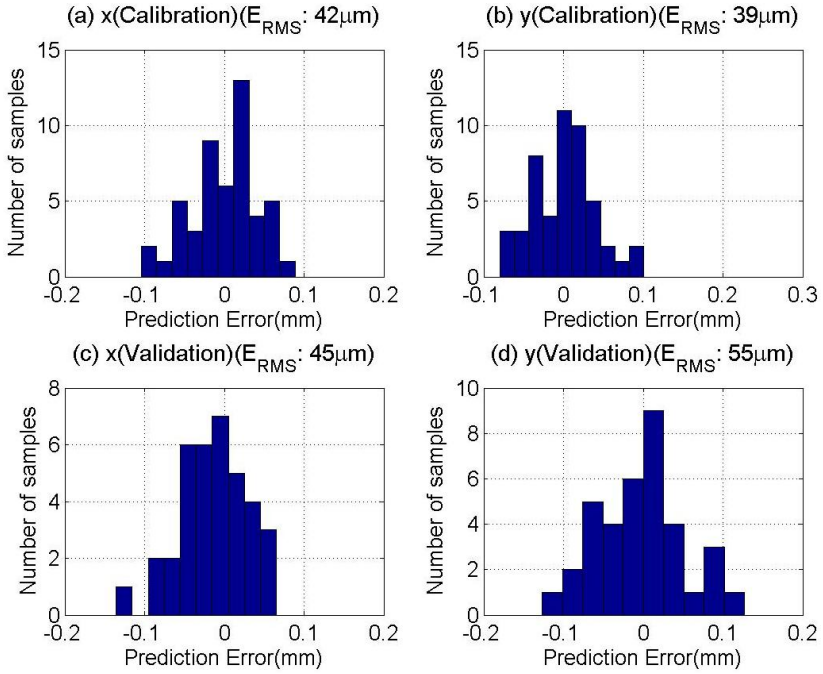

Figure 3.11: Difference of measured and predicted transverse beam position from calibration and validation samples. The applied method is SVD with the first twelve SVD modes. The position resolution is denoted as rms value on each plot.

3.4 Comparison of DLR and SVD

A direct comparison of DLR and SVD on the same samples (split as Fig. 3.2(b)) is shown in Fig. 3.12. The results obtained by the two different methods are similar. The comparisons of the rms prediction errors are listed in Table. 3.1.

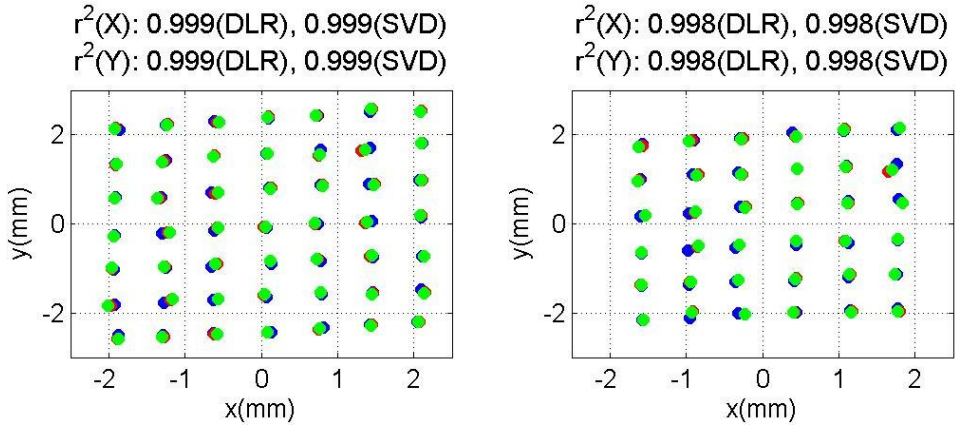

Figure 3.12: Measurement (blue) and prediction of the transverse beam position from calibration (left) and validation (right) samples. The applied method is DLR (red) and SVD with the first twelve SVD modes (green).

Until now, our analysis is based on a specific sample split (Fig. 3.2(b)). To remove sample dependence, a technique namely *cross-validation* is used [32]. As in the discussed example the total sample size is only 85 (49 calibration positions plus 36 validation positions), one can apply the *leave-one-out cross-validation* (LOOCV) [32] technique. LOOCV uses only one from the total samples for the validation and the remainings as calibrations as shown in Fig. 3.13(a) for one example. This is repeated for every sample (85 times in the considered case). Fig. 3.13(b) shows the measurement and the prediction of each validation sample. The method we used is SVD with the first 12 SVD modes. The rms prediction error is then calculated on the prediction error for the validation sample from all 85 different sample splits. The sample-independent rms

Table 3.1: Comparison of rms prediction errors of DLR and SVD corresponding to Fig. 3.4 and Fig. 3.11.

	$\boldsymbol{x}$ (μm)	$\boldsymbol{y}$ (μm)
Calib(DLR)	41	39
Calib(SVD)	42	39
Valid(DLR)	47	56
Valid(SVD)	45	55

prediction error is 50 μm for x and 52 μm for y. Fig. 3.14 shows the sample-independent rms error using the first p SVD modes. Similar to the case of sample split shown in Fig. 3.2(b), the first 12 SVD modes give an optimal prediction accuracy for x and even less SVD modes (the first 7) are needed for y. Since the calibration samples for each of the 85 splits are similar, the sample-independent rms error for the validations is a good estimation of the position resolution. The results are similar compared with the fixed sample split case shown in Table 3.1.

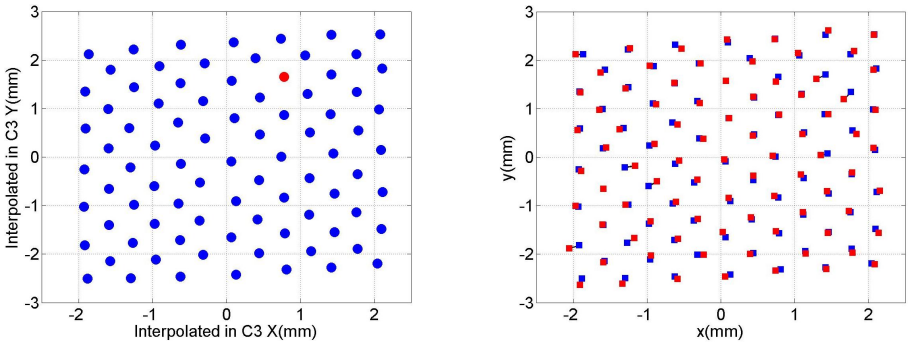

(a) One example (b) LOOCV

Figure 3.13: (a) Calibration (blue) and validation (red) samples from one of the 85 sample splits during the cross validation. (b) Measurement (blue) and prediction (red) of the transverse beam position from each of the 85 sample splits using the cross validation.

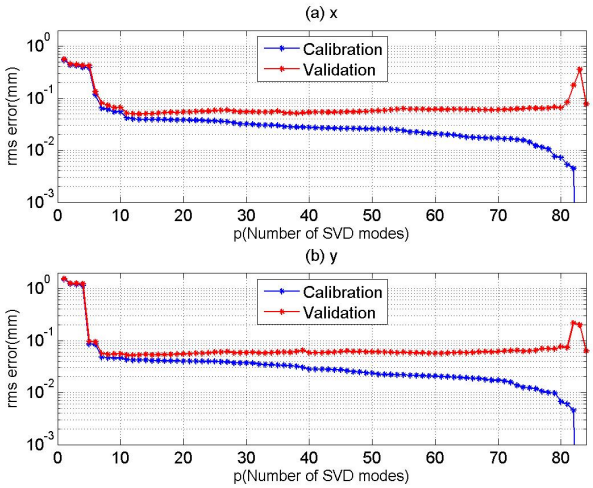

Figure 3.14: Contribution of the first p SVD modes to determine the transverse beam position x and y measured by the sample-independent rms prediction error.

Chapter 4

Position Resolutions

Resolutions for the position determination using various modes are discussed in this chapter. Only one set of modes for each modal option (Table 2.1) is described. The data obtained by the VME digitizer are used for the first two cavity dipole bands and the fifth cavity dipole band, while the μTCA digitizer is used for the beam-pipe modes. The selection is based on data availability for this set of measurements[1]. The data analysis technique used in this chapter is SVD as explained in Chapter 3. The number of SVD modes for regression is determined based on a stable and good position resolution. The results for the first (C1H2) and the last (C4H2) HOM coupler in the four-cavity string are excluded in this chapter. HOM coupler C1H2 picks up the modes transmitted from the first accelerating module, while C4H2 has weak signals. Both the time-domain waveforms and frequency-domain fft amplitudes are studied. The frequency domain is used for comparisons with previous studies using a real-time spectrum analyzer. In general, time-domain signals give better position resolution than frequency-domain fft amplitudes. This proves that the phase information is crucial for the beam position determination. A full list of resolutions for all modes studied with the test electronics can be found in Appendix C along with the number of SVD modes used for a stable and good position determination presented in Appendix D.

4.1 The Localized Beam-pipe Dipole Modes

The LO was set to downconvert 4118 MHz to 70 MHz, and a 20 MHz BPF was then applied to the down-converted signal. Fig. 4.1 shows the down-converted signal after it was processed with the μTCA digitizer, in both the time- and frequency domain (after a fft). As mentioned in the previous chapter, the mathematical ideal filter is applied to the down-converted time-domain waveform for cutting away the other modes after the down-conversion. The final filtered signal is shown as red in Fig. 4.1. Compared with the spectrum analyzer signal obtained in previous studies [20], the displayed signal filtered from 4100 MHz to 4133 MHz has proved to contain the dipole modes localized in the beam pipes. As the BPF was set to 70 MHz with a 10 MHz bandwidth on each side, the main component of the filtered signal is from 4108 MHz to 4128 MHz. The IF signal is undersampled with the 108 MS/s μTCA digitizer.

To determine the beam position, we considered both the time-domain and the frequency-domain (the fft amplitude, discard fft phase) signal. They are shown as red waveform and red spectrum in Fig. 4.1 for one example. The samples have been split in a fixed manner as shown in Fig. 2.8(a) along with a LOOCV case. The position resolution for these modes is shown in Fig. 4.2(a) for time-domain waveform and Fig. 4.2(b) for frequency-domain fft amplitude along with the number of SVD modes used in the respective regression. One may notice that the number of SVD modes is similar for coupler C2H2 and C3H2. Both of these two couplers see clearly orthogonal polarizations of these two peaks from previous studies [20, 22].

[1] The VME digitizer was unavailable when measuring the beam-pipe modes due to technical problems.

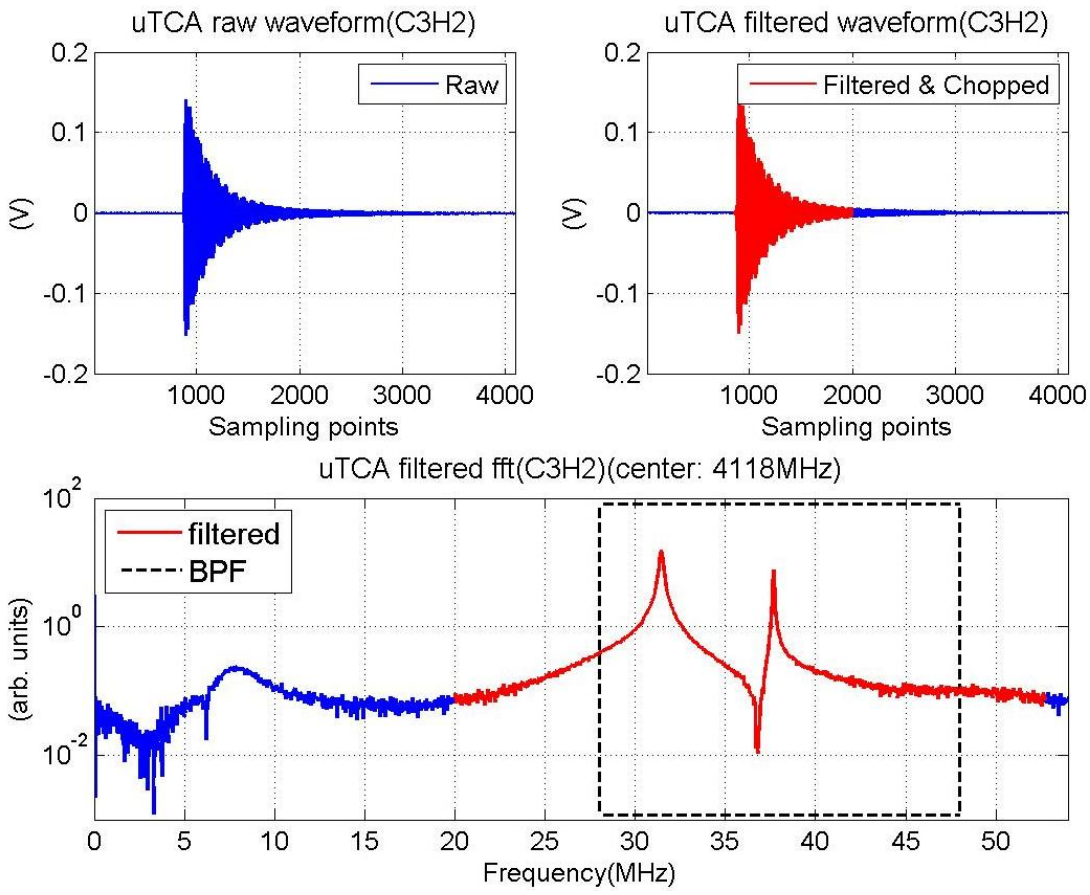

Figure 4.1: HOM signal. The center frequency is 4118 MHz with a 20 MHz BPF.

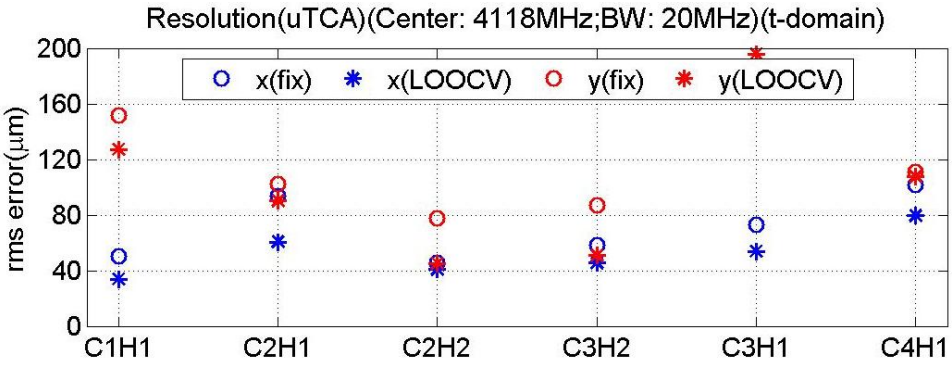

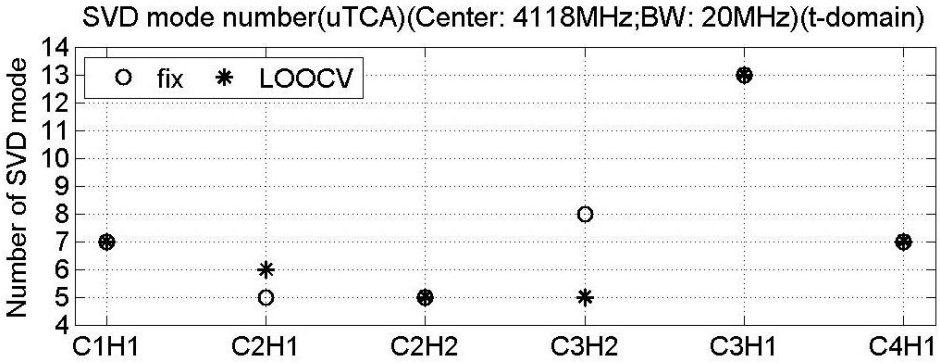

(a) time domain

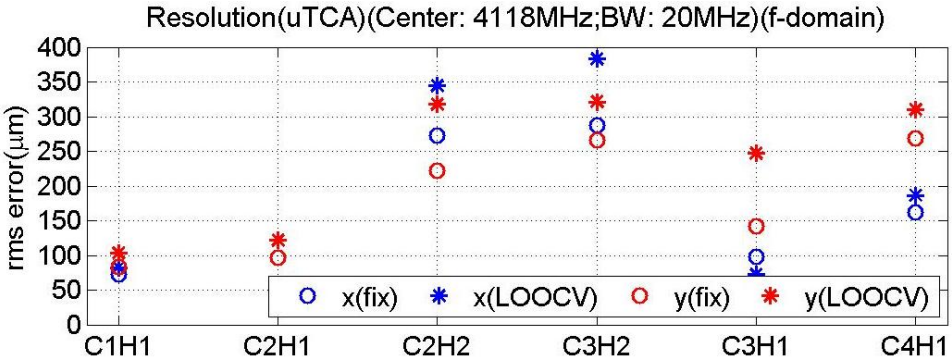

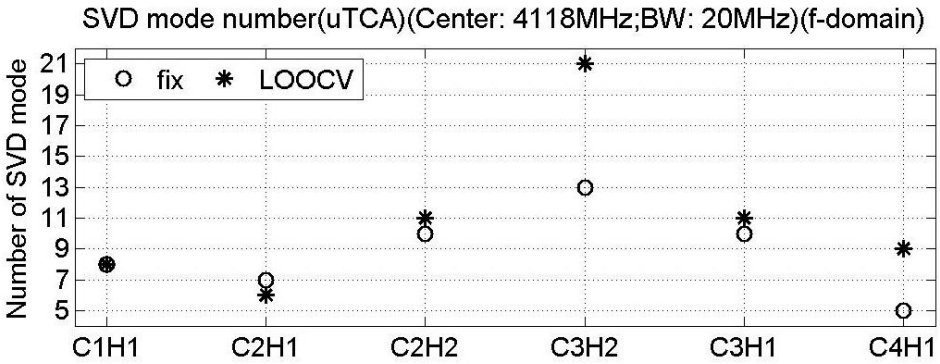

(b) frequency domain

Figure 4.2: Position resolution and SVD mode number used for position determination for both time-domain and frequency-domain. The center frequency is 4118 MHz with a 20 MHz BPF.

The integrated power over the frequency range shown in Fig. 4.1 (red spectrum) is calculated for each beam position. Fig. 4.3 shows the integrated power distribution for each HOM coupler. The position, which has minimum integrated power, is marked with white pentagon. Neither the power distribution nor the power minimum is similar among couplers. This might be a proof that modes are localized inside each beam pipe presented in the frequency region for power integration. It might also be an implication of different electrical axes for individual cavities. This difference can be attributed to asymmetric structure due to couplers and fabrication tolerance of the cavities. Fig. 4.4 decomposes the power distribution plot into horizontal and vertical moves.

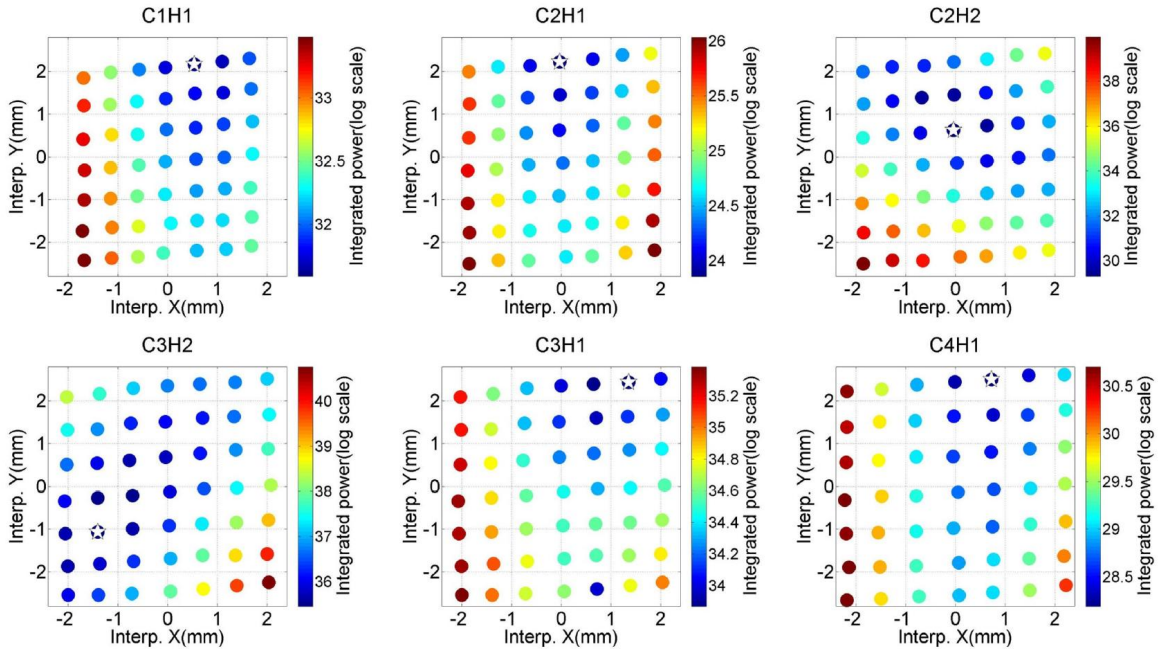

Figure 4.3: Integrated power as a function of transverse position interpolated in each cavity. The log scale magnitude of power is denoted by different color. The minimum power is marked with white pentagon. The center frequency is 4118 MHz with a 20 MHz BPF.

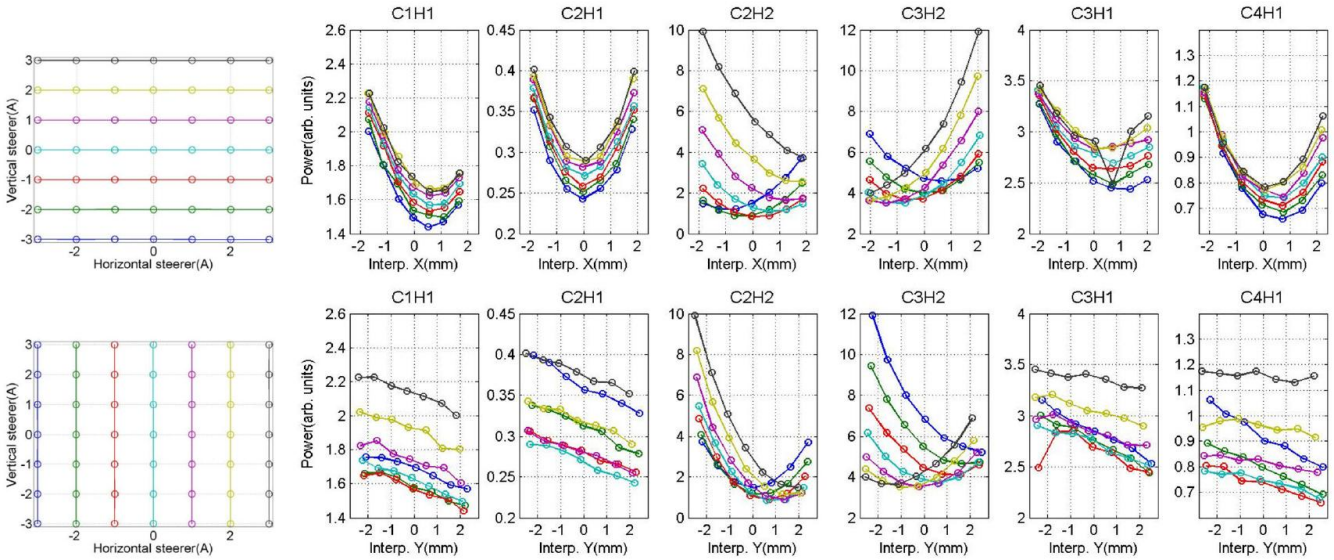

Figure 4.4: Integrated power as a function of transverse position interpolated in each cavity. The center frequency is 4118 MHz with a 20 MHz BPF.

4.2 Coupled Cavity Modes - The First Dipole Band

The LO was set to downconvert 4940 MHz to 70 MHz, and a 20 MHz BPF was then applied to the down-converted signal. Fig. 4.5 shows the down-converted signal after it was processed by the VME digitizer, in both time- and frequency domain (after a fft). Modes in this band are coupled, therefore, the mathematical ideal filter is used only to preserve good signal quality as shown in Fig. 4.5. Compared with the spectrum analyzer signal obtained in previous studies [20], the displayed signal filtered from 4903 MHz to 5009 MHz has proved to contain dipole modes propagating amongst cavities. As the BPF was set to 70 MHz with a 10 MHz bandwidth on each side, the main component of the filtered signal is from 4930 MHz to 4950 MHz.

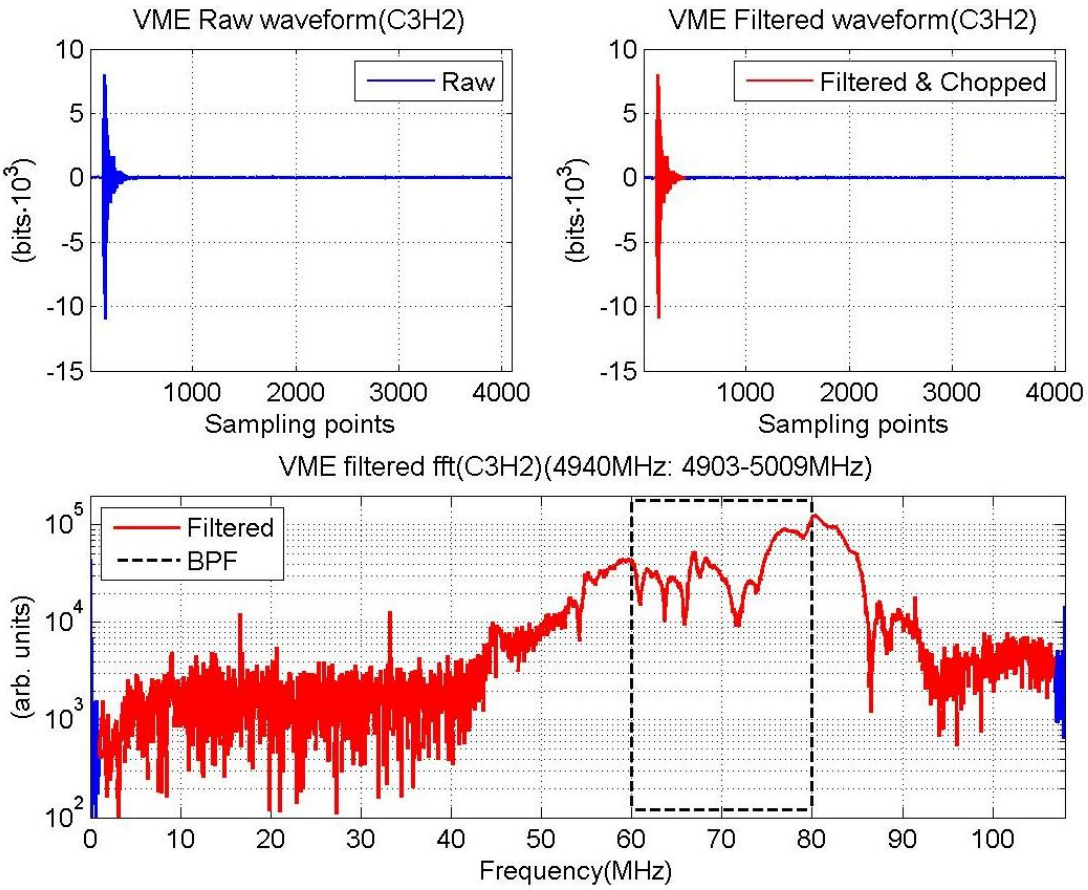

Figure 4.5: HOM signal. The center frequency is 4940 MHz with a 20 MHz BPF.

The position resolution of this band is shown in Fig. 4.6(a) for time-domain waveform and Fig. 4.6(b) for frequency-domain fft amplitude along with the number of SVD modes used in the respective regression. The resolution of y is approximately two times worse than that of x for time-domain, which is not understood.

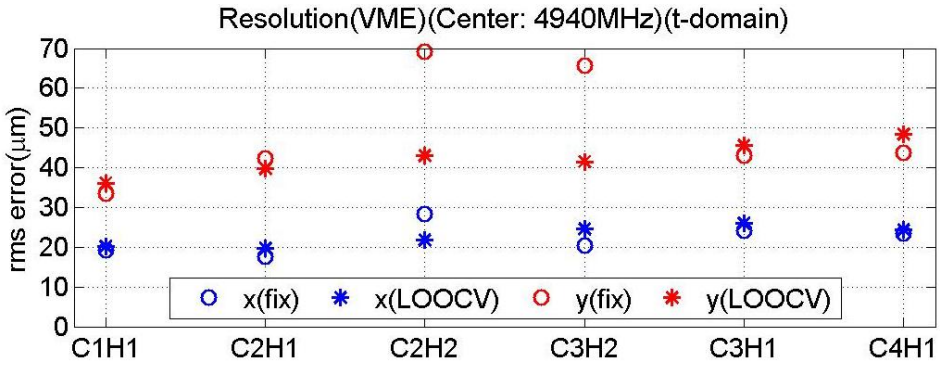

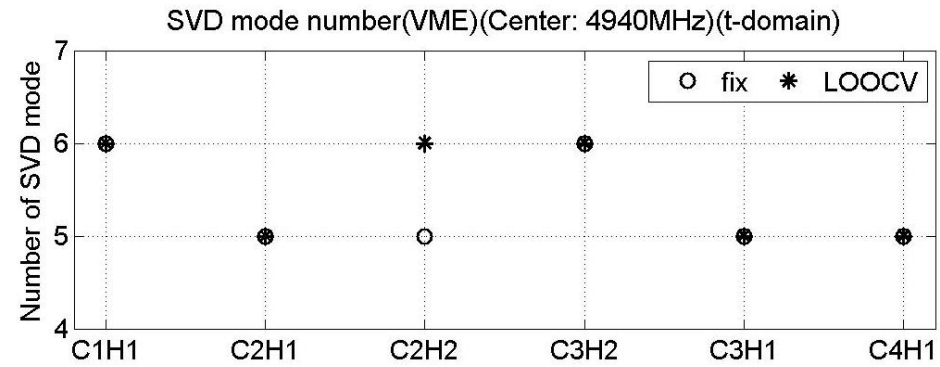

(a) time domain

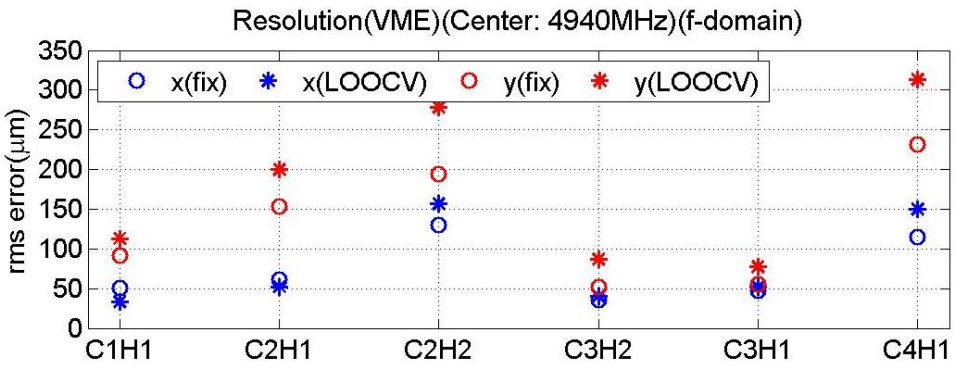

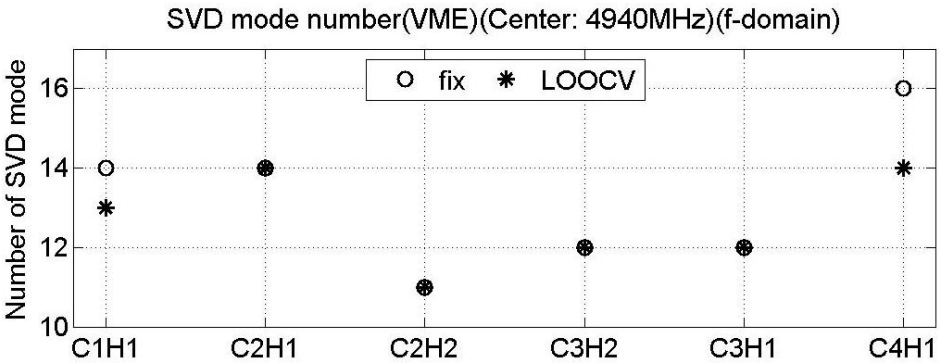

(b) frequency domain

Figure 4.6: Position resolution and SVD mode number used for position determination for both time-domain and frequency-domain. The center frequency is 4940 MHz with a 20 MHz BPF.

The integrated power over the frequency range shown in Fig. 4.5 (red spectrum) is calculated for each beam position. Fig. 4.7 shows the integrated power distribution for each HOM coupler. The position, which has minimum integrated power, is marked with white pentagon. A dissimilar position of the power minimum is found for each of the six HOM couplers. This might be due to different coupling of individual coupler and the longitudinal field distribution of the various modes. Fig. 4.8 decomposes the power distribution plot into horizontal and vertical moves.

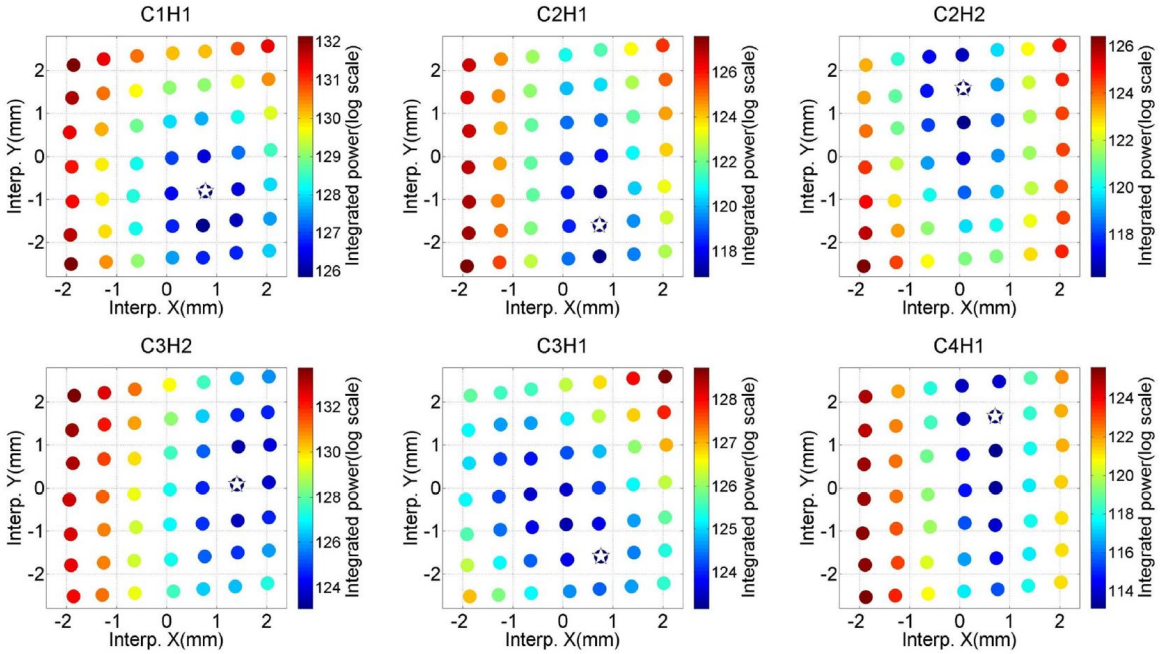

Figure 4.7: Integrated power as a function of transverse position interpolated in each cavity. The log scale magnitude of power is denoted by different color. The minimum power is marked with white pentagon. The center frequency is 4940 MHz with a 20 MHz BPF.

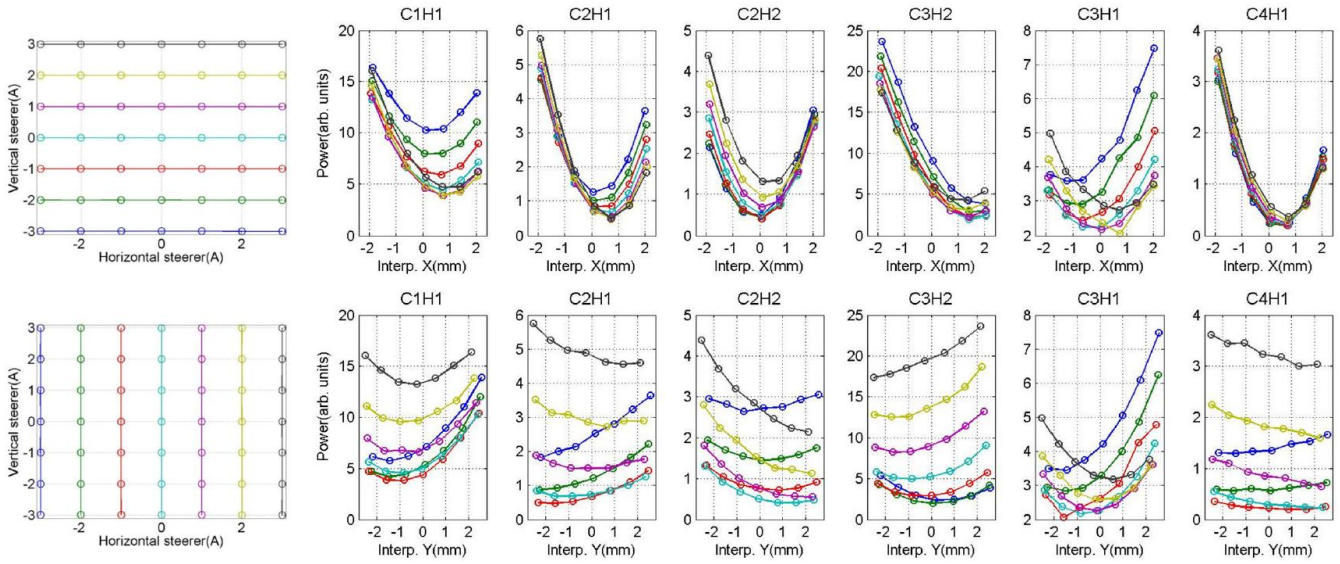

Figure 4.8: Integrated power as a function of transverse position interpolated in each cavity. The center frequency is 4940 MHz with a 20 MHz BPF.

4.3 Coupled Cavity Modes - The Second Dipole Band

The LO was set to downconvert 5437 MHz to 70 MHz, and a 20 MHz BPF was then applied to the down-converted signal. Fig. 4.9 shows the down-converted signal processed by the VME digitizer, in both time- and frequency domain (after a fft). Modes in this band are coupled, therefore, the mathematical ideal filter is only to preserve good signal quality as shown in Fig. 4.9. Compared with the spectrum analyzer signal obtained in previous studies [20], the signal filtered from 5400 MHz to 5506 MHz has proved to contain dipole modes propagating amongst cavities. As the BPF was set to 70 MHz with a 10 MHz bandwidth on each side, the main component of the filtered signal is from 5427 MHz to 5447 MHz.

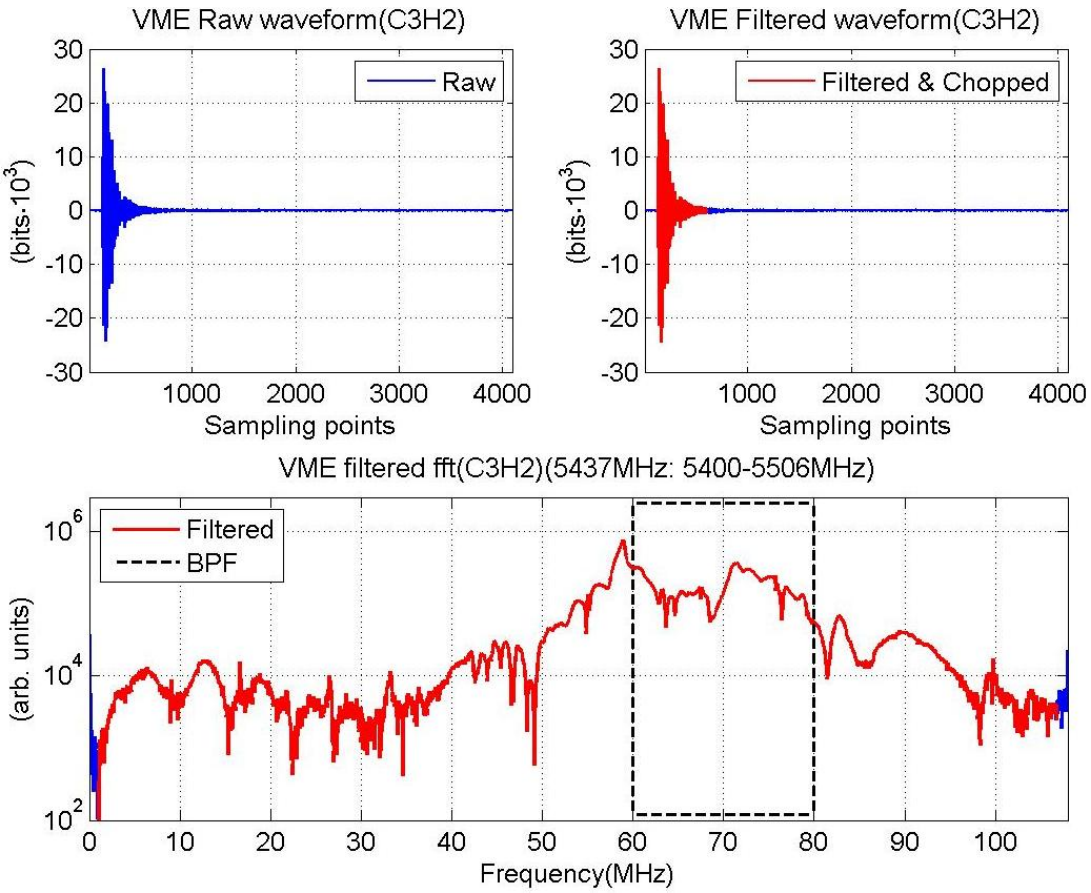

Figure 4.9: HOM signal. The center frequency is 9048 MHz with a 20 MHz BPF.

The position resolution of this band is shown in Fig. 4.10(a) for time-domain waveform and Fig. 4.10(b) for frequency-domain fft amplitude along with the number of SVD modes used in the respective regression. The resolution of y is approximately two times worse than that of x for time-domain. Although the modes are propagating, the HOM signal extracted from each coupler is still different due to the individual coupling effect of each coupler. This is reflected by the dissimilar number of SVD modes used to determine beam position.

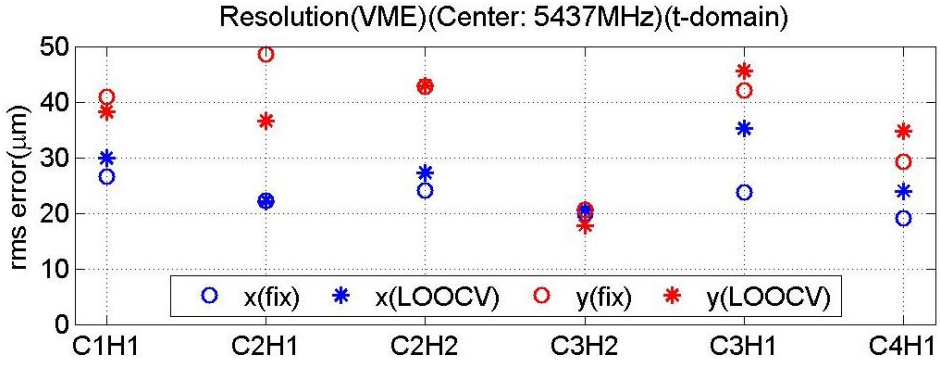

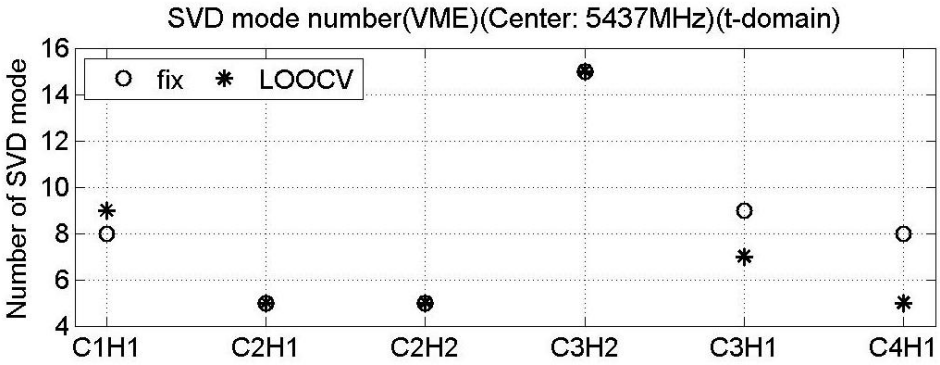

(a) time domain

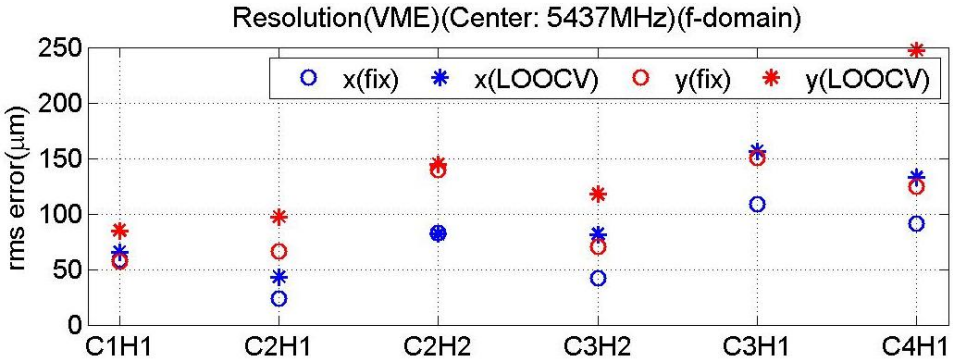

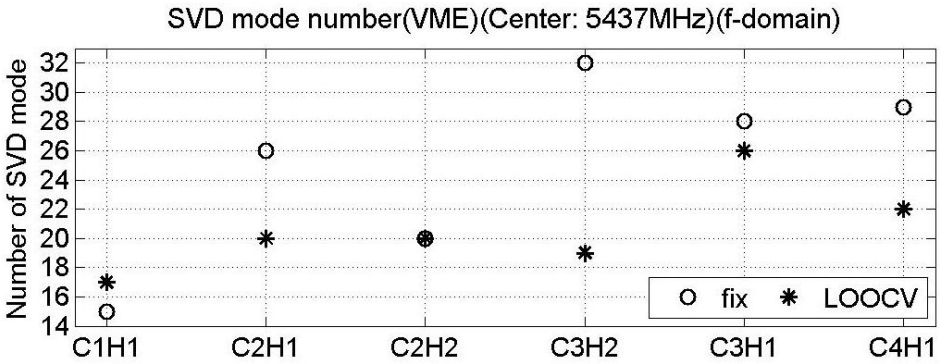

(b) frequency domain

Figure 4.10: Position resolution and SVD mode number used for position determination for both time-domain and frequency-domain. The center frequency is 5437 MHz with a 20 MHz BPF.

The integrated power over the frequency range shown in Fig. 4.9 (red spectrum) is calculated for each beam position. Fig. 4.11 shows the integrated power distribution for each HOM coupler. The position, which has minimum integrated power, is marked with white pentagon. A similar position of the power minimum can be found for all six HOM couplers. This might be a proof that modes are propagating through cavities presented in the frequency range for power integration. Fig. 4.12 decomposes the power distribution plot into horizontal and vertical moves. Around this "common" power-minimum position, we did a smaller scan as shown in Fig. 4.13. The position resolutions for this smaller scan are shown in Fig. 4.14. The position resolution of 30 μm for x and 20 μm for y can be achieved using the signal from each of the six HOM couplers.

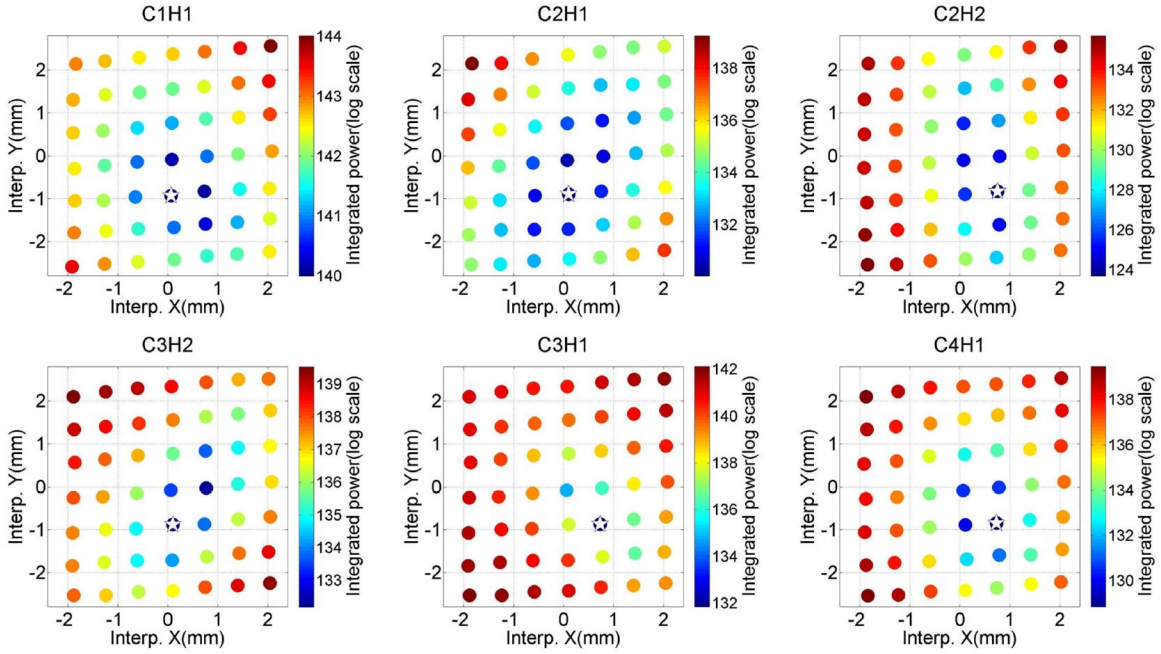

Figure 4.11: Integrated power as a function of transverse position interpolated in each cavity. The log scale magnitude of power is denoted by different color. The minimum power is marked with white pentagon. The center frequency is 5437 MHz with a 20 MHz BPF.

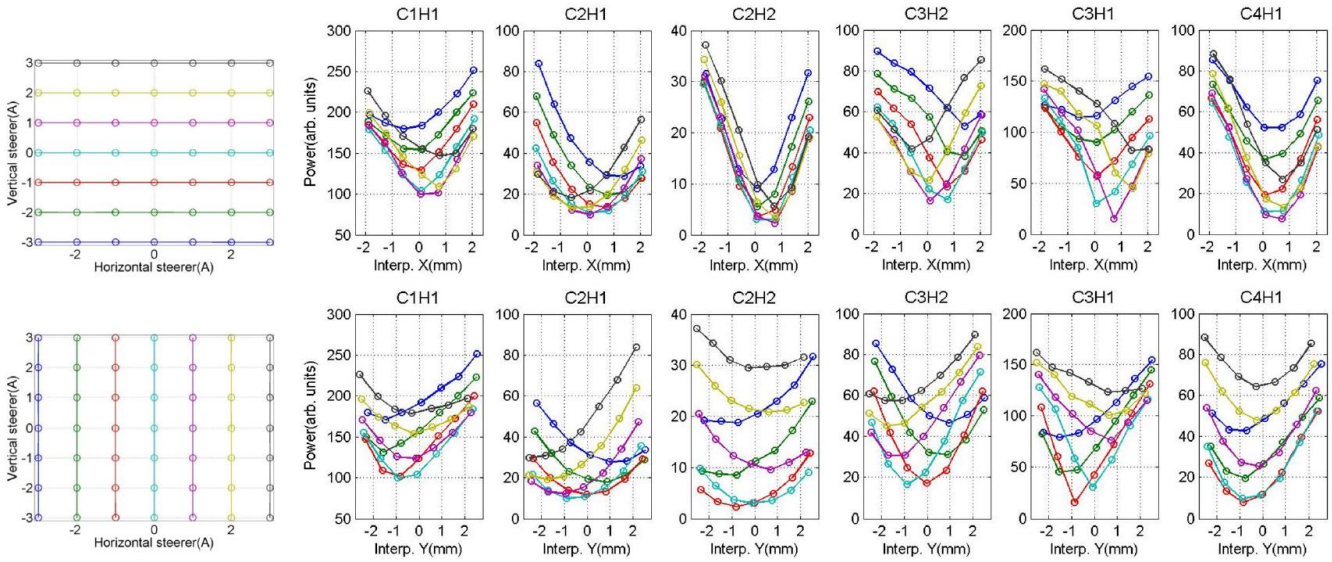

Figure 4.12: Integrated power as a function of transverse position interpolated in each cavity. The center frequency is 5437 MHz with a 20 MHz BPF.

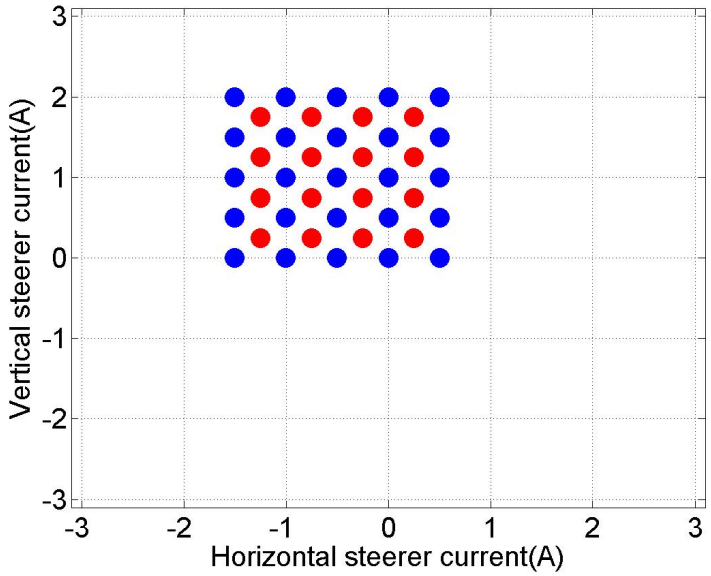

Figure 4.13: Smaller scan around the power minimum. The center frequency is 5437 MHz with a 20 MHz BPF.

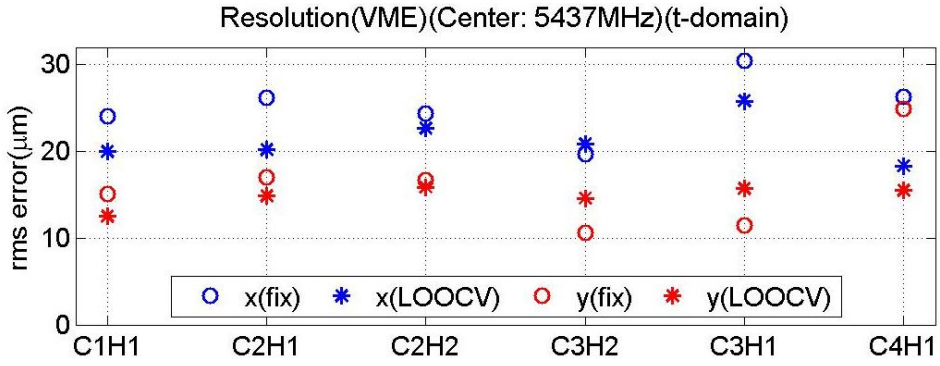

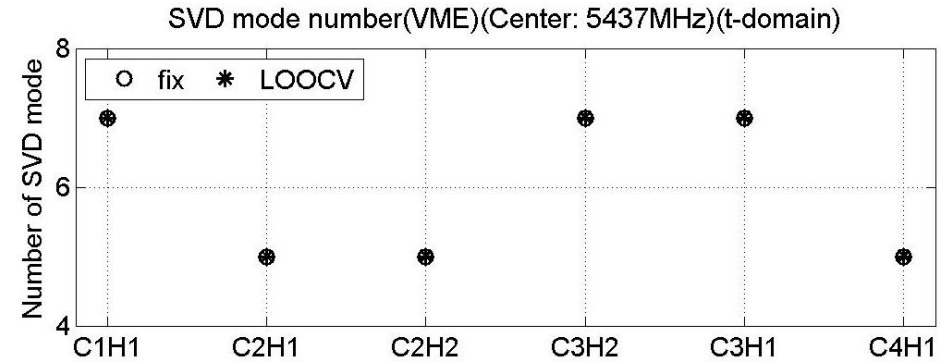

(a) time domain

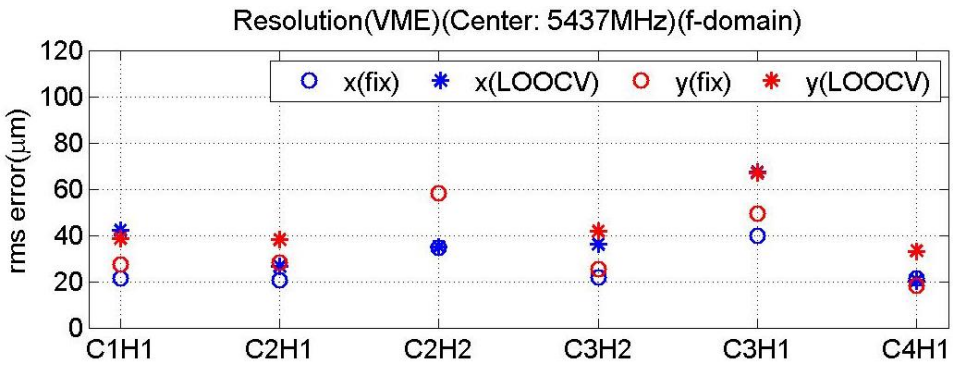

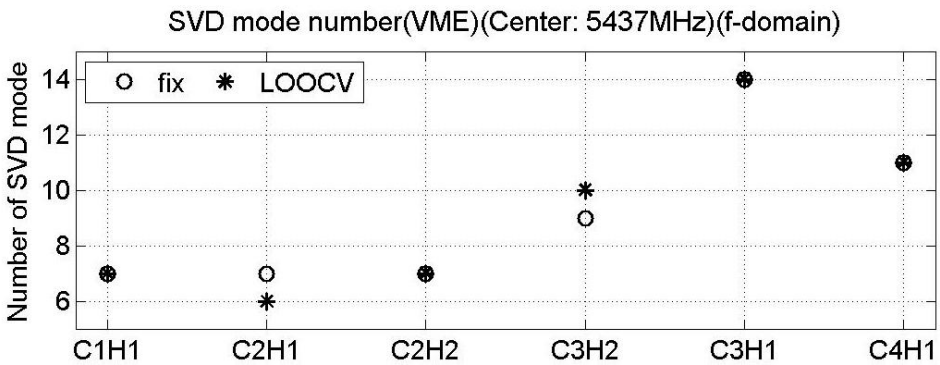

(b) frequency domain

Figure 4.14: Position resolution and SVD mode number used for position determination for both time-domain and frequency-domain. The center frequency is 5437 MHz with a 20 MHz BPF.

4.4 Trapped Cavity Modes - The Fifth Dipole Band

The LO was set to downconvert 9066 MHz to 70 MHz, and a 20 MHz BPF was then applied to the down-converted signal. Fig. 4.15 shows the down-converted signal processed by the VME digitizer, in both time- and frequency domain (after a fft). According to the previous study [24], the double-peak at approximately 55 MHz are coupled modes. Therefore, we applied a mathematical ideal filter to the down-converted time-domain waveform and the filtered signal is shown as red in Fig. 4.15. Compared with the spectrum analyzer signal obtained in previous studies [20], the signal filtered from 9035 MHz to 9080 MHz has proved to contain dipole modes localized inside each cavity. As the BPF was set to 70 MHz with a 10 MHz bandwidth on each side, the main component of the filtered signal is from 9056 MHz to 9076 MHz.

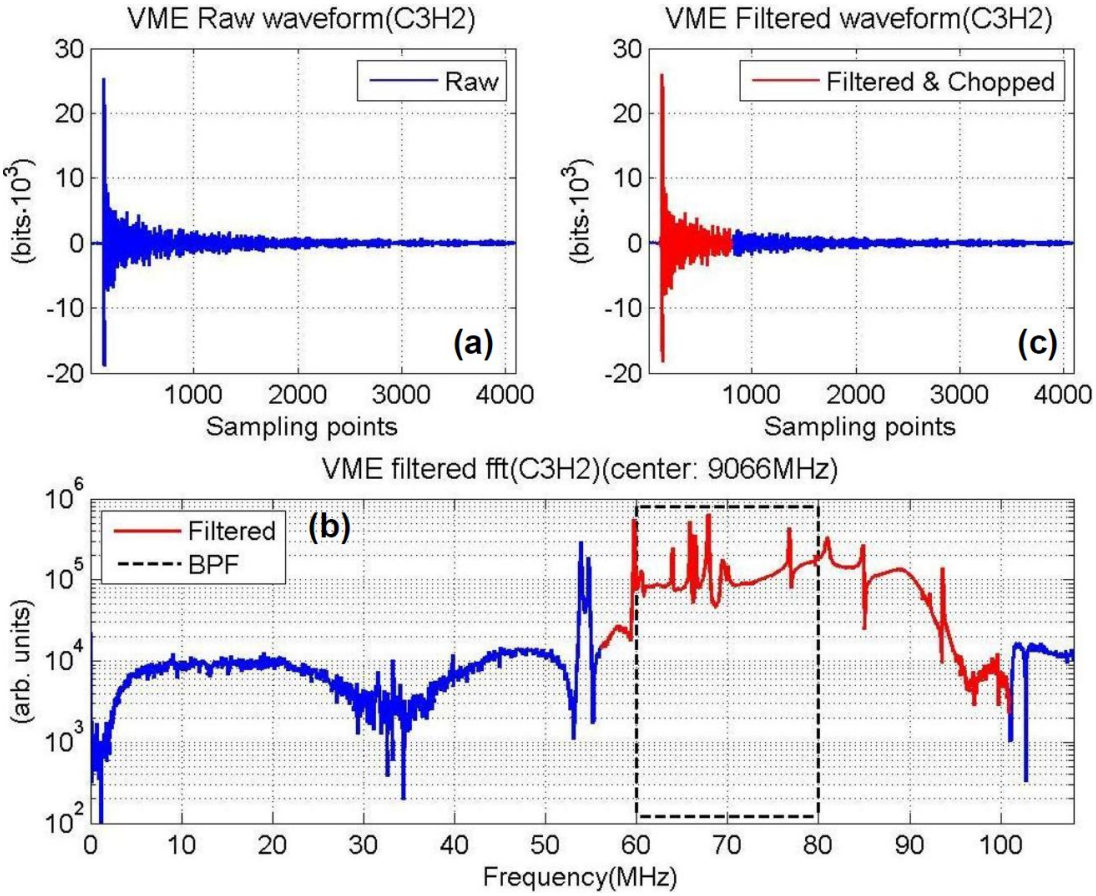

Figure 4.15: HOM signal. The center frequency is 9066 MHz with a 20 MHz BPF.

The position resolution of these modes is shown in Fig. 4.16(a) for time-domain waveform and Fig. 4.16(b) for frequency-domain fft amplitude along with the number of SVD modes used in the respective regression. The number of SVD modes is different for individual couplers due to the dissimilar HOM signal extracted from each coupler.

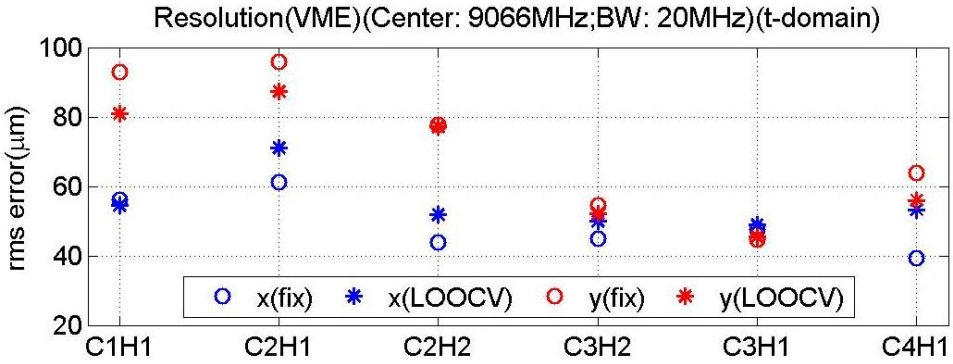

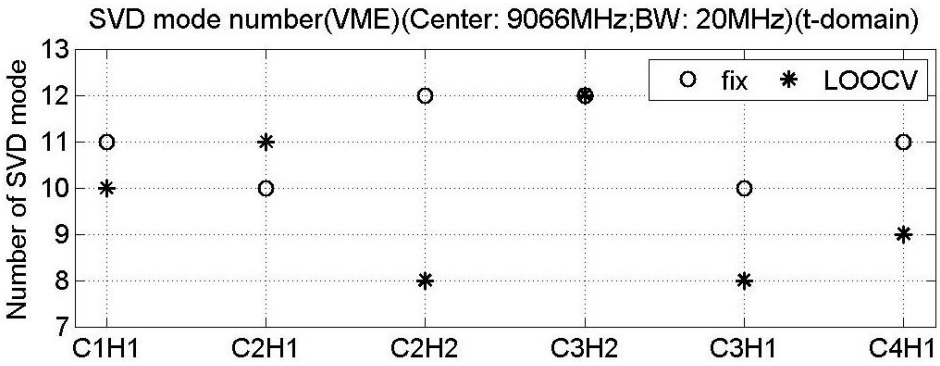

(a) time domain

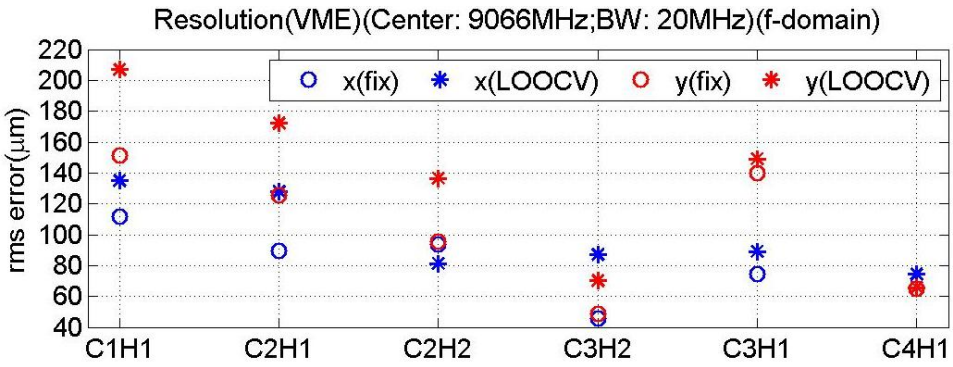

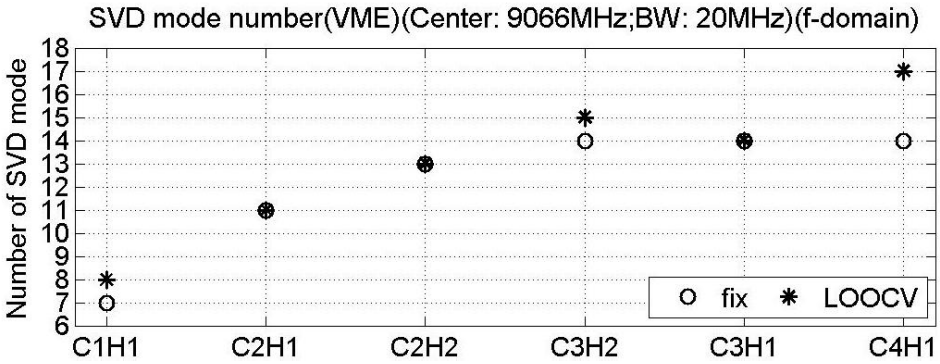

(b) frequency domain

Figure 4.16: Position resolution and SVD mode number used for position determination for both time-domain and frequency-domain. The center frequency is 9066 MHz with a 20 MHz BPF.

The integrated power over the frequency range shown in Fig. 4.15 (red spectrum) is calculated for each beam position. Fig. 4.17 shows the integrated power distribution for each HOM coupler. The position, which has minimum integrated power, is marked with white pentagon. Neither the power distribution nor the power minimum is similar among couplers. This might be a proof that modes are trapped inside each cavity presented in the frequency range for power integration. It might also be an indication of different electrical axes for different dipole modes of individual cavities. This difference can be attributed to asymmetric structure due to couplers and fabrication tolerance of the cavities. Fig. 4.18 decomposes the power distribution plot into horizontal and vertical moves.

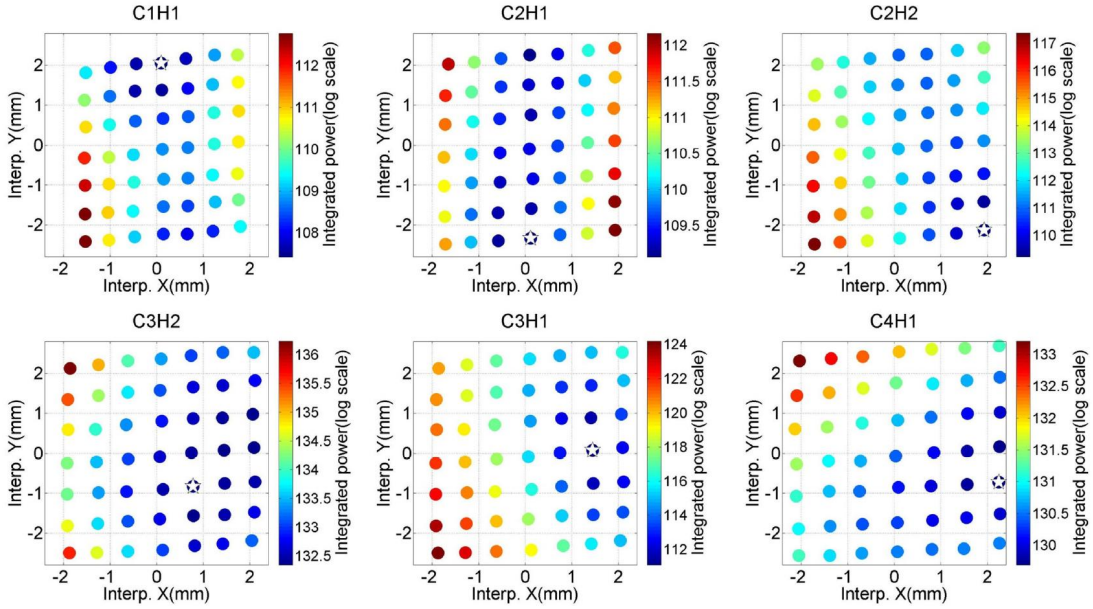

Figure 4.17: Integrated power as a function of transverse position interpolated in each cavity. The log scale magnitude of power is denoted by different color. The minimum power is marked with white pentagon. The center frequency is 9066 MHz with a 20 MHz BPF.

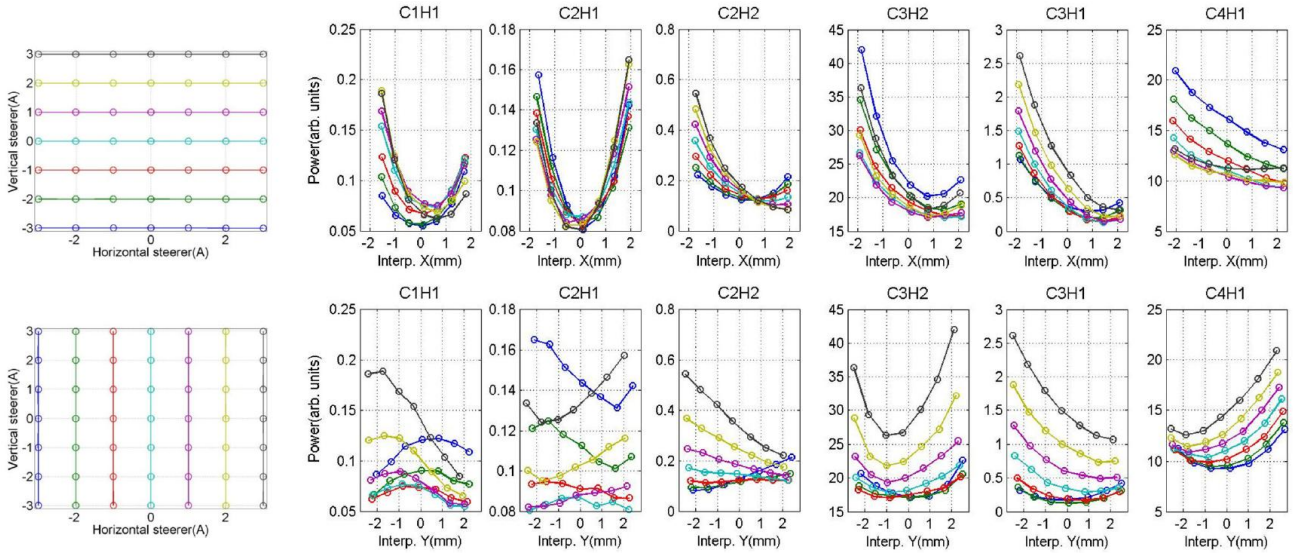

Figure 4.18: Integrated power as a function of transverse position interpolated in each cavity. The center frequency is 9066 MHz with a 20 MHz BPF.

4.5 Estimation of the Resolution

Fundamentally the measurement resolution is limited by the thermal noise, which is unavoidable at non-zero temperature. The smallest measurable thermal energy, U_{th}, is [33]

$$U_{th} = \frac{1}{2} k_B T, \tag{4.1}$$

where T is the temperature in K and k_B is the Boltzmann constant ($8.6 \times 10^{-5}\ eV \cdot K^{-1}$). Assuming a room temperature of 300 K, $U_{th} = 0.0129\ eV$.

A beam with charge q traversing a cavity loses an energy U in a particular mode as [34]

$$U = \frac{\omega}{2} \cdot \left(\frac{R}{Q}\right) \cdot q^2, \tag{4.2}$$

where R/Q (the shunt impedance divided by the quality factor) has the unit of Ω/cm^{-2}, ω is the angular frequency of the mode. This energy radiates to the HOM coupler.

For the third harmonic 3.9 GHz cavity, the strongest coupling mode in the second dipole band has a frequency of 5.4427 GHz and a R/Q value of 20.877 Ω/cm^{-2} [14], and its energy deposited by a 1 nC beam is

$$U[eV/cm^2] = \frac{2\pi \cdot 5.4427 GHz}{2} \cdot 20.877 \Omega/cm^{-2} \cdot (1nC)^2 \cdot 6.2 \times 10^{18} = 2.2 \times 10^{12} eV/cm^2. \tag{4.3}$$

This corresponds to a transverse beam offset

$$r = \sqrt{\frac{U_{th}}{U}} = 0.8\ nm. \tag{4.4}$$

The HOM signals are brought from the coupler inside FLASH tunnel to the HOM patch panel outside the tunnel by long cables. The measured cable loss is approximately 20 dB, the electronics attenuation is 26 dB (10 dB in the RF section and 16 dB in the IF section), this degrades the resolution by a factor of f_{cable} as

$$r^* = f_{cable} \cdot r = 10^{\frac{20dB+26dB}{20}} \cdot r = 199.5 \times 0.8nm = 160\ nm. \tag{4.5}$$

The theoretical minimum resolution is therefore 160 nm, as compared to the observed resolution of 20-50 μm (see Fig. 4.10(a)). This discrepancy may come from three main aspects.

First, HOM signals are all normalized to bunch charge before the position prediction. The bunch charge was recorded from the nearby toroid, which has a measured resolution of 3 pC. The measured bunch charge was ~0.5 nC throughout our studies presented in this report, therefore it corresponds to a relative resolution of ~6%. At 1 mm beam offset, this contributes ~6 μm to the position resolution.

Second, readouts of two BPMs are used to interpolate the beam position into the cavity/module and then to calibrate the HOM signals. These two BPMs have a measured resolution of ~20 μm, contributing to the resolution of the HOM-based system.

Third, the phase noise of the LO used to down-mix the HOM signal can also contribute to the resolution. This need to be studied in future measurements.

Therefore, it can be seen that the measured position resolution is dominated by the BPM resolution used for position interpolation. For the measurement of local position inside each cavity, BPMs can be used to calibrate HOM signals in C1 and C3, the position measured in these two cavities can then be used to make a prediction about the position in C2. In this case, the limitations of BPMs are eliminated from the position prediction in C2, and will consequently improve the resolution.

Chapter 5

Summary

We have studied three modal options with the specially designed test electronics for the third harmonic 3.9 GHz cavities at FLASH. Localized modes are used to determine the individual beam position in each cavity, and the resolution is approximately 50–100 μm. The transverse beam position at the center of the ACC39 module can be determined by using the coupled modes, and the resolution is approximately 20–50 μm due to the strong coupling of these modes to the beam. The resolution estimation with the test electronics for all modal options is shown in Table 5.1. Based on these results we decided to build HOM electronics for the second dipole band and the fifth dipole band, so that we will have both high resolution measurements for the whole module, and localized measurements for individual cavity. A prototype HOM electronics is being built by Fermilab and planned to be tested in FLASH by the end of 2012.

Table 5.1: Resolution estimation for various modal options with the test electronics.

	Localized Modes		**Coupled Modes**	
	Beam-pipe modes	5^{th} dipole band	1^{st} dipole band	2^{nd} dipole band
x (μm)	40−100	40−60	20−30	20−30
y (μm)	80−180	50−100	30−70	20−50

Acknowledgements

We thank Dr. Jacek Sekutowicz for carefully reading this manuscript and many useful comments. This work received support from the European Commission under the FP7 Research Infrastructures grant agreement No.227579.

Bibliography

[1] W. Ackermann *et al.*, "Operation of a free-electron laser from the extreme ultraviolet to the water window," *Nature Photonics*, vol. 1, pp. 336–342, 2007.

[2] J. Sekutowicz, *Multi-cell Superconducting Structures for High Energy e+e- Colliders and Free Electron Laser Linacs*. Warsaw, Poland: Warsaw University of Technology Publishing House, first ed., 2008.

[3] K. Floettmann, T. Limberg and Ph. Piot, "Generation of Ultrashort Electron Bunches by Cancellation of Nonlinear Distortions in the Longitudinal Phase Space," TESLA-FEL Report: TESLA-FEL 2001-06, 2001.

[4] J. Sekutowicz, R. Wanzenberg, W.F.O. Mueller and T. Weiland, "A Design of a 3rd Harmonic Cavity for the TTF 2 Photoinjector," TESLA-FEL Report: TESLA-FEL 2002-05, 2002.

[5] K.L.F. Bane, "Wake Field Effects in a Linear Collider," SLAC Note: SLAC-PUB-4169, 1986.

[6] S. Molloy *et al.*, "High precision superconducting cavity diagnostics with higher order mode measurements," *Phys. Rev. ST Accel. Beams*, vol. 9, p. 112801, 2006.

[7] G. Devanz *et al.*, "HOM Beam Coupling Measurements at the TESLA Test Facility (TTF)," in *Proceedings of EPAC2002*, (Paris, France), pp. 230–232, 2002.

[8] N. Baboi *et al.*, "Preliminary Study on HOM-Based Beam Alignment in the TESLA Test Facility," in *Proceedings of LINAC 2004*, (Lübeck, France), pp. 117–119, 2004.

[9] MAFIA Release 4. CST AG, Darmstadt, Germany.

[10] T. Khabibouline *et al.*, "Higher Order Modes of a 3rd Harmonic Cavity with an Increased End-cup Iris," TESLA-FEL Report: TESLA-FEL 2003-01, 2003.

[11] ANSYS®HFSS. Release 11.2, ANSYS Inc., USA.

[12] I.R.R. Shinton *et al.*, "Compendium of Eigenmodes in Third Harmonic Cavities for FLASH and the XFEL," DESY Report: DESY 12-053, 2012.

[13] CST Microwave Studio®. Ver. 2011, CST AG, Darmstadt, Germany.

[14] P. Zhang, N. Baboi and R.M. Jones, "Eigenmode simulations of third harmonic superconducting accelerating cavities for FLASH and the European XFEL," DESY Report: DESY 12-101, 2012.

[15] I.R.R. Shinton *et al.*, "Higher Order Modes in Third Harmonic Cavities for XFEL/FLASH," in *Proceedings of IPAC'10*, (Kyoto, Japan), pp. 3007–3009, 2010.

[16] I.R.R. Shinton *et al.*, "Higher Order Modes in Third Harmonic Cavities at FLASH," in *Proceedings of Linear Accelerator Conference LINAC2010*, (Tsukuba, Japan), pp. 785–787, 2010.

[17] T. Flisgen *et al.*, "A Concatenation Scheme for the Computation of Beam Excited Higher Order Mode Port Signals," in *Proceedings of IPAC2011*, (San Sebastian, Spain), pp. 2238–2240, 2011.

[18] I.R.R. Shinton *et al.*, "Higher Order Modes in Coupled Cavities of the FLASH Module ACC39," in *Proceedings of IPAC2011*, (San Sebastian, Spain), pp. 2301–2303, 2011.

[19] I.R.R. Shinton *et al.*, "Simulations of higher order modes in the ACC39 module of FLASH," in *IPAC2012*, (New Orleans, USA,), 2012. TUPPR037.

[20] P. Zhang, N. Baboi and R.M. Jones, "Higher order mode spectra and the dependence of localized dipole modes on the transverse beam position in third harmonic superconducting cavities at FLASH," DESY Report: DESY 12-109, 2012.

[21] P. Zhang *et al.*, "First Beam Spectra of SC Third Harmonic Cavity at FLASH," in *Proceedings of Linear Accelerator Conference LINAC2010*, (Tsukuba, Japan), pp. 782–784, 2010.

[22] P. Zhang *et al.*, "Beam-based HOM Study in Third Harmonic SC Cavities for Beam Alignment at FLASH," in *Proceedings of DIPAC2011*, (Hamburg, Germany), pp. 77–79, 2011.

[23] H.-W. Glock *et al.*, "Diode Down-mixing of HOM Coupler Signals for Beam Position Determination in 1.3-GHz- and 3.9-GHz-Cavities at FLASH," in *Proceedings of DIPAC2011*, (Hamburg, Germany), pp. 101–103, 2011.

[24] P. Zhang *et al.*, "Study of Beam Diagnostics with Trapped Modes in Third Harmonic Superconducting Cavities at FLASH," in *Proceedings of IPAC2011*, (San Sebastian, Spain), pp. 2891–2893, 2011.

[25] N. Baboi *et al.*, "Higher Order Modes for Beam Diagnostics in Third Harmonic 3.9 GHz Accelerating Modules," in *Proceedings of SRF2011*, (Chicago, USA), pp. 239–243, 2011.

[26] R.S. Larsen, "PICMG xTCA Standards Extensions for Physics: New Developments and Future Plans," SLAC Note: SLAC-PUB-14182, 2010.

[27] EPICS. http://www.aps.anl.gov/epics/.

[28] DOOCS. http://tesla.desy.de/doocs/.

[29] MATLAB®. Ver. R2011b, The MathWorks Inc., USA.

[30] R.L. Ott and M. Longnecker, *An Introduction to Statistical Methods and Data Analysis*, ch. 11.7, p. 611. Duxbury Press, sixth ed., 2008.

[31] G.H. Golub and C.F. Van Loan, *Matrix Computations*, ch. 2.3, pp. 16–20. The John Hopkins University Press, second ed., 1984.

[32] R. Kohavi, "A Study of Cross-Validation and Bootstrap for Accuracy Estimation and Model Selection," in *Proceedings of the 14th International Joint Conference on Artificial Intelligence*, vol. 2, (Montreal, Quebec, Canada), pp. 1137–1143, 1995.

[33] W.B. Davenport and W.L. Root, *An introduction to the theory of random signals and noise*, ch. 9-4, p. 185. IEEE Press, 1987.

[34] A. Chao and M. Tigner, *Handbook of Accelerator Physics and Engineering*, ch. 3.2.7, p. 213. Singapore: World Scientific, first ed., 1999.

Appendix A

The Analog Box Circuit

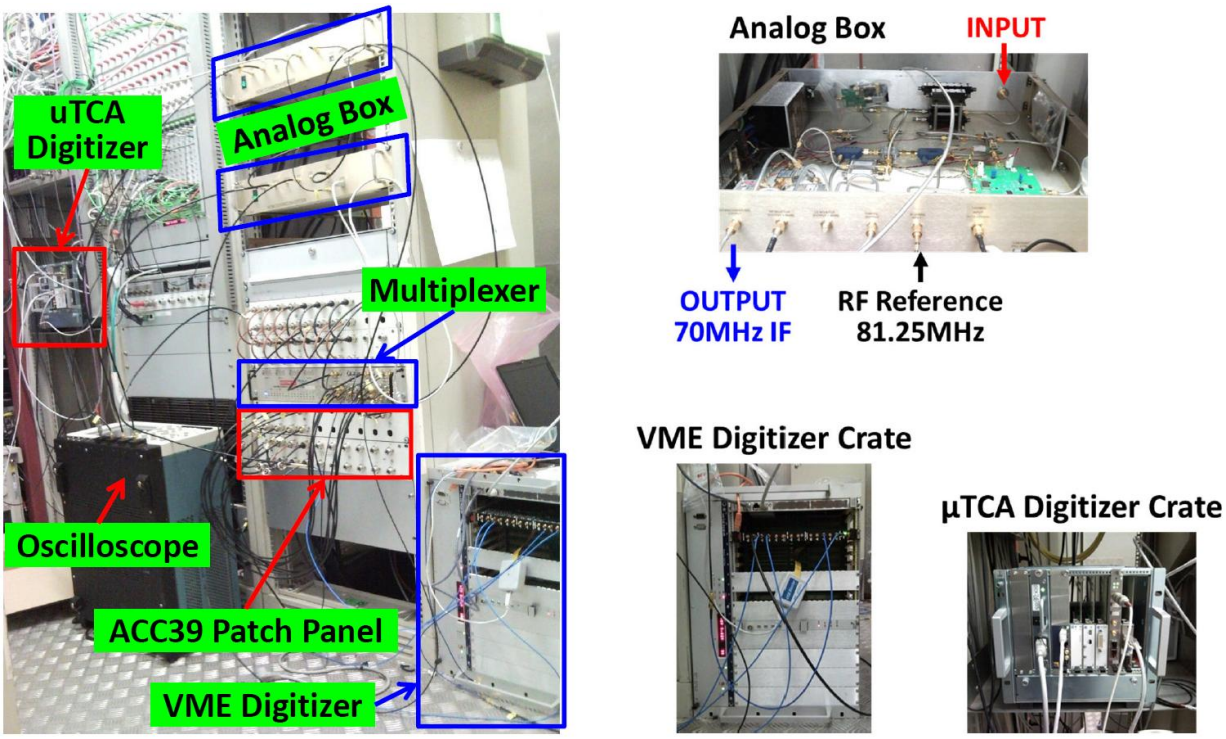

Figure A.1: Photo of the device setup in the FLASH injector barrack outside the tunnel, the analog box and two types of digitizer.

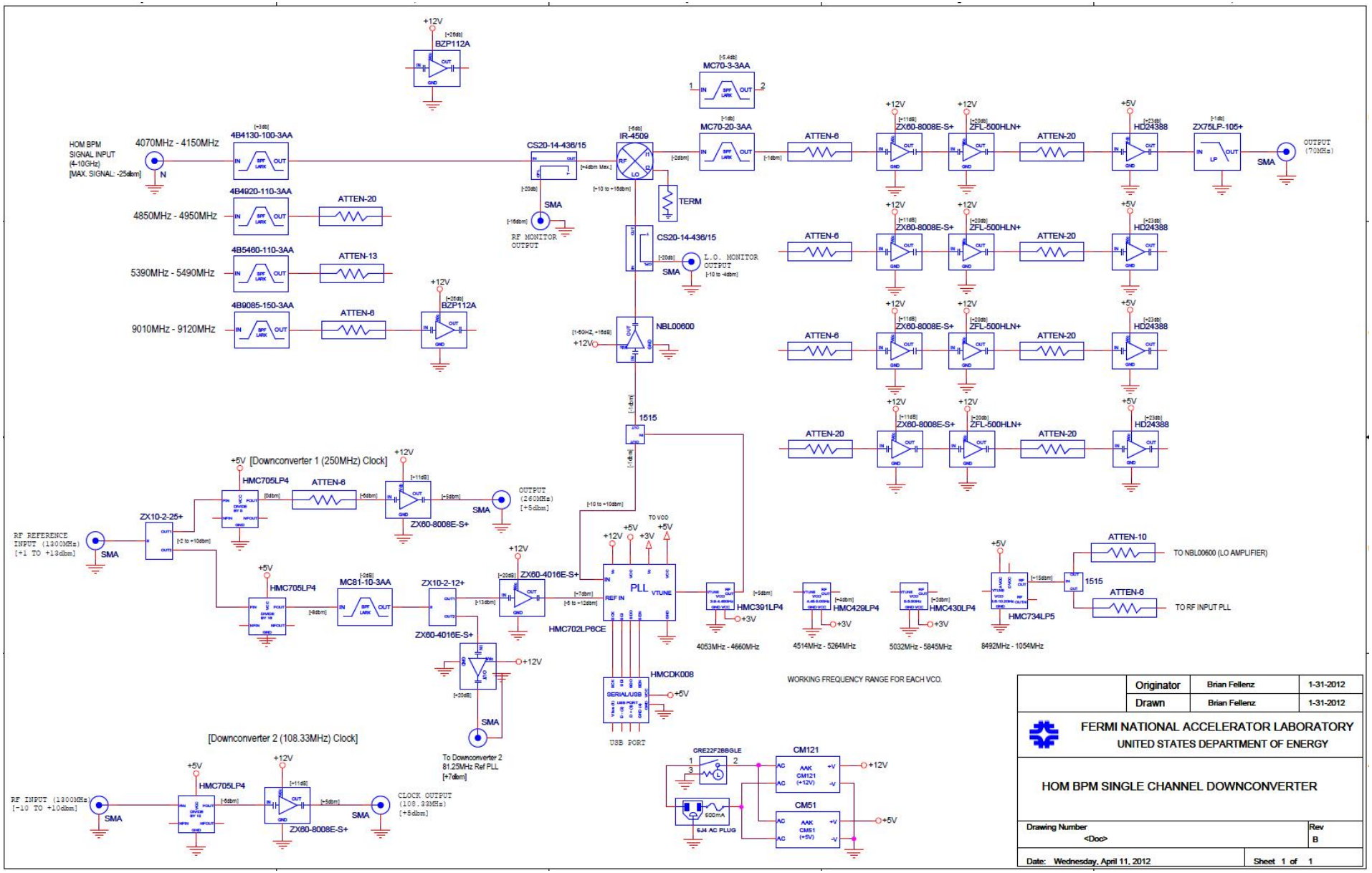

Figure A.2: Drawing of the analog box.

Appendix B

Settings in the Analog Box

HOM signals vary amongst couplers and frequency bands. Therefore various amplification and attenuations were used for each frequency band. They are listed in Table B.1.

Table B.1: Settings in the analog box for each frequency band. "+" means amplification and "−" means attenuation.

Band	Center frequency	Bandwidth	RF section	IF section	Total
Beam-pipe modes	4082 MHz 4118 MHz	20 MHz 20 MHz	+0 dB	+33 dB	+33 dB
1^{st} dipole band	4859 MHz 4904 MHz 4940 MHz 4900 MHz	20 MHz 20 MHz 20 MHz 100 MHz	−13 dB	+32 dB	+19 dB
2^{nd} dipole band	5437 MHz 5464 MHz 5482 MHz 5450 MHz	20 MHz 20 MHz 20 MHz 100 MHz	−10 dB	+36 dB	+26 dB
5^{th} dipole band	9048 MHz 9066 MHz	20 MHz 20 MHz	−6 dB	+52 dB	+46 dB

Appendix C

Tables: Position Resolutions

Resolutions in predicting beam positions for validation samples are listed in this appendix. The method applied is *singular value decomposition* (SVD). The number of SVD modes used for regression is determined based on a stable and good position resolution. These are listed in Appendix D. Both the fixed sample split and a *leave-one-out cross-validation* (LOOCV) are shown. The reading jumps of the BPM-A readouts have been corrected in y plane for all modal options.

C.1 The Localized Beam-pipe modes

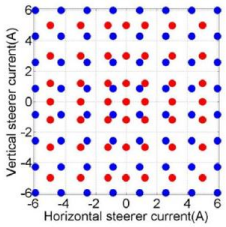

4082MHz (20MHz)			x resolution (μm)								y resolution (μm)							
			C1H2	C1H1	C2H1	C2H2	C3H2	C3H1	C4H1	C4H2	C1H2	C1H1	C2H1	C2H2	C3H2	C3H1	C4H1	C4H2
Fixed split	VME	wfm	n/a	n/a	n/a	n/a	n/a	n/a	n/a	n/a	n/a	n/a	n/a	n/a	n/a	n/a	n/a	n/a
		fft	n/a	n/a	n/a	n/a	n/a	n/a	n/a	n/a	n/a	n/a	n/a	n/a	n/a	n/a	n/a	n/a
	uTCA	wfm	27	28	32	37	30	28	39	38	28	100	88	35	24	46	173	38
		fft	33	68	52	69	64	44	54	46	37	122	93	56	93	103	115	47
LOOCV	VME	wfm	n/a	n/a	n/a	n/a	n/a	n/a	n/a	n/a	n/a	n/a	n/a	n/a	n/a	n/a	n/a	n/a
		fft	n/a	n/a	n/a	n/a	n/a	n/a	n/a	n/a	n/a	n/a	n/a	n/a	n/a	n/a	n/a	n/a
	uTCA	wfm	29	29	27	33	40	35	31	32	30	110	90	40	32	51	98	34
		fft	34	74	43	107	68	47	70	44	40	170	98	66	108	109	142	39

wfm: time-domain waveform; fft: frequency-domain fft amplitude; LOOCV: leave-one-out cross validation

Figure C.1: Position resolutions of beam-pipe modes centered at 4082 MHz with a 20 MHz bandwidth.

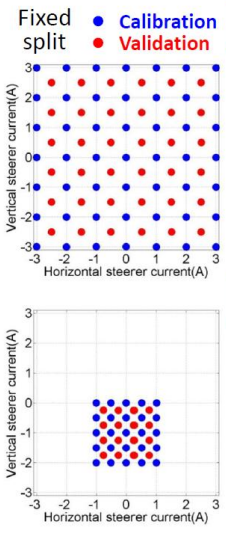

4118MHz (20MHz)			x resolution (μm)								y resolution (μm)							
			C1H2	C1H1	C2H1	C2H2	C3H2	C3H1	C4H1	C4H2	C1H2	C1H1	C2H1	C2H2	C3H2	C3H1	C4H1	C4H2
Fixed split	VME	wfm	n/a	n/a	n/a	n/a	n/a	n/a	n/a	n/a	n/a	n/a	n/a	n/a	n/a	n/a	n/a	n/a
		fft	n/a	n/a	n/a	n/a	n/a	n/a	n/a	n/a	n/a	n/a	n/a	n/a	n/a	n/a	n/a	n/a
	uTCA	wfm	44	50	93	46	58	73	101	60	42	152	102	78	87	186	111	90
		fft	57	72	51	273	287	98	163	85	52	84	97	223	266	141	268	65
LOOCV	VME	wfm	n/a	n/a	n/a	n/a	n/a	n/a	n/a	n/a	n/a	n/a	n/a	n/a	n/a	n/a	n/a	n/a
		fft	n/a	n/a	n/a	n/a	n/a	n/a	n/a	n/a	n/a	n/a	n/a	n/a	n/a	n/a	n/a	n/a
	uTCA	wfm	35	34	61	41	45	54	80	55	41	127	90	45	51	196	108	58
		fft	44	83	54	344	383	72	186	92	52	104	122	317	321	247	310	61

4118MHz (20MHz)			x resolution (μm)								y resolution (μm)							
			C1H2	C1H1	C2H1	C2H2	C3H2	C3H1	C4H1	C4H2	C1H2	C1H1	C2H1	C2H2	C3H2	C3H1	C4H1	C4H2
Fixed split	VME	wfm	n/a	n/a	n/a	n/a	n/a	n/a	n/a	n/a	n/a	n/a	n/a	n/a	n/a	n/a	n/a	n/a
		fft	n/a	n/a	n/a	n/a	n/a	n/a	n/a	n/a	n/a	n/a	n/a	n/a	n/a	n/a	n/a	n/a
	uTCA	wfm	27	28	32	37	30	28	39	38	28	100	88	35	24	46	173	38
		fft	33	68	52	69	64	44	54	46	37	122	93	56	93	103	115	47
LOOCV	VME	wfm	n/a	n/a	n/a	n/a	n/a	n/a	n/a	n/a	n/a	n/a	n/a	n/a	n/a	n/a	n/a	n/a
		fft	n/a	n/a	n/a	n/a	n/a	n/a	n/a	n/a	n/a	n/a	n/a	n/a	n/a	n/a	n/a	n/a
	uTCA	wfm	29	29	27	33	40	35	31	32	30	110	90	40	32	51	98	34
		fft	34	74	43	107	68	47	70	44	40	170	98	66	108	109	142	39

wfm: time-domain waveform; fft: frequency-domain fft amplitude; LOOCV: leave-one-out cross validation

Figure C.2: Position resolutions of beam-pipe modes centered at 4118 MHz with a 20 MHz bandwidth.

C.2 Coupled Cavity Modes - The First Dipole Band

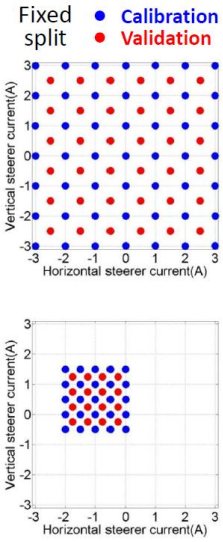

4859MHz (20MHz)			x resolution (μm)								y resolution (μm)							
			C1H2	C1H1	C2H1	C2H2	C3H2	C3H1	C4H1	C4H2	C1H2	C1H1	C2H1	C2H2	C3H2	C3H1	C4H1	C4H2
Fixed split	VME	wfm	n/a	n/a	n/a	n/a	n/a	n/a	n/a	n/a	n/a	n/a	n/a	n/a	n/a	n/a	n/a	n/a
		fft	n/a	n/a	n/a	n/a	n/a	n/a	n/a	n/a	n/a	n/a	n/a	n/a	n/a	n/a	n/a	n/a
	uTCA	wfm	27	36	34	31	28	29	32	33	40	38	84	50	31	44	56	49
		fft	56	80	247	160	116	123	223	117	77	113	268	207	173	251	335	235
LOOCV	VME	wfm	n/a	n/a	n/a	n/a	n/a	n/a	n/a	n/a	n/a	n/a	n/a	n/a	n/a	n/a	n/a	n/a
		fft	n/a	n/a	n/a	n/a	n/a	n/a	n/a	n/a	n/a	n/a	n/a	n/a	n/a	n/a	n/a	n/a
	uTCA	wfm	34	49	48	33	32	62	37	36	40	50	73	45	28	43	54	47
		fft	72	101	242	168	160	171	268	141	70	137	376	264	216	318	430	310

4859MHz (20MHz)			x resolution (μm)								y resolution (μm)							
			C1H2	C1H1	C2H1	C2H2	C3H2	C3H1	C4H1	C4H2	C1H2	C1H1	C2H1	C2H2	C3H2	C3H1	C4H1	C4H2
Fixed split	VME	wfm	n/a	n/a	n/a	n/a	n/a	n/a	n/a	n/a	n/a	n/a	n/a	n/a	n/a	n/a	n/a	n/a
		fft	n/a	n/a	n/a	n/a	n/a	n/a	n/a	n/a	n/a	n/a	n/a	n/a	n/a	n/a	n/a	n/a
	uTCA	wfm	34	36	36	23	31	69	48	45	46	67	98	34	56	51	40	28
		fft	30	110	90	52	41	73	71	55	30	49	60	62	56	92	102	51
LOOCV	VME	wfm	n/a	n/a	n/a	n/a	n/a	n/a	n/a	n/a	n/a	n/a	n/a	n/a	n/a	n/a	n/a	n/a
		fft	n/a	n/a	n/a	n/a	n/a	n/a	n/a	n/a	n/a	n/a	n/a	n/a	n/a	n/a	n/a	n/a
	uTCA	wfm	30	32	28	29	34	32	38	37	47	52	55	49	45	45	56	54
		fft	54	74	107	49	46	58	81	62	55	71	138	74	70	92	176	85

wfm: time-domain waveform; fft: frequency-domain fft amplitude; LOOCV: leave-one-out cross validation

Figure C.3: Position resolutions of cavity modes centered at 4859 MHz with a 20 MHz bandwidth.

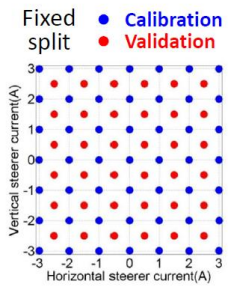

4904MHz (20MHz)			x resolution (μm)								y resolution (μm)							
			C1H2	C1H1	C2H1	C2H2	C3H2	C3H1	C4H1	C4H2	C1H2	C1H1	C2H1	C2H2	C3H2	C3H1	C4H1	C4H2
Fixed split	VME	wfm	n/a	n/a	n/a	n/a	n/a	n/a	n/a	n/a	n/a	n/a	n/a	n/a	n/a	n/a	n/a	n/a
		fft	n/a	n/a	n/a	n/a	n/a	n/a	n/a	n/a	n/a	n/a	n/a	n/a	n/a	n/a	n/a	n/a
	uTCA	wfm	28	35	33	24	38	39	36	33	33	44	73	46	43	46	50	47
		fft	53	54	66	107	60	41	52	110	58	98	166	129	72	56	150	249
LOOCV	VME	wfm	n/a	n/a	n/a	n/a	n/a	n/a	n/a	n/a	n/a	n/a	n/a	n/a	n/a	n/a	n/a	n/a
		fft	n/a	n/a	n/a	n/a	n/a	n/a	n/a	n/a	n/a	n/a	n/a	n/a	n/a	n/a	n/a	n/a
	uTCA	wfm	31	31	37	32	34	39	34	34	37	39	43	33	35	37	43	45
		fft	52	56	102	136	96	43	60	124	57	98	162	150	122	68	189	263

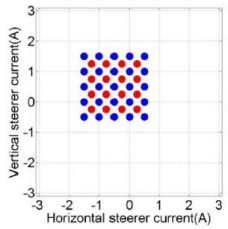

4904MHz (20MHz)			x resolution (μm)								y resolution (μm)							
			C1H2	C1H1	C2H1	C2H2	C3H2	C3H1	C4H1	C4H2	C1H2	C1H1	C2H1	C2H2	C3H2	C3H1	C4H1	C4H2
Fixed split	VME	wfm	n/a	n/a	n/a	n/a	n/a	n/a	n/a	n/a	n/a	n/a	n/a	n/a	n/a	n/a	n/a	n/a
		fft	n/a	n/a	n/a	n/a	n/a	n/a	n/a	n/a	n/a	n/a	n/a	n/a	n/a	n/a	n/a	n/a
	uTCA	wfm	31	33	39	27	25	40	25	26	34	97	127	36	38	46	105	34
		fft	31	62	77	34	32	43	45	36	29	55	54	52	48	83	58	98
LOOCV	VME	wfm	n/a	n/a	n/a	n/a	n/a	n/a	n/a	n/a	n/a	n/a	n/a	n/a	n/a	n/a	n/a	n/a
		fft	n/a	n/a	n/a	n/a	n/a	n/a	n/a	n/a	n/a	n/a	n/a	n/a	n/a	n/a	n/a	n/a
	uTCA	wfm	40	41	29	28	35	35	38	34	40	50	58	48	37	42	53	44
		fft	38	50	37	30	51	38	43	53	52	75	101	59	48	62	70	139

wfm: time-domain waveform; fft: frequency-domain fft amplitude; LOOCV: leave-one-out cross validation

Figure C.4: Position resolutions of cavity modes centered at 4904 MHz with a 20 MHz bandwidth.

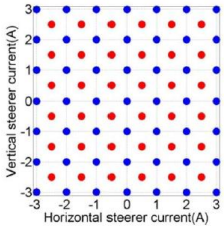

4940MHz (20MHz)			x resolution (μm)								y resolution (μm)							
			C1H2	C1H1	C2H1	C2H2	C3H2	C3H1	C4H1	C4H2	C1H2	C1H1	C2H1	C2H2	C3H2	C3H1	C4H1	C4H2
Fixed split	VME	wfm	26	19	18	28	20	24	23	38	48	33	42	69	66	43	44	44
		fft	34	50	62	130	36	48	115	37	105	92	154	194	51	55	231	106
	uTCA	wfm	40	33	33	39	34	38	41	41	64	36	42	54	63	40	56	60
		fft	92	71	77	207	49	90	119	63	297	111	240	293	74	80	350	167
LOOCV	VME	wfm	24	20	20	22	25	26	24	32	31	36	40	43	41	46	48	46
		fft	52	33	52	157	40	52	150	59	146	113	200	278	87	77	313	192
	uTCA	wfm	35	32	31	37	33	36	35	36	40	43	42	43	42	43	56	51
		fft	103	55	75	249	50	102	147	84	221	127	299	393	109	109	434	184

wfm: time-domain waveform; fft: frequency-domain fft amplitude; LOOCV: leave-one-out cross validation

Figure C.5: Position resolutions of cavity modes centered at 4940 MHz with a 20 MHz bandwidth.

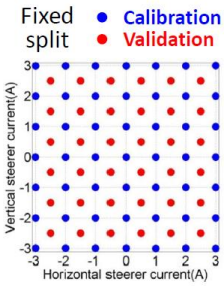

4850-4950MHz			x resolution (μm)								y resolution (μm)							
			C1H2	C1H1	C2H1	C2H2	C3H2	C3H1	C4H1	C4H2	C1H2	C1H1	C2H1	C2H2	C3H2	C3H1	C4H1	C4H2
Fixed split	VME	wfm	25	21	28	24	25	34	21	24	49	30	42	67	64	39	32	55
		fft	42	33	31	67	56	54	46	37	55	53	39	147	64	81	96	81
	uTCA	wfm	36	39	39	46	37	39	47	35	44	51	53	41	36	48	47	66
		fft	64	64	57	119	65	59	64	77	128	106	166	150	59	113	170	134
LOOCV	VME	wfm	27	18	17	20	17	35	20	25	32	27	34	37	31	45	31	51
		fft	52	30	56	62	67	81	34	51	56	53	69	186	100	85	87	139
	uTCA	wfm	31	30	32	33	39	38	32	36	42	39	40	39	37	48	46	51
		fft	62	57	57	113	71	71	55	70	117	80	143	184	75	143	197	126

wfm: time-domain waveform; fft: frequency-domain fft amplitude; LOOCV: leave-one-out cross validation

Figure C.6: Position resolutions of cavity modes from 4850 MHz to 4950 MHz.

C.3 Coupled Cavity Modes - The Second Dipole Band

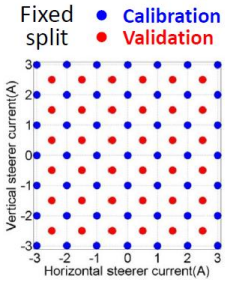

5437MHz (20MHz)			x resolution (μm)								y resolution (μm)							
			C1H2	C1H1	C2H1	C2H2	C3H2	C3H1	C4H1	C4H2	C1H2	C1H1	C2H1	C2H2	C3H2	C3H1	C4H1	C4H2
Fixed split	VME	wfm	26	27	22	24	20	24	19	23	33	41	49	43	21	42	29	20
		fft	25	59	24	83	42	109	91	82	22	57	66	140	70	150	125	79
	uTCA	wfm	42	41	35	39	38	43	35	42	59	75	62	48	62	85	67	48
		fft	54	54	65	88	90	163	81	142	63	74	107	151	85	151	213	91
LOOCV	VME	wfm	23	30	22	27	21	35	24	24	26	38	37	43	18	46	35	21
		fft	36	66	43	82	82	156	133	110	25	85	97	145	118	225	247	109
	uTCA	wfm	29	27	29	31	28	35	28	35	26	30	33	37	32	35	33	35
		fft	40	43	58	64	68	173	75	145	42	72	94	112	73	150	186	92

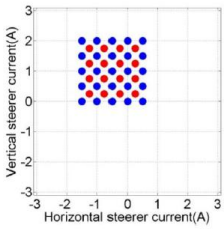

5437MHz (20MHz)			x resolution (μm)								y resolution (μm)							
			C1H2	C1H1	C2H1	C2H2	C3H2	C3H1	C4H1	C4H2	C1H2	C1H1	C2H1	C2H2	C3H2	C3H1	C4H1	C4H2
Fixed split	VME	wfm	20	24	26	24	20	30	26	21	14	15	17	17	11	11	25	13
		fft	21	21	21	35	22	40	21	33	18	28	28	58	25	49	18	30
	uTCA	wfm	35	36	28	29	30	44	26	23	27	31	35	38	35	37	31	42
		fft	36	27	32	43	37	37	46	52	28	42	28	52	51	65	61	49
LOOCV	VME	wfm	18	20	20	23	21	26	18	20	12	12	15	16	15	16	16	13
		fft	33	42	26	35	36	67	20	54	14	39	38	102	42	67	33	64
	uTCA	wfm	35	36	28	29	30	44	26	23	27	31	35	38	35	37	31	42
		fft	36	27	32	43	37	37	46	52	28	42	28	52	51	65	61	49

wfm: time-domain waveform; fft: frequency-domain fft amplitude; LOOCV: leave-one-out cross validation

Figure C.7: Position resolutions of cavity modes centered at 5437 MHz with a 20 MHz bandwidth.

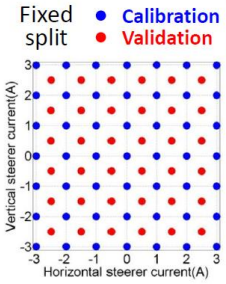

5464MHz (20MHz)			x resolution (μm)								y resolution (μm)							
			C1H2	C1H1	C2H1	C2H2	C3H2	C3H1	C4H1	C4H2	C1H2	C1H1	C2H1	C2H2	C3H2	C3H1	C4H1	C4H2
Fixed split	VME	wfm	n/a	n/a	n/a	n/a	n/a	n/a	n/a	n/a	n/a	n/a	n/a	n/a	n/a	n/a	n/a	n/a
		fft	n/a	n/a	n/a	n/a	n/a	n/a	n/a	n/a	n/a	n/a	n/a	n/a	n/a	n/a	n/a	n/a
	uTCA	wfm	29	25	43	29	47	30	43	24	70	52	50	49	47	61	74	65
		fft	44	44	62	84	58	112	221	98	37	96	88	152	53	153	252	200
LOOCV	VME	wfm	n/a	n/a	n/a	n/a	n/a	n/a	n/a	n/a	n/a	n/a	n/a	n/a	n/a	n/a	n/a	n/a
		fft	n/a	n/a	n/a	n/a	n/a	n/a	n/a	n/a	n/a	n/a	n/a	n/a	n/a	n/a	n/a	n/a
	uTCA	wfm	31	26	34	27	42	30	31	24	34	34	36	31	29	30	37	30
		fft	39	39	67	64	58	92	179	82	32	47	76	100	49	141	192	89

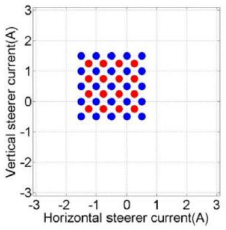

5464MHz (20MHz)			x resolution (μm)								y resolution (μm)							
			C1H2	C1H1	C2H1	C2H2	C3H2	C3H1	C4H1	C4H2	C1H2	C1H1	C2H1	C2H2	C3H2	C3H1	C4H1	C4H2
Fixed split	VME	wfm	34	21	23	23	12	23	22	21	45	48	43	39	24	29	142	40
		fft	21	28	24	25	14	21	20	21	27	35	39	36	39	32	40	34
	uTCA	wfm	60	57	49	36	20	55	42	42	64	59	55	49	47	42	123	49
		fft	37	40	30	36	20	31	47	37	63	84	94	97	92	93	62	68
LOOCV	VME	wfm	26	24	20	20	22	21	17	17	34	29	27	34	29	29	34	31
		fft	28	27	17	24	23	46	51	33	44	51	43	59	70	57	65	56
	uTCA	wfm	27	33	27	25	30	31	30	33	36	36	25	25	27	32	36	34
		fft	24	29	24	26	29	47	58	34	37	46	47	47	40	30	65	50

wfm: time-domain waveform; fft: frequency-domain fft amplitude; LOOCV: leave-one-out cross validation

Figure C.8: Position resolutions of cavity modes centered at 5464 MHz with a 20 MHz bandwidth.

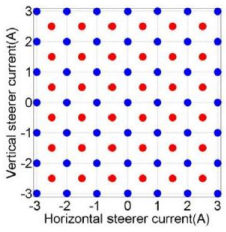

5482MHz (20MHz)			x resolution (μm)								y resolution (μm)							
			C1H2	C1H1	C2H1	C2H2	C3H2	C3H1	C4H1	C4H2	C1H2	C1H1	C2H1	C2H2	C3H2	C3H1	C4H1	C4H2
Fixed split	VME	wfm	n/a	n/a	n/a	n/a	n/a	n/a	n/a	n/a	n/a	n/a	n/a	n/a	n/a	n/a	n/a	n/a
		fft	n/a	n/a	n/a	n/a	n/a	n/a	n/a	n/a	n/a	n/a	n/a	n/a	n/a	n/a	n/a	n/a
	uTCA	wfm	30	51	46	35	35	62	42	45	65	111	154	43	56	112	80	37
		fft	49	52	61	75	43	71	172	44	50	64	49	104	70	89	164	78
LOOCV	VME	wfm	n/a	n/a	n/a	n/a	n/a	n/a	n/a	n/a	n/a	n/a	n/a	n/a	n/a	n/a	n/a	n/a
		fft	n/a	n/a	n/a	n/a	n/a	n/a	n/a	n/a	n/a	n/a	n/a	n/a	n/a	n/a	n/a	n/a
	uTCA	wfm	26	30	31	27	25	31	32	29	30	40	37	36	24	38	41	28
		fft	35	54	46	55	50	76	170	52	25	64	43	109	57	89	160	63

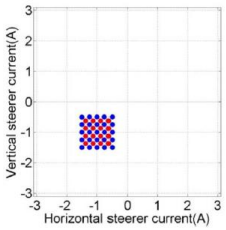

5482MHz (20MHz)			x resolution (μm)								y resolution (μm)							
			C1H2	C1H1	C2H1	C2H2	C3H2	C3H1	C4H1	C4H2	C1H2	C1H1	C2H1	C2H2	C3H2	C3H1	C4H1	C4H2
Fixed split	VME	wfm	13	11	12	13	29	21	15	18	18	15	12	14	9	9	15	16
		fft	17	11	9	10	16	17	11	12	18	17	13	14	10	36	13	12
	uTCA	wfm	30	29	33	37	26	27	29	29	25	24	29	37	25	22	36	34
		fft	32	24	28	33	27	38	33	40	32	25	27	33	20	23	40	40
LOOCV	VME	wfm	16	13	12	10	12	13	13	14	13	11	13	11	11	11	14	14
		fft	16	15	10	15	12	14	18	15	14	14	11	13	12	23	14	17
	uTCA	wfm	25	22	24	24	21	21	23	27	22	24	22	23	20	21	24	20
		fft	30	25	25	27	20	21	23	27	24	23	23	27	22	22	23	24

wfm: time-domain waveform; fft: frequency-domain fft amplitude; LOOCV: leave-one-out cross validation

Figure C.9: Position resolutions of cavity modes centered at 5482 MHz with a 20 MHz bandwidth.

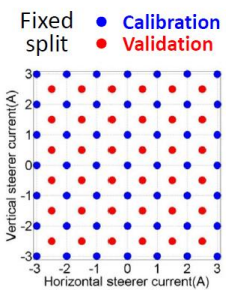

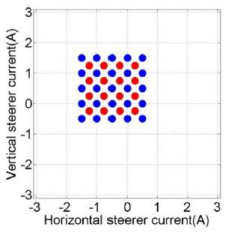

5400-5500MHz			x resolution (μm)								y resolution (μm)							
			C1H2	C1H1	C2H1	C2H2	C3H2	C3H1	C4H1	C4H2	C1H2	C1H1	C2H1	C2H2	C3H2	C3H1	C4H1	C4H2
Fixed split	VME	wfm	24	87	23	20	22	55	29	22	50	60	37	39	43	57	54	36
		fft	38	30	63	52	42	80	49	73	31	43	70	133	58	108	173	81
	uTCA	wfm	37	29	36	41	42	44	32	33	53	51	51	51	59	66	49	63
		fft	39	42	50	63	63	111	59	110	62	66	81	125	147	115	77	105
LOOCV	VME	wfm	24	23	23	22	21	30	21	19	27	33	39	40	35	43	34	29
		fft	27	39	40	59	49	81	65	73	33	41	58	126	65	93	175	76
	uTCA	wfm	32	26	31	32	28	27	25	26	35	34	36	37	35	37	35	33
		fft	36	48	60	48	53	85	72	75	37	54	59	79	91	97	83	83

5400-5500MHz			x resolution (μm)								y resolution (μm)							
			C1H2	C1H1	C2H1	C2H2	C3H2	C3H1	C4H1	C4H2	C1H2	C1H1	C2H1	C2H2	C3H2	C3H1	C4H1	C4H2
Fixed split	VME	wfm	65	30	16	19	17	19	29	35	104	61	36	74	73	64	64	67
		fft	16	18	21	38	21	22	55	23	96	53	53	36	61	70	78	82
	uTCA	wfm	39	48	34	43	41	42	62	46	91	73	87	80	104	106	81	104
		fft	47	48	46	62	46	44	88	43	107	94	87	126	183	156	129	105
LOOCV	VME	wfm	18	19	16	17	17	16	20	19	35	34	35	33	32	32	30	32
		fft	25	24	29	30	24	34	30	60	41	44	66	69	44	44	74	68
	uTCA	wfm	29	28	25	24	20	21	23	26	31	29	29	24	34	35	29	28
		fft	36	31	31	37	26	34	46	35	34	41	35	44	70	56	63	44

wfm: time-domain waveform; fft: frequency-domain fft amplitude; LOOCV: leave-one-out cross validation

Figure C.10: Position resolutions of cavity modes from 5400 MHz to 5500 MHz.

C.4 Trapped Cavity Modes - The Fifth Dipole Band

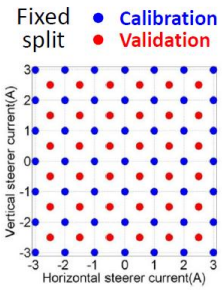

9048MHz (20MHz)			x resolution (μm)								y resolution (μm)							
			C1H2	C1H1	C2H1	C2H2	C3H2	C3H1	C4H1	C4H2	C1H2	C1H1	C2H1	C2H2	C3H2	C3H1	C4H1	C4H2
Fixed split	VME	wfm	49	43	90	58	44	50	79	50	69	83	113	56	53	58	88	127
		fft	29	94	101	66	41	75	33	48	36	163	139	143	68	110	69	339
	uTCA	wfm	60	64	93	57	70	71	66	62	85	94	150	78	73	79	83	200
		fft	39	153	135	60	58	112	57	102	78	183	221	121	74	145	100	306
LOOCV	VME	wfm	39	41	51	55	42	54	43	52	53	59	102	59	55	58	64	115
		fft	25	140	120	82	45	83	40	48	46	175	148	175	61	112	84	294
	uTCA	wfm	34	47	64	43	56	50	53	56	45	66	130	60	43	49	52	158
		fft	32	145	111	81	64	108	44	77	49	187	217	134	59	161	89	343

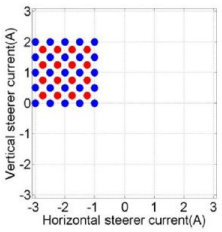

9048MHz (20MHz)			x resolution (μm)								y resolution (μm)							
			C1H2	C1H1	C2H1	C2H2	C3H2	C3H1	C4H1	C4H2	C1H2	C1H1	C2H1	C2H2	C3H2	C3H1	C4H1	C4H2
Fixed split	VME	wfm	13	34	89	39	37	21	20	23	31	49	104	100	18	19	23	107
		fft	12	44	57	52	30	27	22	30	32	77	90	69	31	100	36	120
	uTCA	wfm	29	36	66	48	50	30	49	41	47	86	111	64	31	45	29	79
		fft	66	62	103	53	47	58	53	52	41	156	160	95	45	93	29	236
LOOCV	VME	wfm	11	33	47	29	30	20	24	25	20	48	87	70	20	25	20	99
		fft	19	45	62	55	34	37	33	34	43	83	119	69	34	127	40	177
	uTCA	wfm	29	49	58	33	31	27	34	33	24	81	75	62	36	33	28	73
		fft	32	96	125	51	41	58	41	83	26	191	177	79	34	114	36	260

wfm: time-domain waveform; fft: frequency-domain fft amplitude; LOOCV: leave-one-out cross validation

Figure C.11: Position resolutions of cavity modes centered at 9048 MHz with a 20 MHz bandwidth.

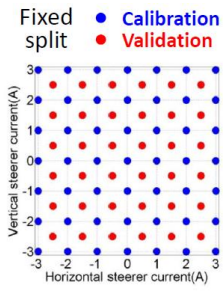

9066MHz (20MHz)			x resolution (μm)								y resolution (μm)							
			C1H2	C1H1	C2H1	C2H2	C3H2	C3H1	C4H1	C4H2	C1H2	C1H1	C2H1	C2H2	C3H2	C3H1	C4H1	C4H2
Fixed split	VME	wfm	39	56	61	44	45	47	39	58	62	93	96	78	55	45	64	110
		fft	34	112	90	94	46	74	65	60	74	151	126	95	49	140	65	196
	uTCA	wfm	53	94	81	79	68	68	64	72	83	172	154	116	77	99	82	89
		fft	67	237	166	99	93	138	71	88	139	325	218	187	67	276	143	235
LOOCV	VME	wfm	37	54	71	52	50	49	53	69	50	81	87	77	52	45	56	67
		fft	43	135	128	81	87	89	74	67	91	207	172	136	70	149	66	243
	uTCA	wfm	33	71	60	56	51	52	52	50	47	106	105	77	56	53	52	58
		fft	41	255	159	106	67	111	72	54	74	351	254	175	59	243	78	225

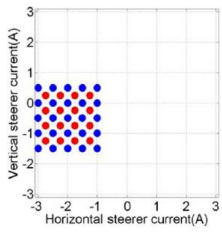

9066MHz (20MHz)			x resolution (μm)								y resolution (μm)							
			C1H2	C1H1	C2H1	C2H2	C3H2	C3H1	C4H1	C4H2	C1H2	C1H1	C2H1	C2H2	C3H2	C3H1	C4H1	C4H2
Fixed split	VME	wfm	12	60	33	21	13	20	24	23	57	129	94	103	42	43	44	90
		fft	31	67	44	48	22	33	21	58	57	134	115	154	44	45	34	231
	uTCA	wfm	28	76	64	40	33	44	35	38	142	181	201	216	105	129	100	106
		fft	43	91	58	79	39	132	39	48	132	239	225	253	101	129	108	191
LOOCV	VME	wfm	20	59	54	31	15	27	21	27	59	127	113	82	37	44	41	34
		fft	37	75	58	66	31	52	34	56	48	137	143	148	51	94	40	250
	uTCA	wfm	24	69	69	41	31	32	40	38	56	118	112	119	35	44	33	39
		fft	34	82	58	91	35	93	47	37	56	219	156	184	36	105	44	201

wfm: time-domain waveform; fft: frequency-domain fft amplitude; LOOCV: leave-one-out cross validation

Figure C.12: Position resolutions of cavity modes centered at 9066 MHz with a 20 MHz bandwidth.

Appendix D

Tables: Number of SVD Modes

This appendix shows the number of SVD modes used in position determination shown in Appendix C. The number of SVD modes used for regression is determined based on a stable and good position resolution.

D.1 The Localized Beam-pipe modes

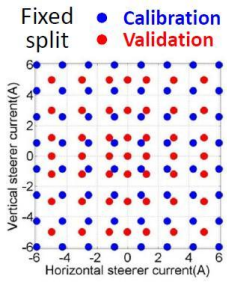

4082MHz (20MHz)			x								y							
			C1H2	C1H1	C2H1	C2H2	C3H2	C3H1	C4H1	C4H2	C1H2	C1H1	C2H1	C2H2	C3H2	C3H1	C4H1	C4H2
Fixed split	VME	wfm	n/a	n/a	n/a	n/a	n/a	n/a	n/a	n/a	n/a	n/a	n/a	n/a	n/a	n/a	n/a	n/a
		fft	n/a	n/a	n/a	n/a	n/a	n/a	n/a	n/a	n/a	n/a	n/a	n/a	n/a	n/a	n/a	n/a
	uTCA	wfm	10	10	10	16	15	14	11	10	10	10	10	16	15	14	11	10
		fft	19	14	8	10	16	19	14	9	19	14	8	10	16	19	14	9
LOOCV	VME	wfm	n/a	n/a	n/a	n/a	n/a	n/a	n/a	n/a	n/a	n/a	n/a	n/a	n/a	n/a	n/a	n/a
		fft	n/a	n/a	n/a	n/a	n/a	n/a	n/a	n/a	n/a	n/a	n/a	n/a	n/a	n/a	n/a	n/a
	uTCA	wfm	9	11	10	16	18	13	11	15	9	11	10	16	18	13	11	15
		fft	20	15	10	20	16	14	7	9	20	15	10	20	16	14	7	9

wfm: time-domain waveform; fft: frequency-domain fft amplitude; LOOCV: leave-one-out cross validation

Figure D.1: Number of SVD modes used for position determination of beam-pipe modes centered at 4082 MHz with a 20 MHz bandwidth.

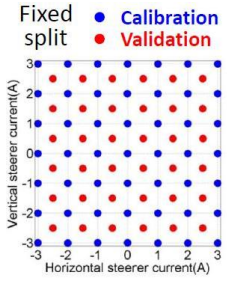

4118MHz (20MHz)			x								y							
			C1H2	C1H1	C2H1	C2H2	C3H2	C3H1	C4H1	C4H2	C1H2	C1H1	C2H1	C2H2	C3H2	C3H1	C4H1	C4H2
Fixed split	VME	wfm	n/a	n/a	n/a	n/a	n/a	n/a	n/a	n/a	n/a	n/a	n/a	n/a	n/a	n/a	n/a	n/a
		fft	n/a	n/a	n/a	n/a	n/a	n/a	n/a	n/a	n/a	n/a	n/a	n/a	n/a	n/a	n/a	n/a
	uTCA	wfm	5	7	5	5	8	13	7	4	5	7	5	5	8	13	7	4
		fft	10	8	7	10	13	10	5	7	10	8	7	10	13	10	5	7
LOOCV	VME	wfm	n/a	n/a	n/a	n/a	n/a	n/a	n/a	n/a	n/a	n/a	n/a	n/a	n/a	n/a	n/a	n/a
		fft	n/a	n/a	n/a	n/a	n/a	n/a	n/a	n/a	n/a	n/a	n/a	n/a	n/a	n/a	n/a	n/a
	uTCA	wfm	5	7	6	5	5	13	7	5	5	7	6	5	5	13	7	5
		fft	15	8	6	11	21	11	9	9	15	8	6	11	21	11	9	9

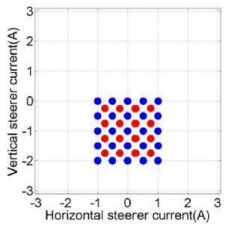

4118MHz (20MHz)			x								y							
			C1H2	C1H1	C2H1	C2H2	C3H2	C3H1	C4H1	C4H2	C1H2	C1H1	C2H1	C2H2	C3H2	C3H1	C4H1	C4H2
Fixed split	VME	wfm	n/a	n/a	n/a	n/a	n/a	n/a	n/a	n/a	n/a	n/a	n/a	n/a	n/a	n/a	n/a	n/a
		fft	n/a	n/a	n/a	n/a	n/a	n/a	n/a	n/a	n/a	n/a	n/a	n/a	n/a	n/a	n/a	n/a
	uTCA	wfm	4	7	4	5	7	6	5	4	4	7	4	5	7	6	5	4
		fft	4	4	3	11	6	5	3	4	4	4	3	11	6	5	3	4
LOOCV	VME	wfm	n/a	n/a	n/a	n/a	n/a	n/a	n/a	n/a	n/a	n/a	n/a	n/a	n/a	n/a	n/a	n/a
		fft	n/a	n/a	n/a	n/a	n/a	n/a	n/a	n/a	n/a	n/a	n/a	n/a	n/a	n/a	n/a	n/a
	uTCA	wfm	4	6	4	5	7	7	4	4	4	6	4	5	7	7	4	4
		fft	5	6	3	8	14	4	3	5	5	6	3	8	14	4	3	5

wfm: time-domain waveform; fft: frequency-domain fft amplitude; LOOCV: leave-one-out cross validation

Figure D.2: Number of SVD modes used for position determination of beam-pipe modes centered at 4118 MHz with a 20 MHz bandwidth.

D.2 Coupled Cavity Modes - The First Dipole Band

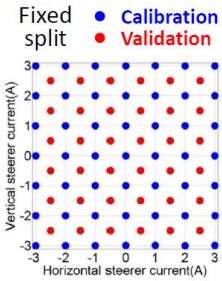

4859MHz (20MHz)			x								y							
			C1H2	C1H1	C2H1	C2H2	C3H2	C3H1	C4H1	C4H2	C1H2	C1H1	C2H1	C2H2	C3H2	C3H1	C4H1	C4H2
Fixed split	VME	wfm	n/a	n/a	n/a	n/a	n/a	n/a	n/a	n/a	n/a	n/a	n/a	n/a	n/a	n/a	n/a	n/a
		fft	n/a	n/a	n/a	n/a	n/a	n/a	n/a	n/a	n/a	n/a	n/a	n/a	n/a	n/a	n/a	n/a
	uTCA	wfm	5	6	3	6	8	6	5	7	5	6	3	6	8	6	5	7
		fft	18	16	30	19	22	14	9	15	18	16	30	19	22	14	9	15
LOOCV	VME	wfm	n/a	n/a	n/a	n/a	n/a	n/a	n/a	n/a	n/a	n/a	n/a	n/a	n/a	n/a	n/a	n/a
		fft	n/a	n/a	n/a	n/a	n/a	n/a	n/a	n/a	n/a	n/a	n/a	n/a	n/a	n/a	n/a	n/a
	uTCA	wfm	5	6	4	7	8	5	6	6	5	6	4	7	8	5	6	6
		fft	21	13	12	19	18	15	13	14	21	13	12	19	18	15	13	14

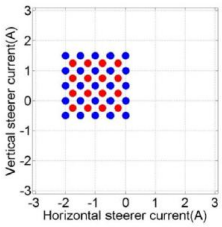

4859MHz (20MHz)			x								y							
			C1H2	C1H1	C2H1	C2H2	C3H2	C3H1	C4H1	C4H2	C1H2	C1H1	C2H1	C2H2	C3H2	C3H1	C4H1	C4H2
Fixed split	VME	wfm	n/a	n/a	n/a	n/a	n/a	n/a	n/a	n/a	n/a	n/a	n/a	n/a	n/a	n/a	n/a	n/a
		fft	n/a	n/a	n/a	n/a	n/a	n/a	n/a	n/a	n/a	n/a	n/a	n/a	n/a	n/a	n/a	n/a
	uTCA	wfm	5	3	3	4	3	2	5	4	5	3	3	4	3	2	5	4
		fft	12	5	6	9	10	5	6	4	12	5	6	9	10	5	6	4
LOOCV	VME	wfm	n/a	n/a	n/a	n/a	n/a	n/a	n/a	n/a	n/a	n/a	n/a	n/a	n/a	n/a	n/a	n/a
		fft	n/a	n/a	n/a	n/a	n/a	n/a	n/a	n/a	n/a	n/a	n/a	n/a	n/a	n/a	n/a	n/a
	uTCA	wfm	4	4	5	4	3	4	5	4	4	4	5	4	3	4	5	4
		fft	4	6	6	9	8	6	6	4	4	6	6	9	8	6	6	4

wfm: time-domain waveform; fft: frequency-domain fft amplitude; LOOCV: leave-one-out cross validation

Figure D.3: Number of SVD modes used for position determination of cavity modes centered at 4859 MHz with a 20 MHz bandwidth.

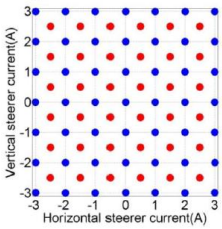

4904MHz (20MHz)			x								y							
			C1H2	C1H1	C2H1	C2H2	C3H2	C3H1	C4H1	C4H2	C1H2	C1H1	C2H1	C2H2	C3H2	C3H1	C4H1	C4H2
Fixed split	VME	wfm	n/a	n/a	n/a	n/a	n/a	n/a	n/a	n/a	n/a	n/a	n/a	n/a	n/a	n/a	n/a	n/a
		fft	n/a	n/a	n/a	n/a	n/a	n/a	n/a	n/a	n/a	n/a	n/a	n/a	n/a	n/a	n/a	n/a
	uTCA	wfm	7	7	7	6	9	11	5	5	7	7	7	6	9	11	5	5
		fft	11	13	11	20	25	12	12	14	11	13	11	20	25	12	12	14
LOOCV	VME	wfm	n/a	n/a	n/a	n/a	n/a	n/a	n/a	n/a	n/a	n/a	n/a	n/a	n/a	n/a	n/a	n/a
		fft	n/a	n/a	n/a	n/a	n/a	n/a	n/a	n/a	n/a	n/a	n/a	n/a	n/a	n/a	n/a	n/a
	uTCA	wfm	7	9	6	9	7	11	5	5	7	9	6	9	7	11	5	5
		fft	12	20	14	20	18	12	11	19	12	20	14	20	18	12	11	19

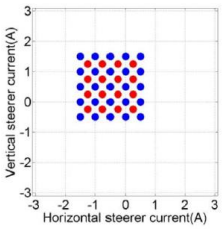

4904MHz (20MHz)			x								y							
			C1H2	C1H1	C2H1	C2H2	C3H2	C3H1	C4H1	C4H2	C1H2	C1H1	C2H1	C2H2	C3H2	C3H1	C4H1	C4H2
Fixed split	VME	wfm	n/a	n/a	n/a	n/a	n/a	n/a	n/a	n/a	n/a	n/a	n/a	n/a	n/a	n/a	n/a	n/a
		fft	n/a	n/a	n/a	n/a	n/a	n/a	n/a	n/a	n/a	n/a	n/a	n/a	n/a	n/a	n/a	n/a
	uTCA	wfm	4	7	4	4	4	6	5	4	4	7	4	4	4	6	5	4
		fft	6	12	4	4	5	6	4	7	6	12	4	4	5	6	4	7
LOOCV	VME	wfm	n/a	n/a	n/a	n/a	n/a	n/a	n/a	n/a	n/a	n/a	n/a	n/a	n/a	n/a	n/a	n/a
		fft	n/a	n/a	n/a	n/a	n/a	n/a	n/a	n/a	n/a	n/a	n/a	n/a	n/a	n/a	n/a	n/a
	uTCA	wfm	4	5	6	4	4	6	4	4	4	5	6	4	4	6	4	4
		fft	6	11	6	6	6	8	6	7	6	11	6	6	6	8	6	7

wfm: time-domain waveform; fft: frequency-domain fft amplitude; LOOCV: leave-one-out cross validation

Figure D.4: Number of SVD modes used for position determination of cavity modes centered at 4904 MHz with a 20 MHz bandwidth.

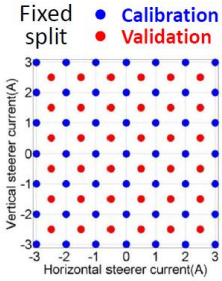

4940MHz (20MHz)			x								y							
			C1H2	C1H1	C2H1	C2H2	C3H2	C3H1	C4H1	C4H2	C1H2	C1H1	C2H1	C2H2	C3H2	C3H1	C4H1	C4H2
Fixed split	VME	wfm	4	6	5	5	6	5	5	5	4	6	5	5	6	5	5	5
		fft	19	14	14	11	12	12	16	6	19	14	14	11	12	12	16	6
	uTCA	wfm	5	7	5	5	6	5	5	6	5	7	5	5	6	5	5	6
		fft	21	13	13	8	11	13	11	7	21	13	13	8	11	13	11	7
LOOCV	VME	wfm	7	6	5	6	6	5	5	5	7	6	5	6	6	5	5	5
		fft	24	13	14	11	12	12	14	6	24	13	14	11	12	12	14	6
	uTCA	wfm	7	7	5	5	6	5	6	6	7	7	5	5	6	5	6	6
		fft	20	13	14	8	12	10	12	6	20	13	14	8	12	10	12	6

wfm: time-domain waveform; fft: frequency-domain fft amplitude; LOOCV: leave-one-out cross validation

Figure D.5: Number of SVD modes used for position determination of cavity modes centered at 4940 MHz with a 20 MHz bandwidth.

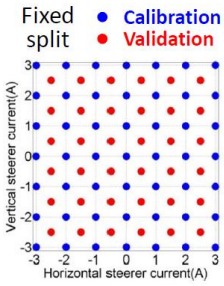

4850-4950MHz			x								y							
			C1H2	C1H1	C2H1	C2H2	C3H2	C3H1	C4H1	C4H2	C1H2	C1H1	C2H1	C2H2	C3H2	C3H1	C4H1	C4H2
Fixed split	VME	wfm	4	12	4	5	6	10	7	5	4	12	4	5	6	10	7	5
		fft	20	19	22	17	15	21	22	21	20	19	22	17	15	21	22	21
	uTCA	wfm	3	11	6	5	10	8	7	5	3	11	6	5	10	8	7	5
		fft	19	18	17	13	15	14	14	12	19	18	17	13	15	14	14	12
LOOCV	VME	wfm	5	12	8	5	10	11	8	5	5	12	8	5	10	11	8	5
		fft	14	22	12	15	15	22	21	18	14	22	12	15	15	22	21	18
	uTCA	wfm	7	13	9	8	10	13	10	7	7	13	9	8	10	13	10	7
		fft	22	17	19	14	13	15	11	10	22	17	19	14	13	15	11	10

wfm: time-domain waveform; fft: frequency-domain fft amplitude; LOOCV: leave-one-out cross validation

Figure D.6: Number of SVD modes used for position determination of cavity modes from 4850 MHz to 4950 MHz.

D.3 Coupled Cavity Modes - The Second Dipole Band

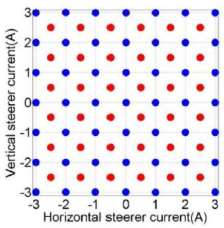

5437MHz (20MHz)			x								y							
			C1H2	C1H1	C2H1	C2H2	C3H2	C3H1	C4H1	C4H2	C1H2	C1H1	C2H1	C2H2	C3H2	C3H1	C4H1	C4H2
Fixed split	VME	wfm	7	8	5	5	15	9	8	10	7	8	5	5	15	9	8	10
		fft	20	15	26	20	32	28	29	23	20	15	26	20	32	28	29	23
	uTCA	wfm	7	9	5	5	11	7	8	6	7	9	5	5	11	7	8	6
		fft	11	17	13	26	20	19	20	23	11	17	13	26	20	19	20	23
LOOCV	VME	wfm	10	9	5	5	15	7	5	13	10	9	5	5	15	7	5	13
		fft	20	17	20	20	19	26	22	22	20	17	20	20	19	26	22	22
	uTCA	wfm	13	12	5	5	12	16	10	7	13	12	5	5	12	16	10	7
		fft	17	17	17	21	21	19	21	21	17	17	17	21	21	19	21	21

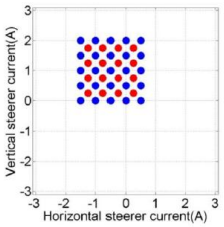

5437MHz (20MHz)			x								y							
			C1H2	C1H1	C2H1	C2H2	C3H2	C3H1	C4H1	C4H2	C1H2	C1H1	C2H1	C2H2	C3H2	C3H1	C4H1	C4H2
Fixed split	VME	wfm	4	7	5	5	7	7	5	5	4	7	5	5	7	7	5	5
		fft	7	7	7	7	9	14	11	11	7	7	7	7	9	14	11	11
	uTCA	wfm	4	5	6	2	7	4	4	3	4	5	6	2	7	4	4	3
		fft	4	9	6	7	8	14	10	10	4	9	6	7	8	14	10	10
LOOCV	VME	wfm	5	7	5	5	7	7	5	5	5	7	5	5	7	7	5	5
		fft	8	7	6	7	10	14	11	12	8	7	6	7	10	14	11	12
	uTCA	wfm	4	6	5	5	7	8	4	5	4	6	5	5	7	8	4	5
		fft	6	7	6	13	9	14	12	10	6	7	6	13	9	14	12	10

wfm: time-domain waveform; fft: frequency-domain fft amplitude; LOOCV: leave-one-out cross validation

Figure D.7: Number of SVD modes used for position determination of cavity modes centered at 5437 MHz with a 20 MHz bandwidth.

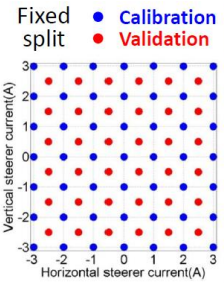

5464MHz (20MHz)			x								y							
			C1H2	C1H1	C2H1	C2H2	C3H2	C3H1	C4H1	C4H2	C1H2	C1H1	C2H1	C2H2	C3H2	C3H1	C4H1	C4H2
Fixed split	VME	wfm	n/a	n/a	n/a	n/a	n/a	n/a	n/a	n/a	n/a	n/a	n/a	n/a	n/a	n/a	n/a	n/a
		fft	n/a	n/a	n/a	n/a	n/a	n/a	n/a	n/a	n/a	n/a	n/a	n/a	n/a	n/a	n/a	n/a
	uTCA	wfm	8	7	7	5	8	6	7	14	8	7	7	5	8	6	7	14
		fft	13	15	15	22	20	21	12	16	13	15	15	22	20	21	12	16
LOOCV	VME	wfm	n/a	n/a	n/a	n/a	n/a	n/a	n/a	n/a	n/a	n/a	n/a	n/a	n/a	n/a	n/a	n/a
		fft	n/a	n/a	n/a	n/a	n/a	n/a	n/a	n/a	n/a	n/a	n/a	n/a	n/a	n/a	n/a	n/a
	uTCA	wfm	6	7	7	9	9	7	7	13	6	7	7	9	9	7	7	13
		fft	11	19	15	22	18	15	22	23	11	19	15	22	18	15	22	23

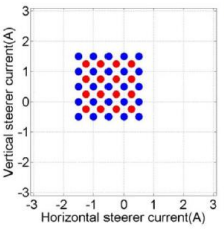

5464MHz (20MHz)			x								y							
			C1H2	C1H1	C2H1	C2H2	C3H2	C3H1	C4H1	C4H2	C1H2	C1H1	C2H1	C2H2	C3H2	C3H1	C4H1	C4H2
Fixed split	VME	wfm	4	5	5	6	8	8	7	7	4	5	5	6	8	8	7	7
		fft	6	9	7	9	11	14	12	10	6	9	7	9	11	14	12	10
	uTCA	wfm	4	5	4	6	5	8	6	7	4	5	4	6	5	8	6	7
		fft	6	4	3	5	14	12	15	7	6	4	3	5	14	12	15	7
LOOCV	VME	wfm	4	4	5	6	7	5	5	7	4	4	5	6	7	5	5	7
		fft	3	8	10	11	8	10	12	10	3	8	10	11	8	10	12	10
	uTCA	wfm	4	4	5	6	6	4	5	5	4	4	5	6	6	4	5	5
		fft	4	7	8	12	9	12	7	11	4	7	8	12	9	12	7	11

wfm: time-domain waveform; fft: frequency-domain fft amplitude; LOOCV: leave-one-out cross validation

Figure D.8: Number of SVD modes used for position determination of cavity modes centered at 5464 MHz with a 20 MHz bandwidth.

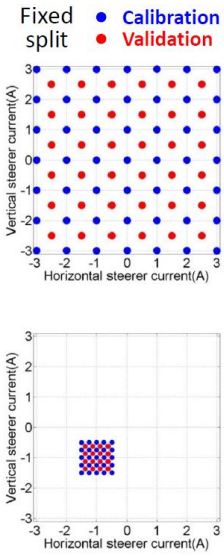

5482MHz (20MHz)			x								y							
			C1H2	C1H1	C2H1	C2H2	C3H2	C3H1	C4H1	C4H2	C1H2	C1H1	C2H1	C2H2	C3H2	C3H1	C4H1	C4H2
Fixed split	VME	wfm	n/a	n/a	n/a	n/a	n/a	n/a	n/a	n/a	n/a	n/a	n/a	n/a	n/a	n/a	n/a	n/a
		fft	n/a	n/a	n/a	n/a	n/a	n/a	n/a	n/a	n/a	n/a	n/a	n/a	n/a	n/a	n/a	n/a
	uTCA	wfm	10	6	6	4	4	6	2	4	10	6	6	4	4	6	2	4
		fft	10	21	11	19	22	25	19	18	10	21	11	19	22	25	19	18
LOOCV	VME	wfm	n/a	n/a	n/a	n/a	n/a	n/a	n/a	n/a	n/a	n/a	n/a	n/a	n/a	n/a	n/a	n/a
		fft	n/a	n/a	n/a	n/a	n/a	n/a	n/a	n/a	n/a	n/a	n/a	n/a	n/a	n/a	n/a	n/a
	uTCA	wfm	9	4	6	2	9	4	6	10	9	4	6	2	9	4	6	10
		fft	13	16	11	17	22	20	15	20	13	16	11	17	22	20	15	20

5482MHz (20MHz)			x								y							
			C1H2	C1H1	C2H1	C2H2	C3H2	C3H1	C4H1	C4H2	C1H2	C1H1	C2H1	C2H2	C3H2	C3H1	C4H1	C4H2
Fixed split	VME	wfm	5	4	4	4	4	4	4	8	5	4	4	4	4	4	4	8
		fft	3	3	4	3	3	3	5	7	3	3	4	3	3	3	5	7
	uTCA	wfm	5	6	4	3	3	5	4	4	5	6	4	3	3	5	4	4
		fft	4	3	4	4	3	6	2	5	4	3	4	4	3	6	2	5
LOOCV	VME	wfm	4	4	4	4	4	4	4	6	4	4	4	4	4	4	4	6
		fft	3	3	4	4	5	4	5	7	3	3	4	4	5	4	5	7
	uTCA	wfm	4	6	4	4	5	4	3	4	4	6	4	4	5	4	3	4
		fft	4	3	3	4	4	4	4	5	4	3	3	4	4	4	4	5

wfm: time-domain waveform; fft: frequency-domain fft amplitude; LOOCV: leave-one-out cross validation

Figure D.9: Number of SVD modes used for position determination of cavity modes centered at 5482 MHz with a 20 MHz bandwidth.

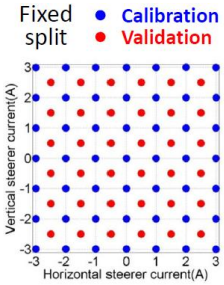

5400-5500MHz			x								y							
			C1H2	C1H1	C2H1	C2H2	C3H2	C3H1	C4H1	C4H2	C1H2	C1H1	C2H1	C2H2	C3H2	C3H1	C4H1	C4H2
Fixed split	VME	wfm	4	5	7	7	8	9	4	7	4	5	7	7	8	9	4	7
		fft	12	22	16	32	21	22	15	24	12	22	16	32	21	22	15	24
	uTCA	wfm	8	8	6	4	7	6	4	7	8	8	6	4	7	6	4	7
		fft	11	17	20	14	24	22	18	26	11	17	20	14	24	22	18	26
LOOCV	VME	wfm	11	8	7	4	8	15	6	7	11	8	7	4	8	15	6	7
		fft	15	22	29	33	26	34	25	26	15	22	29	33	26	34	25	26
	uTCA	wfm	7	8	6	5	8	15	5	7	7	8	6	5	8	15	5	7
		fft	11	15	23	24	27	22	18	26	11	15	23	24	27	22	18	26

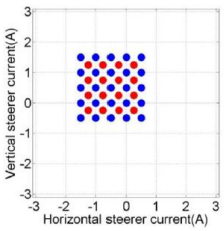

5400-5500MHz			x								y							
			C1H2	C1H1	C2H1	C2H2	C3H2	C3H1	C4H1	C4H2	C1H2	C1H1	C2H1	C2H2	C3H2	C3H1	C4H1	C4H2
Fixed split	VME	wfm	5	6	6	5	5	4	4	6	5	6	6	5	5	4	4	6
		fft	8	3	3	8	10	16	4	12	8	3	3	8	10	16	4	12
	uTCA	wfm	5	5	8	3	5	4	3	6	5	5	8	3	5	4	3	6
		fft	8	14	11	11	11	12	9	12	8	14	11	11	11	12	9	12
LOOCV	VME	wfm	4	5	4	5	4	4	4	6	4	5	4	5	4	4	4	6
		fft	5	8	7	9	13	14	15	10	5	8	7	9	13	14	15	10
	uTCA	wfm	4	5	3	5	5	4	5	6	4	5	3	5	5	4	5	6
		fft	7	12	9	11	15	10	12	12	7	12	9	11	15	10	12	12

wfm: time-domain waveform; fft: frequency-domain fft amplitude; LOOCV: leave-one-out cross validation

Figure D.10: Number of SVD modes used for position determination of cavity modes from 5400 MHz to 5500 MHz.

D.4 Trapped Cavity Modes - The Fifth Dipole Band

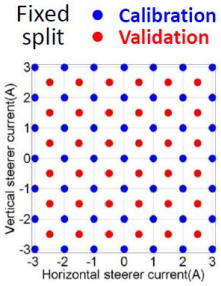

9048MHz (20MHz)			x								y							
			C1H2	C1H1	C2H1	C2H2	C3H2	C3H1	C4H1	C4H2	C1H2	C1H1	C2H1	C2H2	C3H2	C3H1	C4H1	C4H2
Fixed split	VME	wfm	7	7	8	9	15	8	8	9	7	7	8	9	15	8	8	9
		fft	15	9	8	12	21	14	13	26	15	9	8	12	21	14	13	26
	uTCA	wfm	6	6	9	8	11	10	4	9	6	6	9	8	11	10	4	9
		fft	11	7	6	15	20	12	17	7	11	7	6	15	20	12	17	7
LOOCV	VME	wfm	10	7	8	9	14	8	8	9	10	7	8	9	14	8	8	9
		fft	15	10	10	15	21	16	13	10	15	10	10	15	21	16	13	10
	uTCA	wfm	8	5	8	8	11	5	7	12	8	5	8	8	11	5	7	12
		fft	16	7	7	12	20	12	18	11	16	7	7	12	20	12	18	11

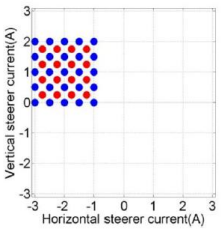

9048MHz (20MHz)			x								y							
			C1H2	C1H1	C2H1	C2H2	C3H2	C3H1	C4H1	C4H2	C1H2	C1H1	C2H1	C2H2	C3H2	C3H1	C4H1	C4H2
Fixed split	VME	wfm	7	4	5	7	8	5	4	8	7	4	5	7	8	5	4	8
		fft	5	3	4	5	7	4	9	3	5	3	4	5	7	4	9	3
	uTCA	wfm	4	4	5	9	8	4	4	5	4	4	5	9	8	4	4	5
		fft	8	4	3	6	8	5	5	4	8	4	3	6	8	5	5	4
LOOCV	VME	wfm	8	4	5	8	8	5	6	5	8	4	5	8	8	5	6	5
		fft	5	3	5	8	7	7	11	3	5	3	5	8	7	7	11	3
	uTCA	wfm	8	4	7	8	8	4	4	5	8	4	7	8	8	4	4	5
		fft	8	3	4	5	11	5	6	4	8	3	4	5	11	5	6	4

wfm: time-domain waveform; fft: frequency-domain fft amplitude; LOOCV: leave-one-out cross validation

Figure D.11: Number of SVD modes used for position determination of cavity modes centered at 9048 MHz with a 20 MHz bandwidth.

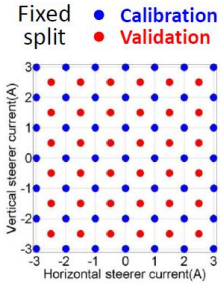

9066MHz (20MHz)			x								y							
			C1H2	C1H1	C2H1	C2H2	C3H2	C3H1	C4H1	C4H2	C1H2	C1H1	C2H1	C2H2	C3H2	C3H1	C4H1	C4H2
Fixed split	VME	wfm	9	11	10	12	11	10	11	9	9	11	10	12	11	10	11	9
		fft	17	7	11	13	14	14	14	8	17	7	11	13	14	14	14	8
	uTCA	wfm	9	12	10	10	8	7	9	8	9	12	10	10	8	7	9	8
		fft	14	7	8	9	16	11	14	12	14	7	8	9	16	11	14	12
LOOCV	VME	wfm	7	10	11	8	11	8	9	9	7	10	11	8	11	8	9	9
		fft	18	8	11	13	15	14	17	7	18	8	11	13	15	14	17	7
	uTCA	wfm	9	8	10	9	13	7	9	8	9	8	10	9	13	7	9	8
		fft	18	7	9	11	19	14	14	12	18	7	9	11	19	14	14	12

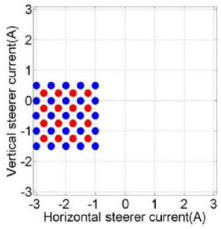

9066MHz (20MHz)			x								y							
			C1H2	C1H1	C2H1	C2H2	C3H2	C3H1	C4H1	C4H2	C1H2	C1H1	C2H1	C2H2	C3H2	C3H1	C4H1	C4H2
Fixed split	VME	wfm	4	6	8	8	11	4	8	5	4	6	8	8	11	4	8	5
		fft	6	8	14	7	9	7	9	14	6	8	14	7	9	7	9	14
	uTCA	wfm	5	5	5	4	9	4	8	4	5	5	5	4	9	4	8	4
		fft	13	3	3	9	7	4	8	7	13	3	3	9	7	4	8	7
LOOCV	VME	wfm	4	7	4	10	11	4	8	6	4	7	4	10	11	4	8	6
		fft	6	4	5	11	9	6	9	10	6	4	5	11	9	6	9	10
	uTCA	wfm	5	5	4	7	8	4	8	4	5	5	4	7	8	4	8	4
		fft	7	3	2	4	7	5	8	7	7	3	2	4	7	5	8	7

wfm: time-domain waveform; fft: frequency-domain fft amplitude; LOOCV: leave-one-out cross validation

Figure D.12: Number of SVD modes used for position determination of cavity modes centered at 9066 MHz with a 20 MHz bandwidth.